

**University of Alberta**

**Steam-Assisted Gravity Drainage Process Enhancement**

by

Jian Gong



A thesis submitted to the Faculty of Graduate Studies and Research in partial fulfillment  
of the requirements of the degree of Master of Science

in

Petroleum Engineering

Department of Civil and Environmental Engineering

Edmonton, Alberta, Canada

Fall 2002



National Library  
of Canada

Acquisitions and  
Bibliographic Services

395 Wellington Street  
Ottawa ON K1A 0N4  
Canada

Bibliothèque nationale  
du Canada

Acquisitions et  
services bibliographiques

395, rue Wellington  
Ottawa ON K1A 0N4  
Canada

*Your file Votre référence*

*Our file Notre référence*

The author has granted a non-exclusive licence allowing the National Library of Canada to reproduce, loan, distribute or sell copies of this thesis in microform, paper or electronic formats.

The author retains ownership of the copyright in this thesis. Neither the thesis nor substantial extracts from it may be printed or otherwise reproduced without the author's permission.

L'auteur a accordé une licence non exclusive permettant à la Bibliothèque nationale du Canada de reproduire, prêter, distribuer ou vendre des copies de cette thèse sous la forme de microfiche/film, de reproduction sur papier ou sur format électronique.

L'auteur conserve la propriété du droit d'auteur qui protège cette thèse. Ni la thèse ni des extraits substantiels de celle-ci ne doivent être imprimés ou autrement reproduits sans son autorisation.

0-612-81399-1

**University of Alberta**  
**Library Release Form**

**Name of Author:** Jian Gong


**Title of Thesis:** Steam-Assisted Gravity Drainage Process Enhancement

**Degree:** Master of Science

**Year this Degree Granted:** 2002

Permission is hereby granted to the University of Alberta Library to reproduce single copies of this thesis and to lend or sell such copies for private, scholarly, or scientific research purposes only.

The author reserves all other publication and other rights in association with the copyright in the thesis, and except as herein before provided, neither the thesis nor any substantial portion thereof may be printed or otherwise reproduced in any material form whatever without the author's prior written permission.


  
\_\_\_\_\_  
3B 9201 112 ST N.W.  
Edmonton, Alberta  
Canada  
T6G 2C5

Date: Sept. 25, 2002

University of Alberta

Faculty of Graduate Studies and Research

The undersigned certify that they have read, and recommend to the Faculty of Graduate Studies and Research for acceptance, a thesis entitled *Steam-Assisted Gravity Drainage Process Enhancement* submitted by Jian Gong in partial fulfillment of the requirements for the degree of Master of Science in Petroleum Engineering.



---

Dr. Marcel Polikar

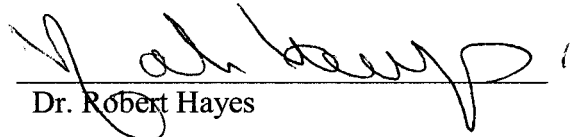
Supervisor



---

Dr. Richard Chalaturnyk

Committee Chair & Examiner



---

Dr. Robert Hayes

Committee Member

Date: September 25, 2002



## **ABSTRACT**

In the past two decades, Canada's remaining reserves of conventional crude oil have been declining. Heavy and extra-heavy oil reservoirs located in Western Canada (Alberta and Saskatchewan provinces) are one of the largest accumulations of hydrocarbons in the world, and constitute Canada's major remaining resources. This fact has led to the development of several methods of exploiting heavy oil deposits.

This research outlines a new variation of the Steam-Assisted Gravity Drainage (SAGD) process, called Fast-SAGD. Simply, Fast-SAGD is operated in a combined SAGD and Cyclic Steam Stimulation (CSS) process, in which the CSS process is applied to an offset well. Numerical simulation of the Fast-SAGD process using a thermal reservoir simulation software package is performed to investigate the operating strategy. Geomechanical issues have been recognized as one of the important factors, as the steam is introduced into the reservoir, especially from an offset well in a cyclic injection mode. A geomechanical model is used to analyze the impact of geomechanics on the recovery process. It is concluded from this study that, besides gravity, steam drive, shear failure, and pore volume deformation are additional mechanisms in this recovery process. Clearly, Fast-SAGD is a process with high productivity and low cumulative steam-oil ratio.

## **ACKNOWLEDGEMENTS**

I wish to express my appreciation and gratitude for the support and opportunity provided by my supervisor, Dr. Marcel Polikar. The guidance given by Dr. Polikar is highly acknowledged. The assistance of the author's co-supervisor, Dr. Richard Chalaturnyk, is also appreciated. I enjoyed our regular meetings and your guidance and suggestion. Without your help, I would not have accomplished my studies.

I am grateful to my colleague, Pingke Li, for our many hours of discussion throughout this research especially in the late stages of thesis completion.

A special thank to Dr. Ramon Bentsen for his kindness and assistance in reading through my thesis and giving me helpful suggestions.

To all my friends, especially Rufus Ayodele and Hyundon Shin. Your friendship and encouragement strongly supported me in finishing my research and writing.

To my dear parents and my brother, who encouraged and supported me to study abroad. Your love does and will lead my dream to come true.

## TABLE OF CONTENTS

Chapter	Page
1.0 INTRODUCTION.....	1
2.0 REVIEW OF LITERATURE.....	3
2.1 SAGD and its Variation .....	3
2.2 Cyclic Steam Stimulation.....	7
2.3 Coupled Reservoir/Geomechanics Stimulation .....	8
2.4 Geomechanical Mechanism in SAGD .....	12
3.0 STATEMENT OF THE PROBLEM .....	14
4.0 NUMERICAL INVESTIGATION OF FAST-SAGD .....	15
4.1 Background of the Thermal Recovery Process .....	15
4.2 Fast-SAGD Process.....	15
4.3 Numerical Model.....	16
4.3.1 Geometry and Gridding.....	17
4.3.2 Reservoir Properties .....	17
4.3.3 Well Position, Constraint and Boundary Conditions .....	19
4.3.4 Initial Pressure.....	20
4.3.5 Conditions of Numerical Runs.....	20
4.4 Reservoir Simulation Results and Discussion.....	22
4.4.1 Operating Pressure for the SAGD Well Pair.....	22
4.4.2 Comparison of Simulation Results between SAGD and Fast-SAGD .....	22
4.4.3 Extra Steam Injection from the SAGD Injector .....	25
4.4.4 Injection Pressure and Start-up Time of the Offset Well .....	25
4.5 Proposal for an Operating Strategy after the First Offset Well.....	27
4.6 Summary .....	29
5.0 NUMERICAL INVESTIGATION OF GEOMECHANICAL RESPONSE ON FAST-SAGD.....	30
5.1 Development of the Reservoir/Geomechanical Model .....	30
5.1.1 Thickness of Overburden and Oil Sands.....	31
5.1.2 Initial Stress Conditions .....	32
5.1.3 Grid Development and Boundary Conditions.....	32

5.2 Geomechanical Results and Discussion.....	34
5.2.1 Initial Stress State.....	35
5.2.2 Stress Path and Volume Strain Increment.....	35
5.2.3 Shear Failure Zone .....	40
5.2.4 Stress-Induced Porosity and Absolute Permeability Changes .....	41
5.3 Summary .....	42
6.0 CONCLUSIONS AND FUTURE WORK .....	43
7.0 REFERENCES.....	44
Appendix A: Fluid and Rock Properties .....	49
Appendix B: Impact of Hydrostatic Pressure on SAGD Operation.....	51
Appendix C: Reservoir Simulation Results for Cases 1-9 .....	61
Appendix D: Geomechanical Properties of Oil Sands .....	99
Appendix E: Geomechanical Simulation Results for Cases 1, 6 and 8.....	104
Appendix F: Reservoir Simulation Set (STARS) .....	124
Appendix G: Geomechanical Simulation Set (FLAC) .....	133
Appendix F: Interfacial Program of Data Transformation.....	142

## LIST OF TABLES

Table	Page
Table 4-1. Reservoir Properties.....	18
Table 4-2. Properties of the Three Zones.....	19
Table 4-3. Fast-SAGD Simulation Cases.....	21
Table 4-4. Simulation Results of Fast-SAGD.....	24
Table 4-5. Simulation Summary of CSS Components.....	26
Table 5-1. Geomechanical Properties .....	32
Table B-1. Initial Conditions and Reservoir Properties .....	52
Table B-2. Simulation Sets of Cases A to D .....	53
Table B-3. Simulation Results of Cases A to D .....	53

## LIST OF FIGURES

Figure	Page
Figure 2-1. Steam-Assisted Gravity Drainage Concept .....	3
Figure 2-2. Schematic of the Interaction between Rock Deformation, Fluid Flow and Temperature in a Deformable Reservoir .....	9
Figure 2-3. Schematic Showing Possible Increase in Horizontal Stresses in SAGD .....	12
Figure 4-1. Schematic of Fast-SAGD .....	16
Figure 4-2. Grid System .....	18
Figure 4-3. Steam Enthalpy .....	23
Figure 4-4. Comparison of Steam Chamber Sizes .....	23
Figure 4-5. Cumulative Production and SOR .....	24
Figure 4-6. Comparison for Cases 4 and 8 (extra steam) .....	25
Figure 4-7. Production History of the SAGD Producer in the Fast-SAGD Process .....	27
Figure 4-8. Temperature Profile @ 10 Years after 2nd Offset Well .....	28
Figure 4-9. Cumulative Oil and SOR Curves for Proposed Case .....	28
Figure 5-1. Schematic of the Decoupled Method .....	30
Figure 5-2. Three Zones and their Pore Pressure and Stress .....	31
Figure 5-3. Comparison of the Grid Systems .....	33
Figure 5-4. Geomechanical Model and Boundary Conditions .....	34
Figure 5-5. Element Locations Used in Describing Stress Path History within Reservoir .....	35
Figure 5-6. Stress Path in Thermal Recovery Process .....	36
Figure 5-7. Stress Path for 1st Element .....	38
Figure 5-8. Stress Path for 2nd Element .....	38
Figure 5-9. Stress Path for 3rd Element .....	39
Figure 5-10. Volume Strain Increment for 1st Element .....	39
Figure 5-11. Volume Strain Increment for 2nd Element .....	40
Figure 5-12. Failure Zone @ 10 Years (Case 8, $K_0=1.5$ ) .....	41
Figure 5-13. $\phi/\phi_0$ Ratio @ 10 Years .....	42
Figure 5-14. $k/k_0$ Ratio @ 10 Years .....	42
Figure A-1. Bitumen Viscosity .....	49

Figure A-2. Relative Permeability Curves for C1 .....	49
Figure A-3. Relative Permeability Curves for C2.....	50
Figure A-4. Relative Permeability Curves for C3 .....	50
Figure B-1. Grid System of 30 m Pay Zone Reservoir Model.....	55
Figure B-2. Grid System of 60 m Pay Zone Reservoir Model.....	55
Figure B-3. Comparison of Cumulative Oil and SOR (30m) .....	56
Figure B-4. Comparison of Cumulative Oil and SOR (60m) .....	56
Figure B-5. Pressure and Temperature Profiles (Constant Pressure; 30m).....	57
Figure B-6. Pressure and Temperature Profiles (Hydrostatic Pressure; 30m) .....	58
Figure B-7. Pressure and Temperature Profiles (Constant Pressure; 60m).....	59
Figure B-8. Pressure and Temperature Profiles (Hydrostatic Pressure; 60m) .....	60
Figure C-1. Pressure and Temperature Profiles for Case 1 .....	61
Figure C-2. Pressure and Temperature Profiles for Case 2.....	62
Figure C-3. Pressure and Temperature Profiles for Case 3 .....	63
Figure C-4. Pressure and Temperature Profiles for Case 4.....	64
Figure C-5. Pressure and Temperature Profiles for Case 5.....	65
Figure C-6. Pressure and Temperature Profiles for Case 6.....	66
Figure C-7. Pressure and Temperature Profiles for Case 7 .....	67
Figure C-8. Pressure and Temperature Profiles for Case 8.....	68
Figure C-9. Pressure and Temperature Profiles for Case 9.....	69
Figure C-10. Oil Saturation Profiles for Case 1 .....	70
Figure C-11. Oil Saturation Profiles for Case 2 .....	71
Figure C-12. Oil Saturation Profiles for Case 3 .....	72
Figure C-13. Oil Saturation Profiles for Case 4.....	73
Figure C-14. Oil Saturation Profiles for Case 5 .....	74
Figure C-15. Oil Saturation Profiles for Case 6 .....	75
Figure C-16. Oil Saturation Profiles for Case 7 .....	76
Figure C-17. Oil Saturation Profiles for Case 8 .....	77
Figure C-18. Oil Saturation Profiles for Case 9 .....	78
Figure C-19. Injection and Production Rate for Case 1 .....	79
Figure C-20. Injection and Production Rate for Case 2 .....	80

Figure C-21. Injection and Production Rate for Case 3 .....	81
Figure C-22. Injection and Production Rate for Case 4 .....	82
Figure C-23. Injection and Production Rate for Case 5 .....	83
Figure C-24. Injection and Production Rate for Case 6 .....	84
Figure C-25. Injection and Production Rate for Case 7 .....	85
Figure C-26. Injection and Production Rate for Case 8 .....	86
Figure C-27. Injection and Production Rate for Case 9 .....	87
Figure C-28. Bottom-hole Pressure of Wells for Case 1.....	88
Figure C-29. Bottom-hole Pressure of Wells for Case 2.....	89
Figure C-30. Bottom-hole Pressure of Wells for Case 3.....	90
Figure C-31. Bottom-hole Pressure of Wells for Case 4.....	91
Figure C-32. Bottom-hole Pressure of Wells for Case 5.....	92
Figure C-33. Bottom-hole Pressure of Wells for Case 6.....	93
Figure C-34. Bottom-hole Pressure of Wells for Case 7.....	94
Figure C-35. Bottom-hole Pressure of Wells for Case 8.....	95
Figure C-36. Bottom-hole Pressure of Wells for Case 9.....	96
Figure C-37. Cumulative Oil and SOR Curves for Cases 2 and 6.....	97
Figure C-38. Cumulative Oil and SOR Curves for Cases 3 and 7.....	97
Figure C-39. Cumulative Oil and SOR Curves for Cases 4 and 8.....	98
Figure C-40. Cumulative Oil and SOR Curves for Cases 5 and 9.....	98
Figure D-1. Principal Stresses.....	99
Figure D-2. Stress Variation with Depth.....	101
Figure D-3. Idealized Relation for Dilation Angle .....	102
Figure E-1. Stress Paths for Case 1 ( $K_0=1.5$ ).....	104
Figure E-2. Stress Paths for Case 1 ( $K_0=1.0$ ).....	105
Figure E-3. Stress Paths for Case 6 ( $K_0=1.5$ ).....	106
Figure E-4. Stress Paths for Case 6 ( $K_0=1.0$ ).....	107
Figure E-5. Stress Paths for Case 8 ( $K_0=1.5$ ).....	108
Figure E-6. Stress Paths for Case 8 ( $K_0=1.0$ ).....	109
Figure E-7. Volume Strain Increment for Case 1 ( $K_0=1.5$ ) .....	110
Figure E-8. Volume Strain Increment for Case 1 ( $K_0=1.0$ ) .....	111



Figure E-9. Volume Strain Increment for Case 6 ( $K_0=1.5$ ) .....	112
Figure E-10. Volume Strain Increment for Case 6 ( $K_0=1.0$ ) .....	113
Figure E-11. Volume Strain Increment for Case 8 ( $K_0=1.5$ ) .....	114
Figure E-12. Volume Strain Increment for Case 8 ( $K_0=1.0$ ) .....	115
Figure E-13. Failure Zone @ 10 Years for Case 6 ( $K_0=1.5$ ) .....	116
Figure E-14. Failure Zone @ 10 Years for Case 6 ( $K_0=1.0$ ) .....	116
Figure E-15. Failure Zone @ 10 Years for Case 8 ( $K_0=1.5$ ) .....	117
Figure E-16. Failure Zone @ 10 Years for Case 8 ( $K_0=1.0$ ) .....	117
Figure E-17. Ratio $\phi/\phi_0$ @ 10 Years for Case 1 ( $K_0=1.5$ ).....	118
Figure E-18. Ratio $k/k_0$ @ 10 Years for Case 1 ( $K_0=1.5$ ).....	118
Figure E-19. Ratio $\phi/\phi_0$ @ 10 Years for Case 1 ( $K_0=1.0$ ).....	119
Figure E-20. Ratio $k/k_0$ @ 10 Years for Case 1 ( $K_0=1.0$ ).....	119
Figure E-21. Ratio $\phi/\phi_0$ @ 10 Years for Case 6 ( $K_0=1.5$ ).....	120
Figure E-22. Ratio $k/k_0$ @ 10 Years for Case 6 ( $K_0=1.5$ ).....	120
Figure E-23. Ratio $\phi/\phi_0$ @ 10 Years for Case 6 ( $K_0=1.0$ ).....	121
Figure E-24. Ratio $k/k_0$ @ 10 Years for Case 6 ( $K_0=1.0$ ).....	121
Figure E-25. Ratio $\phi/\phi_0$ @ 10 Years for Case 8 ( $K_0=1.5$ ).....	122
Figure E-26. Ratio $k/k_0$ @ 10 Years for Case 8 ( $K_0=1.5$ ).....	122
Figure E-27. Ratio $\phi/\phi_0$ @ 10 Years for Case 8 ( $K_0=1.0$ ).....	123
Figure E-18. Ratio $k/k_0$ @ 10 Years for Case 8 ( $K_0=1.0$ ).....	123

## NOMENCLATURE

$g$	= acceleration due to gravity
$h$	= thickness
$K_0$	= initial stress ratio
$k$	= absolute permeability
$k_{row}$	= relative permeability of oil to water
$k_{rw}$	= relative permeability of water
$k_{rog}$	= relative permeability of oil to gas
$k_{rg}$	= relative permeability of gas
$m$	= dimensionless parameter (typically 3-4) which is determined by the viscosity - temperature characteristics of the oil
$p$	= pore pressure
$q$	= flow rate
$s$	= saturation
$T$	= temperature
$c$	= cohesion
$E$	= Young's Modulus
$f^s$	= yield function
$G$	= Shear Modulus

### *Subscript*

$h$	= horizontal
$o$	= oil
$t$	= tensile
$v$	= vertical
$0$	= initial
$x$	= x axis
$y$	= y axis
$z$	= z axis
$1$	= major

2 = intermediate

3 = minor

### *Superscript*

' = effective

### *Greek symbols*

$\alpha$  = thermal diffusivity of reservoir

$\phi$  = fractional porosity of reservoir

$\nu$  = kinematic viscosity

$\sigma$  = stress

$\gamma$  = density

$\psi$  = dilation angle

$\varepsilon_v$  = volume strain

### *Abbreviation*

AOSTRA = Alberta Oil Sands Technology and Research Authority

CSS = Cyclic Steam Stimulation

SAGD = Steam-Assisted Gravity Drainage

SOR = Steam Oil Ratio

UTF = Underground Test Facility

## 1.0 INTRODUCTION

Over the past two decades, the reserves of conventional crude oil have declined. Heavy and extra-heavy oil reserves will play a major role as their replacement. The efficient and economic recovery of heavy oil and bitumen from reservoirs in Canada, Venezuela, and elsewhere is a major technical challenge and task. A new recovery method – Steam Assisted Gravity Drainage (SAGD) – was developed by Butler et al<sup>(1)</sup>. In this process, a pair of horizontal wells is placed near the bottom of the oil sands pay zone, with the injector on the top. Steam is injected through the upper well. It condenses on the cold oil sands to heat the bitumen. Heated oil drains by gravity along the steam chamber down to the lower producer. The process was subsequently reduced to practice in the field at the Underground Test Facility (UTF)<sup>(2)</sup>, in the Athabasca Oil Sands in northern Alberta in 1987. Since then, there have been many other demonstration projects of the SAGD process in all of the three Alberta oil sands deposits and in the heavy oil deposits of Alberta and Saskatchewan.

Cyclic steam stimulation (CSS) has been applied in Venezuela, California, Indonesia and other heavy oil areas. CSS, as employed in Alberta, is different from those mentioned above. Injection of any fluid into the oil sands is problematic because of the very low mobility of the in situ bitumen. As a result, the injection pressure is increased to a level to part the formation. Especially in Cold Lake, injection pressures of 12 MPa have been reached, and the steam introduced into the formation at rates as high as about 200 m<sup>3</sup>/day. CSS is now a proven commercial process in Cold Lake.

A variation of SAGD, called Fast-SAGD, has been proposed<sup>(3)</sup>. Simply, Fast-SAGD is a combination of SAGD and CSS. After the SAGD process has been developed, a single horizontal well, called the offset well, located 50 m away from the SAGD well pair, is cyclically operated to propagate the steaming process down the reservoir. Simulation shows that Fast-SAGD is a process with relatively high productivity and low operating pressure.

The purpose of this research is to further the understanding of the proposed Fast-SAGD process and to make improvements to numerical models to provide more accurate prediction for these types of steam-based processes. Geomechanical mechanisms are studied for this process, especially during the phases where the oil sands is loaded and unloaded cyclically. The model is then used to simulate and determine the causes of the synergy between the two processes of SAGD and CSS.

## 2.0 REVIEW OF LITERATURE

### 2.1 SAGD and Its Variations

Steam Assisted Gravity Drainage (SAGD) was introduced by Butler et al.<sup>(1)</sup>. This concept is shown in Figure 2-1. In this process, horizontal well pairs are used for SAGD, since gravity does not provide an adequate drive to move heated bitumen to a conventional vertical or deviated well at an economic rate. Two horizontal wells, an injector above a producer, are drilled in the lower part of a formation. Both wells and the reservoir between the two wells are first heated by means of steam circulation between the wells. When communication is established between the two wells, steam injection is continued in the upper well, creating a “steam chamber”, which rises above the injector, in the reservoir. Meanwhile, bitumen and condensate drain by gravity along the sides of the steam chamber to the lower horizontal well. In order to keep live steam in the reservoir, a steam trap control mechanism is devised to operate the producer at a temperature a few degrees lower than the steam injection temperature, thereby allowing only hot bitumen and condensate to be produced.

Mechanism:

- Steam condenses at interface
- Oil and condensate drain to well at bottom
- Flow is caused by gravity
- Chamber grows upwards and sideways

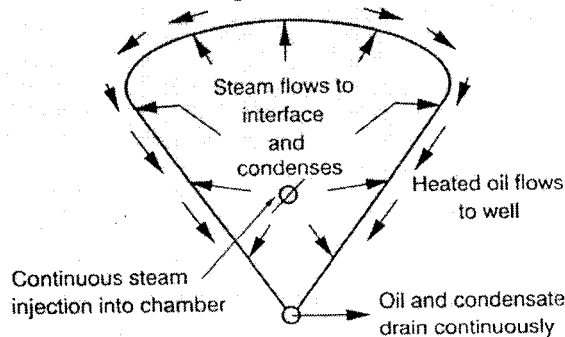


Figure 2-1. Steam-Assisted Gravity Drainage Concept (after Butler et al.<sup>(1)</sup>)

The general expression for the rate of oil production,  $q_o$ , is:

$$q_o = \sqrt{\frac{2\phi\Delta s_o k g \alpha h}{m v_s}} \quad (2-1)$$

This equation indicates that the rate of drainage is a function of the drainage height ( $h$ ), reservoir permeability ( $k$ ) and kinematic viscosity ( $v_s$ ) of the oil at the steam temperature.

Butler and Stephens<sup>(4)</sup> modified the theory using the TANDRAIN assumption (the interface curve of flow is replaced by tangents drawn from the well) to reduce the rate of drainage of oil. The constant 2 in the Equation (2-1) is replaced by 1.5. Experimental data showed the equation to be in good agreement with the theory. A variation called LINDRAIN<sup>(5)</sup> was also developed. In this variation, it is assumed that the interface is straight, right up to the top of the reservoir. With this assumption, the constant of Equation (2-1) is replaced by 1.3.

In all the above variations of Equation (2-1), it was assumed that the temperature distribution ahead of the advancing front was steady state. A new approach that avoids the steady state heat assumption was described by Butler<sup>(6)</sup>. The interface is divided into small elements, and the heat storage ahead of each element is calculated at successive time steps using an approximate differential equation. For each time step, the flow of oil behind the element is calculated and then the movement of the interface is obtained from material balance considerations.

Scott Ferguson and Butler<sup>(7)</sup> developed a new calculation procedure, which allowed the prediction of the effects of varying steam injection rates, pressures, and the duration of injection cycles on heavy oil recovery by gravity drainage. Previous models assumed maintenance of a constant steam chamber pressure and temperature. The model uses an approximate mathematical method to obtain the heat transfer to the receding oil bank and to the overburden. It is shown that considerable increases in cumulative oil-steam ratios are to be gained by stopping steam injection before the recoverable reserves in a pattern

have been produced completely. It is also indicated that higher injection pressures and rates accelerate production and do not reduce the cumulative oil-steam ratio significantly. Little benefit results from multiple injection cycles within the same production pattern.

Laboratory studies on the SAGD process were conducted by Chung and Butler<sup>(8)</sup> to investigate the effect of steam injection on the formation of emulsions in the SAGD process. They observed in their experiments that there is a meandering and counter-current flow of steam and heated heavy oil within the steam chamber. The pressure of the injected steam has little effect on the emulsified water content of the produced fluid.

Producing conventional heavy oil by SAGD from reservoirs containing bottom water is one of the most challenging problems. Experiments performed by Sugianto and Butler<sup>(9)</sup>, using a scaled, two-dimensional reservoir model, showed that the process may produce heavy oil economically and reduce the water production by operating the production wells at a pressure close to that of the aquifer. The thickness of the bottom water zone and the well configurations employed had a significant effect on the cumulative oil recovery.

Yang and Butler<sup>(10)</sup> developed experiments to simulate heterogeneous reservoirs. These included reservoirs with thin shale layers or with horizontal layers of different permeability. The experimental results showed that a short horizontal barrier had not too much effect on the general performance. A long horizontal barrier decreased the production rate but not nearly as much as expected in some configurations. It was found that production was faster when a higher permeability layer was located above a lower permeability layer than when these conditions were reversed.

Sawhney et al.<sup>(11)</sup> focused on the vertical injection wells for SAGD. The reason for using vertical injection wells is that they may be available from previous field development. However, the main problem of using vertical wells is that the steam chamber has to grow in the direction of the axis of the horizontal well as well as transversely. As a result, the effective length of the production well could be less than its physical length, at least until



the operation becomes mature. Experiments were carried out using a three-dimensional, scaled, cylindrical, physical model with central vertical injection wells in order to investigate this impact. A theoretical model to predict the growth of the steam chamber around the vertical injection well was presented. This study shows that a horizontal injector rather than vertical injectors will be more economical for SAGD.

Based on Chung's experimental data from the physical model, a two-dimensional, three-phase (bitumen, water and steam) and two-component (water and bitumen) black oil numerical model for the SAGD process was developed by Chow and Butler<sup>(12)</sup> using the CMG "STARS" thermal simulator. Both the "Spreading Steam Chamber" and the "Rising Steam Chamber" processes were observed in the simulation results. The simulation results for cumulative oil production, recovery percentage and temperature profiles matched the measured data well.

Recently, interest has appeared in using a single dual-stream horizontal well in SAGD applications. In this technology, steam is injected into the tubing and fluid is produced through the annulus. Oballa and Buchanan<sup>(13)</sup> examined this idea of a single horizontal well by using new simulation technology (hybrid grid surrounding a discretized wellbore). They concluded that the drainage process is dominated by varying conditions in the wellbore, and the energy efficiency is very poor when the drainage process is applied in heavy oil or bitumen reservoirs with steam injection. Therefore, it may be very difficult to operate such a well, and more study is needed to improve this strategy.

Shen<sup>(14)</sup> advanced numerical investigation of the SAGD process using a single horizontal well. His study showed that the undulation of a horizontal wellbore has the potential to overcome the capillary pressure constraint on steam entering the formation. However, its effectiveness is very limited and this approach is unlikely to be an economic solution in field applications. Gas/liquid top-to-bottom co-current circulation is the dominant fluid exchange pattern around the wellbore when using the single-well configuration. The oil rate of single-well SAGD is relatively low in comparison with the dual-well SAGD. This comes about because of the different fluid exchange patterns in the two processes.

A modified process named SAGD-ISSLW was introduced by Sasaki et al<sup>(15)</sup>. Instead of continuous production from the lower producer, it was intermittently stimulated by steam injection, in conjunction with steam injection in the upper injector. Using this method, the time to generate a near breakthrough condition between two wells was shortened, and oil production was enhanced at the rising chamber stage as compared with that of the conventional SAGD process.

A new process called Fast-SAGD, proposed by Polikar et al.<sup>(3)</sup>, was simulated numerically. In this process, after starting the first pair of horizontal wells with the SAGD process, a set of equidistant single horizontal wells is used to propagate the steaming process down the reservoir. These single horizontal wells, called offset wells, are placed parallel to, but 50 metres away from the initial SAGD pair and from each other, and have the same length and are equidepth with the SAGD producer at the base of the pay zone. Once the steam chamber has developed fully and reached the top of the pay zone, cyclic steam injection is started in the first offset well. The offset wells are operated both as injectors and producers. Steam injection takes place at a pressure and flow rate higher than those used in the SAGD operation, but they do not exceed the fracture conditions of the formation. The purpose of injecting steam into the offset well is to accelerate the growth and propagation of the steam chamber without disturbing the sand matrix. Also, during the production phase, the steam trap control mechanism is used for the offset well, whether or not a soak period existed after the steam injection. The results obtained are very encouraging: markedly increased rate of production of bitumen and reduced steam-oil ratio.

## **2.2 Cyclic Steam Stimulation**

Cyclic steam stimulation (CSS) was first utilized in Western Venezuela in 1959 and developed in the field. In Alberta, injection of any fluid into oil sands is problematic because of the very low mobility of the in situ bitumen. As a result, the injection pressure is increased to a level sufficient to part the formation.

Denbina et al.<sup>(16)</sup> developed a two-dimensional, radial, single well numerical model to investigate the drive mechanisms of the CSS operation in Cold Lake. They concluded that formation compaction, solution gas and fluid expansion were the main drive mechanisms. Gravity drainage contributed very little of the oil produced in the first two cycles, but the amount of aid due to gravity drainage may increase significantly in subsequent cycles.

A reservoir deformation model was developed by Beattie et al.<sup>(17)</sup> to represent appropriately the oil sands dilation and re-compaction occurring during CSS at Cold Lake. The model can reasonably match injection and production pressures and flowback times. The relative permeability hysteresis model presented provides a simple and effective means of modeling history-dependent behavior. However, the deformation was dominated by pore pressure instead of stress.

A multiwell CSS process was simulated by Vittoratos et al.<sup>(18)</sup>, to understand the interwell communication observed in the Cold Lake area. Simulations showed that the impact of steaming strategy on bitumen production was not significant until later cycles.

Walters et al.<sup>(19)</sup> studied the poroelastic effects of cyclic steam stimulation in the Cold Lake deposit. A coupled geomechanical and reservoir model was developed to understand the aquifer response. A coupled modeling method could help to better understand the geomechanical response and guide reservoir management.

### **2.3 Coupled Reservoir/Geomechanics Simulation**

Reservoir simulation technology is already highly developed in handling multiphase flow and heat transfer in porous media using the finite difference method. Most current simulators use pressure-dependent compressibility and permeability to approximate geomechanical effects, which is not accurate. Stress models are also highly developed, most of which use the finite element method to simulate stress and strain. Some models capture certain features of multiphase flow, but they are very simplistic as compared to reservoir simulators. Fracture propagation models deal mostly with problems in

impermeable rocks, and have been adapted to porous media in the petroleum industry. But most of them simplify the fluid flow and use two-dimensional analytical approaches. Thus, none of the above approaches is satisfactory for problems where strong coupling of fluid mechanics and geomechanics exists, especially in in-situ bitumen recovery processes.

In a fluid flow/stress problem, pressure and temperature changes, due to multiphase flow in porous media, cause strain and stress changes in the formation. Conversely, the geomechanical response affects the pore volume and stress-sensitive absolute permeability and relative permeability, which dominate the fluid flow in porous media. Introducing coupling between stress and flow is a way to communicate the response from both sides. The interaction between fluid flow and in-situ stress is schematically shown in Figure 2-2. Normally, two main components of coupling, pore volume and flow properties (absolute and relative permeability), are considered. The degree of coupling may affect the accuracy of the solution as well as the computational efficiency.

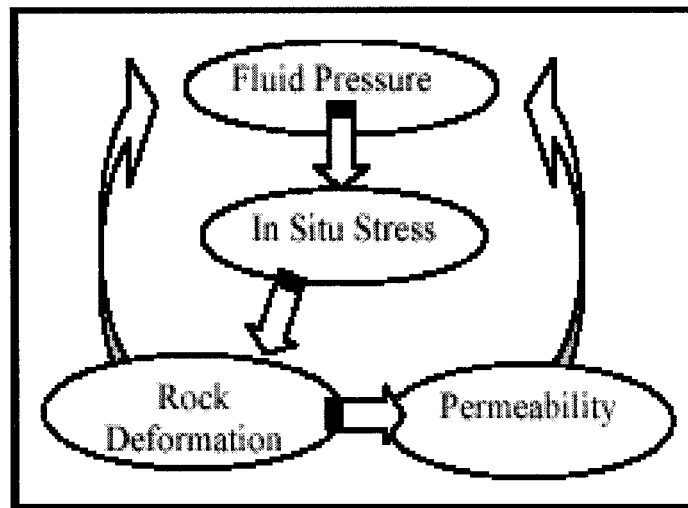


**Figure 2-2. Schematic of the Interaction between Rock Deformation, Fluid Flow and Temperature in a Deformable Reservoir**  
(after Gutierrez et al.<sup>(20)</sup>)

According to Settari and Walters<sup>(21)</sup>, four approaches are used to couple these two models. The “Uncoupled” method introduces a reservoir simulation solution to a stress model that computes a transient stress solution. In the “Explicitly Coupled” method, the stress-induced property changes are fed back by lagging the coupling terms one time step behind. In the “Iteratively Coupled” method, a repeated solution of the flow and stress equations is computed until convergence during each time step. The “Explicitly Coupled” method is a special case of the “Iteratively Coupled” method in which only one iteration per time step is performed. The “Fully Coupled” approach integrates stress and fluid flow as a full system and solves the stress and flow equations simultaneously. However, a large development effort is still needed to achieve good results with this method.

Volumetric changes of porous rock, which depend on elastic parameters, were first described by Geertsma<sup>(22)</sup>. Three types of compressibility (rock matrix compressibility, rock bulk compressibility and pore compressibility) were discussed in detail. Finally, relationships were developed, which give the compressibility of both pore and bulk volume as a function of the elastic and viscous deformation constants of rock materials for an isotropic and homogeneous porous medium.

A coupled reservoir and geomechanical model was first introduced by Settari<sup>(23)</sup> to simulate the thermal flow and soil mechanics in unconsolidated porous media. A one-dimensional nonlinear stress equation was partially decoupled externally with a one-dimensional two-phase flow equation. The deformation change by pressure and stress is described by the relative volume of the element. Absolute permeability is a function of the minimum effective stress and sand failure. The relative permeability is not changed in this model. An example showed a new feature of reservoir mechanics in reservoirs where strong coupling of fluid-flow and soil-mechanics exists.

A three dimensional finite element linear elastic stress model was applied by Settari and Mourits<sup>(24)</sup> in the coupled model to simulate bitumen recovery in unconsolidated oil sands. By using the partially coupled method, a reservoir thermal simulator was iterated to convergence after coupled components were fed back from a stress model at each time

step. Effective porosity, as a function of pressure, temperature and mean stress, is matched to the conventional reservoir engineering “porosity” concept. The absolute permeability is calculated explicitly at each time step as a function of effective stress. Changes in relative permeability were not considered in this model. However, the results demonstrated that this method is very effective. Later Settari and Mourits<sup>(25)</sup> extended this method to a nonlinear elastic stress model.

A subsequent study by Fung and Buchanan<sup>(26)</sup> set up an iteratively coupled model. A new stress model, an elasto-plastic deformation model, is coupled with STARS, a thermal multiphase flow reservoir simulation model. In this coupling, at the end of each time step, temperature and pressure changes were introduced into the stress model to compute the distribution of stress and strain corresponding to the reservoir grid. The pore volume change was calculated directly from the stress model and fed back through a conventional reservoir engineering concept - rock compressibility - in a way which is different than that of Settari and Mourits<sup>(25)</sup>. The relative permeability was changed in the shear zone due to substantial dilation by defining an additional set of relative permeability tables. However, neglect of absolute permeability change in the reservoir is a shortcoming of this model.

Meanwhile, a lot of effort has been expended to set up a fully coupled fluid-flow/geomechanics model. One of the fully coupled models was developed by Fung<sup>(27)</sup> using the finite element procedure. However, it is restricted to isothermal flow, two immiscible fluids, and a hyperbolic dilatant stress-strain case.

Another fully coupled thermal-fluid flow/stress mathematics model was attempted by Tortike and Farouq Ali<sup>(28,29)</sup>. However, due to computational convergence problems, more study is needed. Therefore, these authors preferred the iteratively coupled method between the thermal-fluid, three-phase, three-dimensional finite difference flow model and a plastic stress model. They showed examples of the importance of coupling in order to better understand the mechanics of oil recovery in unconsolidated oil sands.

## 2.4 Geomechanical Mechanism in SAGD

The impact of geomechanical response in SAGD was realized during AOSTRA's Underground Test Facility SAGD operation. Chalaturnyk and Scott<sup>(30)</sup> discuss the principal geomechanical mechanisms which appeared in SAGD and concluded that permeability increases resulted from dilation ahead of the steam chamber. Also, several factors that affected the geomechanical response were discussed, such as reservoir depth, initial stress ratio, and well pair spacing.

To illustrate how geomechanics impacts the SAGD process, the formation properties of the SAGD process were investigated by Chalaturnyk and Scott<sup>(32)</sup> both in theory and in experiments, and compared with field measured formation response. Ahead of the steam chamber, increases in absolute permeability of 30% to 50% may occur (Figure 2-3).

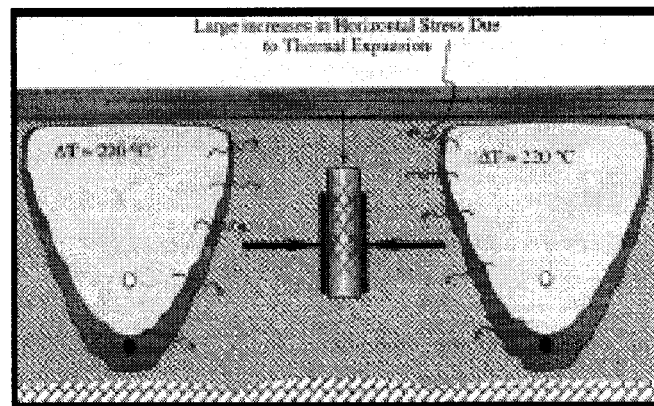


**Figure 2-3. Schematic Showing Possible Increase in Horizontal Stresses in SAGD  
(after Chalaturnyk<sup>(31)</sup>)**

In the numerical simulation of the SAGD process at the Hangingstone pilot, Ito and Suzuki<sup>(33)</sup> first discussed the role of geomechanical effects. Their simulator allows one to change porosity, permeability and relative permeability as a function of pressure only to reflect the shear failure. The results indicated that the geomechanical response of the reservoir changed the steam chamber shape and increased the oil recovery. They proved that geomechanics play an important role in SAGD.

Chalaturnyk and Li<sup>(34)</sup> discussed in more detail the sensitivity of the factors which affect the geomechanical response. Injection pressure and temperature, reservoir depth, and initial stress state showed a more complicated geomechanical response for the SAGD process.



### 3.0 STATEMENT OF THE PROBLEM

The purpose of this research is to develop further the Fast-SAGD process<sup>(35)</sup> and to make improvements to numerical models so as to provide more accurate predictions for these types of steam-based processes. Initial numerical work has indicated the advantages of this process by showing increased heavy oil production and decreased steam-oil ratio (less steam injection, hence less energy input into the system) with the addition of only one offset horizontal well and the manner in which it is operated.

Fast-SAGD is operated in a combined SAGD-CSS process, in which the CSS process is applied to the offset well. Although the previous reservoir simulation work<sup>(3)</sup> has shown that the Fast-SAGD process requires less steam and less wells for the same production levels as SAGD, much work remains to be done to understand fully the recovery mechanism involved in this process, especially in geomechanical terms.

Fully coupled thermal-stress-fluid-flow models are complex and beyond the scope of this study. Consequently, a decoupled geomechanical simulation will be performed with the thermal reservoir simulation. Initial in-situ effective stress, offset well injection pressures and temperatures, and offset well injection start-up time are considered in the simulations. Stress response is studied to analyze pore volume and permeability changes in the Fast-SAGD process. Finally the strategy for combining the SAGD and CSS processes is discussed in order to produce heavy oil effectively.

Fast-SAGD is currently the only process that can be made to work with multilateral horizontal wells. After Fast-SAGD is initiated, an operating strategy for multilateral offset well needs to be devised.

## **4.0 NUMERICAL INVESTIGATION OF FAST-SAGD**

### **4.1 Background of the Thermal Recovery Process**

Cyclic steam stimulation was first used in Western Venezuela in 1959 and developed in the field. In Alberta, injection of any fluid in oil sands is problematic because of the very low mobility of the in-situ bitumen. As a result, the injection pressure is increased to a level high enough to part the formation. In Cold Lake, this is achieved with an injection pressure of 12 MPa, and the steam is introduced into the formation at rates of about 200 m<sup>3</sup>/day<sup>(36)</sup>. However, the major problem with CSS, as it is practiced in Alberta, is that typically 15 to 20% of the bitumen is recovered from the resource, even in a pattern comprised of closely spaced vertical wells. For a reservoir with a gas cap or bottom water, parting of the formation probably results in the leakage of more heat into the over/under-burden by heat convection and thereby decreases the heat efficiency.

The Steam-Assisted Gravity Drainage process was developed in the 1980s. Currently several commercial projects are operated in Alberta. In this process, steam is injected continuously into a horizontal well, located parallel to and above a horizontal production well, located at the base of the reservoir. Heated oil drains by gravity and the steam fills in the pore volume vacated by the hot oil. It has been reported that the SAGD process is attractive, and results in high recovery and a low steam-oil ratio (SOR)<sup>(37)</sup>. However, a challenge for operating the SAGD process efficiently is promoting the lateral expansion of the steam chamber<sup>(38)</sup>.

A new process, called Fast-SAGD, which combines SAGD and CSS, was recently proposed<sup>(35)</sup>. Reservoir simulation has shown that Fast-SAGD is a process with relatively high productivity and low operating pressure.

### **4.2 Fast-SAGD Process**

Fast-SAGD is a combination using both the SAGD and CSS processes, as can be seen in Figure 4-1. After the SAGD process is implemented, steam is injected into a single horizontal well, called the offset well, 50 metres away from the SAGD well pair in a

cyclic mode to help propagate the steam chamber expansion down the reservoir. The first cycle lasts one year, consisting of nine months of steam injection followed by three months of production. In the second cycle, after six months of steam injection, the offset well is converted to a production well for the remainder of the project life. At this time, additional steam is injected into the SAGD injector to maintain and expand the huge steam chamber that is generated by the offset well. A two-week soak period is used in the cyclic steaming of the offset well. It should be noted that steam-trap control is used for all the production wells to avoid producing live steam.

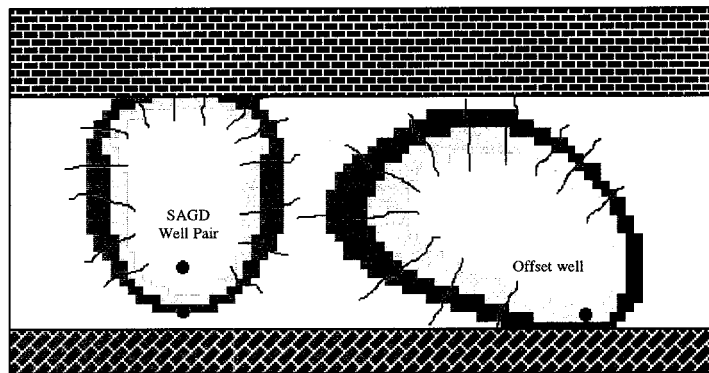


**Figure 4-1. Schematic of Fast-SAGD**

In this section, the strategy of operating the Fast-SAGD process is investigated in more detail, based on previous work, and a suitable start-up time for the offset well is discussed based on the relationship between the vertical and lateral heat communication in the reservoir.

### **4.3 Numerical Model**

STARS<sup>(39)</sup>, a computer software model released by the Computer Modeling Group, is an advanced thermal reservoir simulator useful for simulating thermal recovery processes including steam injection in any form. It has been reported that SAGD process simulations<sup>(3,12,40,41,42,43)</sup> have been conducted successfully. In the simulations conducted here, STARS was used in all the runs. The reservoir model used for this study is based on the Clearwater formation of the Cold Lake deposits.

#### **4.3.1 Geometry and Gridding**

A two-dimensional (x-z) model was developed. The model considered half of the reservoir area, which has a width (x direction) of 200 m and a thickness (z direction) of 38 m. The length (y direction) was selected to be 900 m. It is believed that the two-dimensional model provides an adequate representation of the Fast-SAGD process, while allowing fine gridding in both the x and z directions. Depth of the formation is approximately 400 m.

Small gridding of the order of one to two metres in the x and z directions was selected to study the Fast-SAGD process. One-metre grid blocks were used in the z direction. In the x direction, the first 101 blocks of 1-m length were used around the SAGD well pair and the offset well. The next 50 blocks had a length of 2 metres. In the y direction, there was only one block of 900 metres, which is the length of the horizontal wells. Figure 4-2 shows the grid system used in the simulations.

#### **4.3.2 Reservoir Properties**

The Clearwater formation of the Cold Lake deposit is the basis for the reservoir model. Initial reservoir conditions and petrophysical properties are shown in Table 4-1. The formation can be divided into three zones with varying properties. C1 is the lowest zone and consists of interbedded sand and clay. C2, the middle zone, is the cleanest (least clay), and C3, the upper zone, is the most variable. The thickness of the C1, C2 and C3 is approximately 12, 21 and 5 metres, respectively. Table 4-2 shows the pay zone properties in each layer.

Three components, water, bitumen, and methane, were chosen in this numerical simulation model. Initially, methane is dissolved in the bitumen. Fluid properties are defined in order to describe their behavior with respect to pressure and temperature correctly. Bitumen and light oil viscosity versus temperature are given in Appendix A. Relative permeability curves for each zone are also included in Appendix A. The gas-bitumen and water-bitumen capillary pressures were neglected in this study.

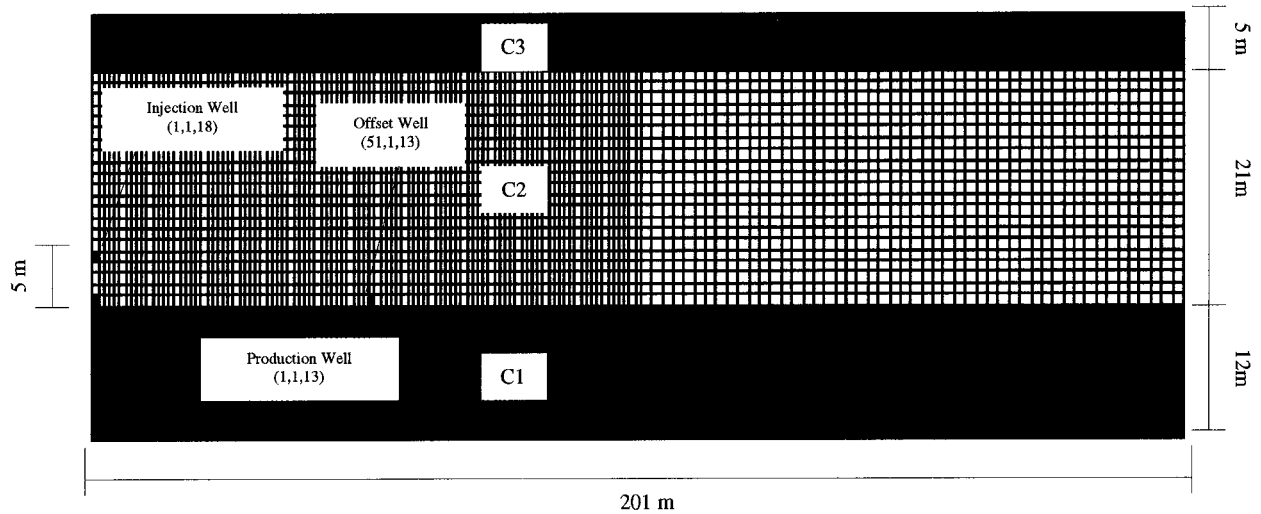


**Figure 4-2. Grid System**

**Table 4-1. Reservoir Properties**

Reservoir Pressure	3100 kPa
Reservoir Temperature	18 °C
Reference Pressure	101.3 kPa
Reference Temperature	20 °C
Capillary Pressure	0 kPa
CH <sub>4</sub>	11 mole%
Formation Heat Capacity	2350 kJ/m <sup>3</sup> -°K
Rock Compressibility	$9.6 \times 10^{-6}$ kPa <sup>-1</sup>
Rock Thermal Conductivity	$6.6 \times 10^5$ J/m-d-°C
Oil Thermal Conductivity	$1.15 \times 10^4$ J/m-d-°C
Water Thermal Conductivity	$5.35 \times 10^4$ J/m-d-°C
Gas Thermal Conductivity	$1.4 \times 10^2$ J/m-d-°C
Dead Oil Viscosity @ 20°C	21,500 cp

**Table 4-2. Properties of the Three Zones**

Zone	C1	C2	C3
h (m)	12	21	5
$\phi$ (%)	0.32	0.35	0.30
$k_v$ (D)	0.20	1.25	0.30
$k_h$ (D)	1.00	2.50	1.50
$S_w$ (%)	0.60	0.30	0.45
$S_o$ (%)	0.40	0.70	0.55

#### 4.3.3 Well Position, Constraint and Boundary Conditions

The C1 is highly saturated with water ( $S_w=60\%$ ). Therefore, Fast-SAGD is only being applied in the two best zones – C2 and C3. The SAGD wells were located at the base of the C2 pay zone instead of the C1, with the injector placed 5 m above the producer. The offset well was 50 m away from the SAGD well pair and at the same depth as that of the SAGD producer. The well positions are shown in Figure 4-2.

During the initial pre-heat stage to establish communication between the SAGD injector and the producer, the formation is stimulated by circulating steam through both wells for 52 days. For all the simulations, the length of the horizontal wells is 900 m. All simulations were performed for a ten-year period. All production wells were operated by steam trap control at the reservoir pressure. The rates for the SAGD injection were selected as 400 to 800 m<sup>3</sup>/d of cold water equivalent (CWE). The injection pressure was set 10 kPa higher than the production pressure. The injection rate for the offset well was set at the maximum of 800 m<sup>3</sup>/d.

A symmetry boundary condition is used for the left side, and a no flow boundary for the right side. At both the upper and lower boundaries, there is no fluid flow but only heat conduction. A semi-analytical model is used for heat transfer to or from the over- or under-burden of infinite extent<sup>(39)</sup>.

#### **4.3.4 Initial Pressure**

In thermal simulation, constant pressure is normally assumed in the reservoir. However, when the simulation is run, the reservoir pore pressure would reach the equilibrium hydrostatic pressure due to gravity at an early stage of the process. SAGD is a gentle recovery process in which the bitumen drains by gravity. It is the hydrostatic pressure distribution in the reservoir that affects the SAGD operating pressure strategy and its simulation performance, especially in those reservoirs where a thick pay zone, gas cap or bottom water exists. A difference was observed between the hydrostatic pressure case and the constant pressure case. The numerical simulation results have indicated that, in order to predict the production correctly, the hydrostatic pressure naturally occurring in the reservoir should be considered in the thermal numerical simulations. Otherwise, the actual oil production is over-predicted when a constant pressure is considered in the reservoir. This difference becomes larger as the pay zone thickness increases. The detailed results and a discussion comparing these two pressure cases are given in Appendix B. In the reservoir simulation conducted here, hydrostatic pressure was set before the model was run.

#### **4.3.5 Conditions of Numerical Runs**

The first numerical simulation was a baseline SAGD case. Based on Cold Lake field pilot tests, steam injection into the SAGD injector was selected as 400 m<sup>3</sup>/d CWE at a pressure of 3110 kPa, 10 kPa higher than the production pressure. The production well was operated at the reservoir pressure of 3100 kPa and a steam trap control was set.

For the Fast-SAGD cases, one parameter that was investigated was the start-up time of the steaming from the offset well. The start-up time of the offset well was set at 1, 2, 3, and 4 years after that of the SAGD well pair operation. In the offset well, steam was injected at a maximum rate of 800 m<sup>3</sup>/d CWE and a pressure of 8000 kPa, as indicated in Table 4-3. The first steam cycle lasted one year, with nine months of steam injection followed by three months of production. The second cycle consisted of six months of steam injection, followed by production for the remainder of the simulation. A two-week soak period was considered between the injection and production cycles. It should be

noted that steam trap control was also used for the offset well during the periods of production. The control was set at the same pressure (3100 kPa) as that used for the SAGD producer. In this way, steam was not blown off, after steam injection at the offset well, as would happen in the CSS process, but rather it stayed in the formation to aid in the propagation of the initial steam chest created by the SAGD process.

In addition to the SAGD baseline simulation (Case 1), Cases 2 to 5 (400 m<sup>3</sup>/d for SAGD and 800 m<sup>3</sup>/d for the offset well starting after 1, 2, 3 and 4 years) and Cases 6 to 9 (same as 2 to 5, extra steam for SAGD after two cycles) are presented (Table 4-3).

**Table 4-3. Fast-SAGD Simulation Cases**

Case	SAGD Well Pair				Offset Well			
	Max. Injection Pressure Set (kPa)	Max. Injection Rate Set (m <sup>3</sup> /d)	Extra Steam Set After CSS (m <sup>3</sup> /d)	Min. production Pressure Set (kPa)	Max. Injection Pressure Set (kPa)	Max. Injection Rate Set (m <sup>3</sup> /d)	Start-up Time (year)	Min. Production Pressure Set (kPa)
1	3110	400	N/A	3100	N/A	N/A	N/A	N/A
2			0		8000	800	1	3100
3			0		8000	800	2	
4			0		8000	800	3	
5			0		8000	800	4	
6			400		8000	800	1	
7			400		8000	800	2	
8			400		8000	800	3	
9			400		8000	800	4	



## **4.4 Reservoir Simulation Results and Discussion**

### **4.4.1 Operating Pressure for the SAGD Well Pair**

The total enthalpy of wet steam is the sum of the latent heat of evaporation and the sensible heat of hot water. As the steam quality drops from 100% to 0%, the latent heat is released completely. As is shown in Figure 4-3, the latent heat of the steam increases while the saturation pressure decreases. The latent heat of steam comprises most of the heat that is transferred to the formation in the SAGD process. The amount of latent heat transported per unit mass of saturated steam is highest at low pressures and least at high pressures. However, at the low pressures, the volume of steam is highest, and the rate at which it can be transmitted to a condensing zone and the concomitant reduction of viscosity of the bitumen are least. Therefore, the operating pressure is of primary concern for SAGD schemes, and in practice the optimal pressure is fairly high.

Edmunds and Chhina<sup>(44)</sup> showed that low-pressure SAGD results in low productivity, and in a low cumulative SOR. Conversely, high-pressure SAGD brings high productivity and a high cumulative SOR. It appears evident that the economics of any SAGD project are highly sensitive to the cost of oil and the operating pressure. In field operations, sufficient pressure is required in order to enable the gas lift process to raise the bitumen and steam condensate to the surface. Therefore, in our study, the injection pressure was set 10 kPa higher than the reservoir pressure of 3100 kPa. As discussed below, the main operating pressure in the reservoir remains low despite short periods of high pressure during the cyclic injection of steam. Therefore, Fast-SAGD still stays in a relatively low cumulative SOR regime.

### **4.4.2 Comparison of Simulation Results between SAGD and Fast-SAGD**

Owing to the CSS operation at the offset well, the steam chamber for the Fast-SAGD process at the end of ten years is much larger than that of the traditional SAGD (Figure 4-4). Fast-SAGD results in a high productivity with 94% incremental cumulative production in Case 8 (best case) over the base case. All the Fast-SAGD cases produced much more bitumen, with a constant cumulative SOR, except for case 4 and 5, as shown in Table 4-4 and Figure 4-5.

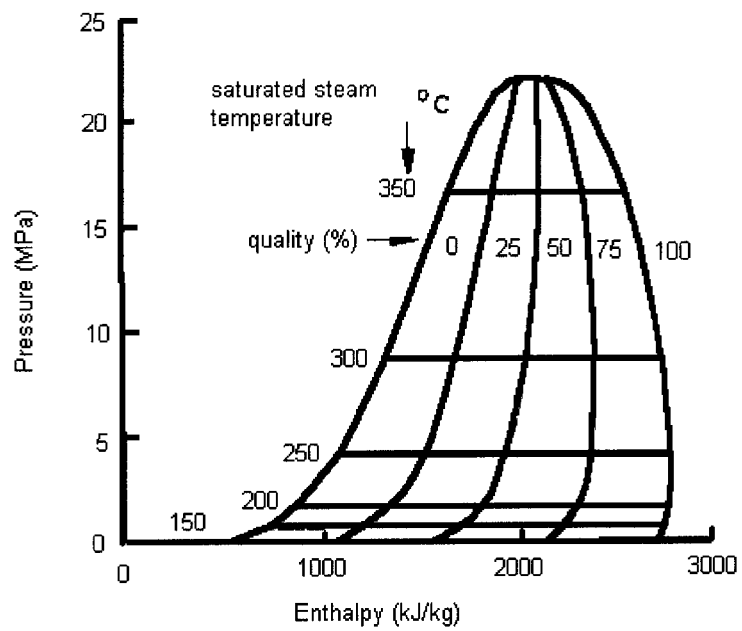


**Figure 4-3. Steam Enthalpy (after Butler<sup>(5)</sup>)**

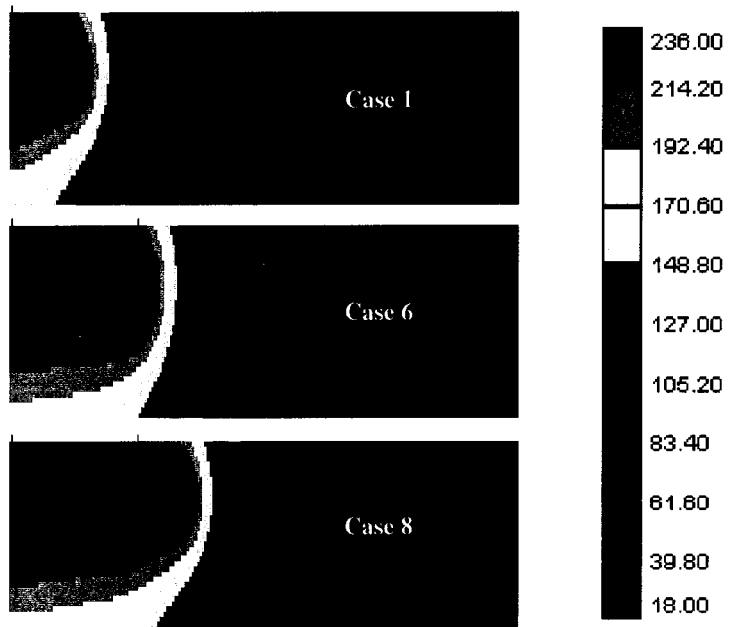


**Figure 4-4. Comparison of Steam Chamber Sizes**

**Table 4-4. Simulation Results of Fast-SAGD**

Case	1	2	3	4	5	6	7	8	9
Cum. Bitumen ( $10^6\text{m}^3$ )	0.195	0.286	0.292	0.239	0.245	0.346	0.355	0.379	0.369
Cum. Inj. Water ( $10^6\text{m}^3$ )	0.603	0.823	0.884	0.921	0.931	0.964	1.016	1.128	1.097
Cum. SOR	3.10	2.88	3.03	3.85	3.80	2.79	2.86	2.98	2.97
Cum. Bitumen from SAGD Well ( $10^6\text{m}^3$ )	0.195	0.170	0.200	0.205	0.215	0.166	0.202	0.226	0.236
Cum. Bitumen from Offset Well ( $10^6\text{m}^3$ )	N/A	0.116	0.092	0.034	0.030	0.180	0.153	0.153	0.133

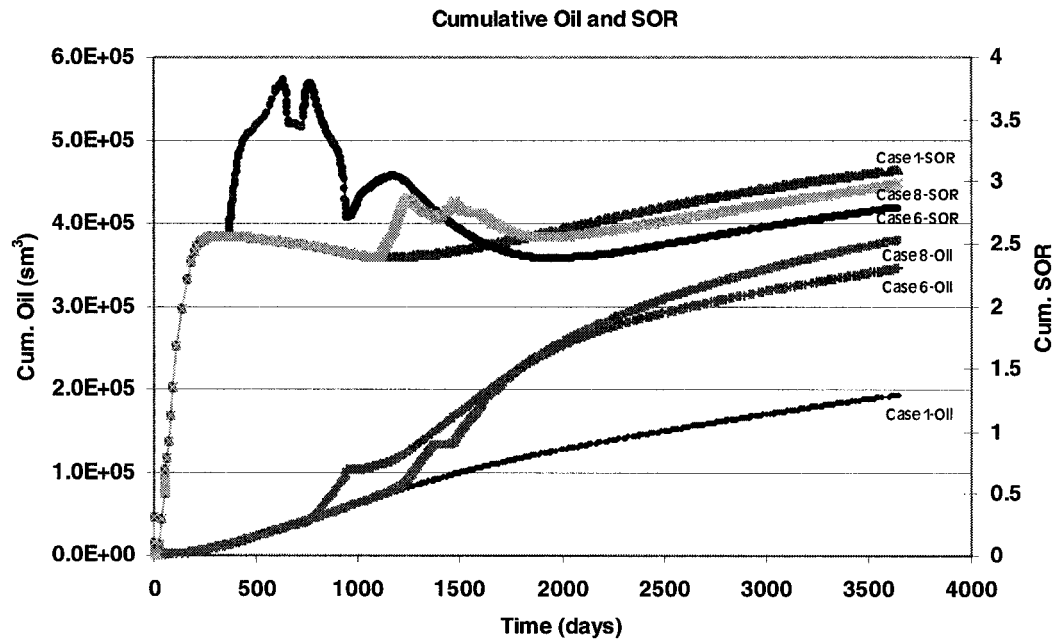


**Figure 4-5. Cumulative Production and SOR**

#### 4.4.3 Extra Steam Injection into the SAGD Injector

It can be seen, from the Table 4-4 and Figure 4-6, that extra steam injection into the SAGD injector generates more recovery after two cycle of steaming at the offset well. The cumulative production in Cases 2 to 5 is less than that in Cases 6 to 9. Since the cyclic process results in greater communication between the SAGD well pair and the offset well, a huge steam chamber is established in a short time. In order to maintain and expand this huge chamber, extra steam is injected into the SAGD injector. Otherwise the steam chamber would collapse and productivity would drop off too.

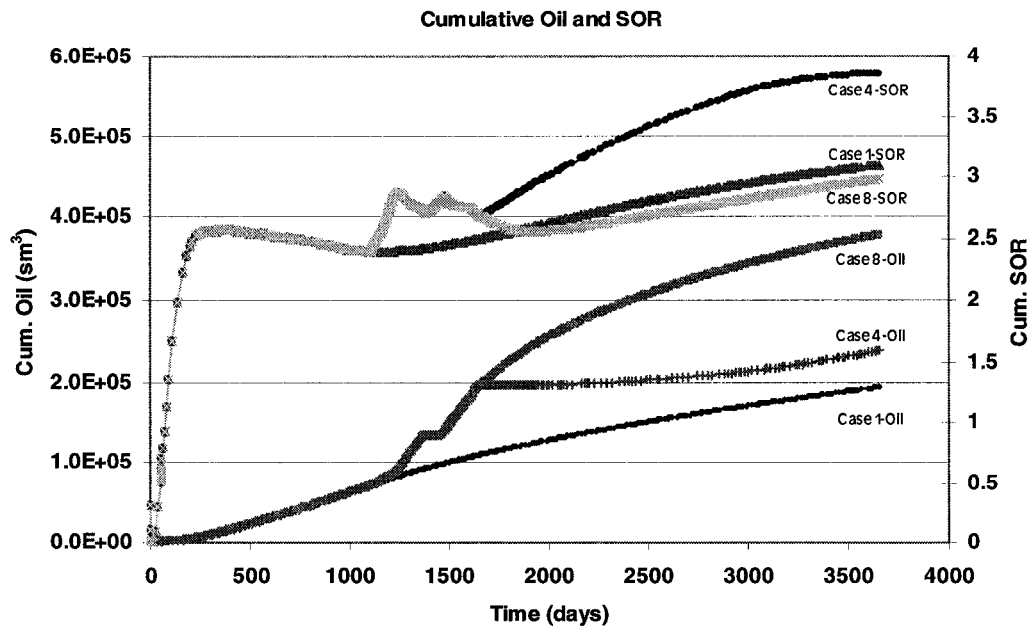


Figure 4-6. Comparison for Cases 4 and 8 (extra steam)

#### 4.4.4 Injection Pressure and Start-up Time of the Offset Well

In a traditional CSS field operation in the Cold Lake deposit, the formation is fractured with a steam injection pressure of 12 MPa. In the Fast-SAGD process, the maximum injection pressure of the offset well during the cyclic operation is set at 8 MPa, so that the formation is not fractured. Owing to the different start-up times of the offset well, the cyclic injection pressure history varied and the reservoir pressure changed dramatically during the cyclic period. In Cases 2 and 6, the heat communication between the SAGD well pair and the offset well was established in the second cycle. In Cases 4 and 8, however, the injection pressure of the offset well dropped quickly from 8 MPa to 3.7

MPa just in the first cycle, and heat communication was developed soon after the injection of steam into the offset well in the first cycle. It can be seen from the Table 4-5 that the steam injection volume into the offset well is much larger in Cases 2 and 6 than in Cases 4 and 8 because of the lower injection pressure. The zone between the offset well and the SAGD well pair is preheated longer by heat conduction from the SAGD operation in Cases 4 and 8. It is, therefore, easier to develop flow communication and push the mobile oil toward the SAGD producer during the cyclic steam injection. A temperature of 40 °C between these two steam chambers, which corresponds to a bitumen viscosity of 2000 cp, is observed to initiate the flow communication. Figure 4-7 shows that during the CSS period, the SAGD production jumps to a high level in Case 8. The function of the offset well is to accelerate the heat communication in the CSS process. Steam drive then becomes another important recovery mechanism to produce the oil from the SAGD producer.

The pressure of Cases 3 and 7 is intermediate between that of Cases 2 and 6 and Cases 4 and 8. However, when the offset well is started after 4 years in Cases 5 and 9, the injection pressure of the offset well increases from 3.5 to 4.1 MPa in the second cycle due to the over-heating of the pay zone (Table 4-5). All the simulation results are shown in Appendix C.

**Table 4-5. Simulation Summary of CSS Components**

Case	2/6	3/7	4/8	5/9
Initial Injection Pressure in the 1st Cycle (kPa)	8000.0	8000.0	8000.0	8000.0
Low Injection Pressure in the 1st Cycle (kPa)	8000.0	4282.6	3694.4	3512.4
Cum. Injection Volume in the 1st Cycle ( $10^3 \times m^3$ )	72.2	136.9	181.1	204.4
Initial Injection Pressure in the 2nd Cycle (kPa)	7017.4	3823.9	3574.1	3472.2
Low Injection Pressure in the 2nd Cycle (kPa)	5733.7	3731.6	3527.3	4061.4
Cum. Injection volume in the 2nd Cycle ( $10^3 \times m^3$ )	144.8	144.8	144.8	144.8

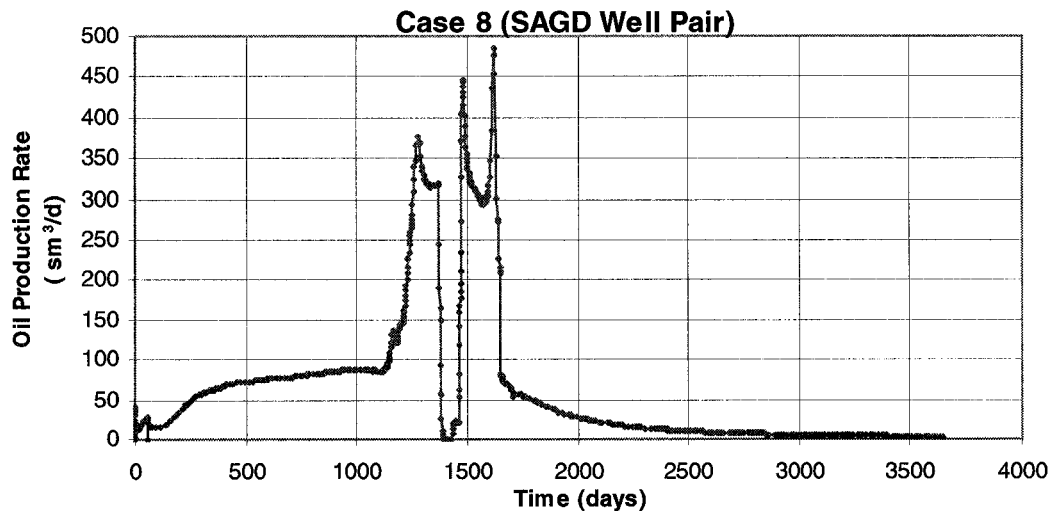


**Figure 4-7. Production History of the SAGD Producer in the Fast-SAGD Process**

It is concluded that the start-up time of the offset well is dependent on the development of lateral heat rather than vertical heat communication especially in the thick pay zone. From this point of view, Case 7 is feasible and Case 8 is the best case, in which the SAGD steam chamber would reach the top of the pay zone after 3 years.

#### **4.5 Possible Operating Strategy after the First Offset Well**

A major concern after the first offset well is put into operation is how to propagate continuously the steam chamber down the reservoir. A suggestion as to how this might be achieved is discussed below. However, more study is needed to optimize this process.

After two cycles of CSS at the first offset well, the offset well becomes a production well for another year. During this time, another equidistant offset well is drilled beside the first offset well. The second offset well is operated by CSS, in the same manner as the first one for two cycles, then converted to a production well. At that time, the SAGD well pair ceases to operate. The first offset well is switched from producer to injector. Figures 4-8 and 4-9 show the temperature profile and the production data, respectively, for such a scheme. Finally, the process is operated with two wells only, one horizontal injection

well and another equidepth horizontal producer, located 50 metres away. Preliminary simulation results show that this post-process strategy is efficient at recovering more oil.

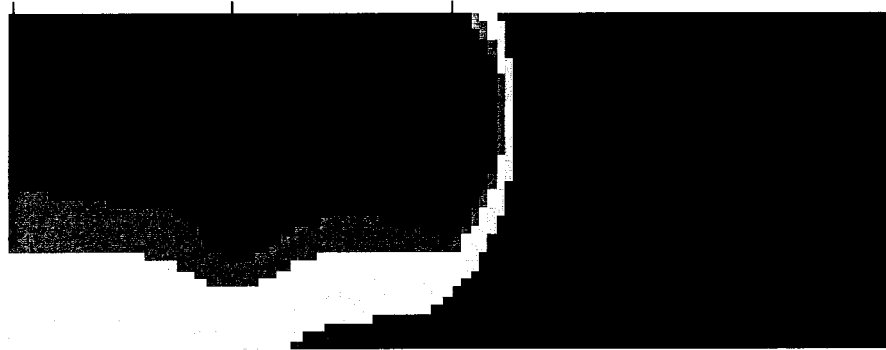


**Figure 4-8. Temperature Profile @ 10 Years after 2nd Offset Well**

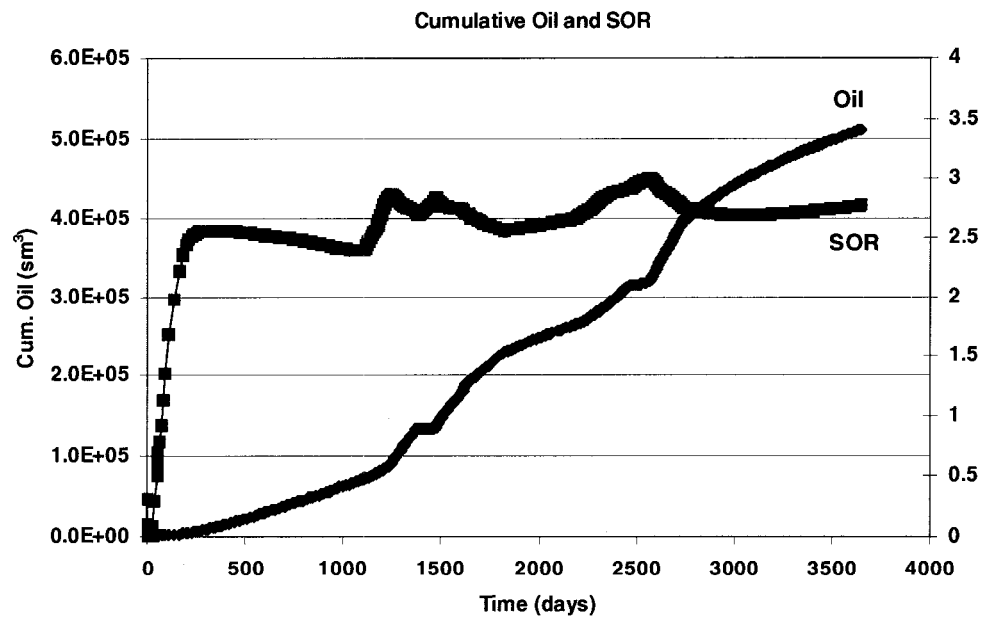


**Figure 4-9. Cumulative Oil and SOR Curves for Proposed Case**

#### **4.6 Summary**

1. Compared to SAGD, Fast-SAGD generates a much larger steam chamber, resulting in 94% incremental cumulative production.
2. The cumulative SOR for Fast-SAGD stays at the same level as that of SAGD.
3. Besides helping the steam chamber expand down the reservoir, the offset well induces a steam drive for producing additional bitumen from the SAGD producer during the CSS.
4. Lateral heat communication of the steam chamber is a significant factor in making the Fast-SAGD process more efficient.
5. Fast-SAGD is a way to operate the process at a relatively lower pressure and higher productivity mode.
6. Extra steam must be injected into the SAGD injector in order to maintain and expand the steam chamber.
7. Due to the different start-up times of the offset well, the reservoir pressure varies dramatically in the CSS stage, especially in Cases 2 and 6, in which steam is injected into the offset well at very high pressure in the unheated part of the reservoir.



## 5.0 NUMERICAL INVESTIGATION OF GEOMECHANICAL RESPONSE ON FAST-SAGD

### 5.1 Development of the Reservoir/Geomechanical Model

As discussed before, there are several different methods to couple fluid flow and stress models. A lot of effort has been made to develop a fully coupled thermal-stress-fluid-flow model. There is no commercial software to conduct iteratively-coupled models as well. In this study, a decoupled method is used to simulate the geomechanical response and predict the effect on bitumen recovery. A two-dimensional three-phase fluid flow thermal model (STARS) decoupled with a two-dimensional, elastoplastic stress model (FLAC<sup>(45)</sup>) is developed in this study. Failure is based on the Mohr-Coulomb failure criterion.

The coupling schematic is shown in Figure 5-1. In this decoupled method, only temperature and pressure changes are introduced into the stress model. There is no feedback from FLAC into STARS, although the permeability and pore volume changes could be computed. However, the effect on bitumen production and recovery can be predicted from an analysis of the geomechanical response.

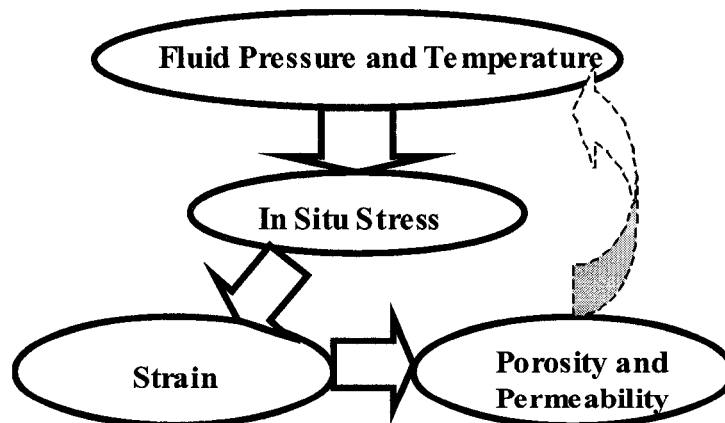


Figure 5-1. Schematic of the Decoupled Method

In this study, the simulation results of Fast-SAGD from the last chapter are used directly, and the pressure and temperature changes are introduced into FLAC through an interface program.

### 5.1.1 Thickness of Overburden and Oil Sands

The Clearwater formation was deposited to a depth of 402 m. According to the geological structure of this reservoir, the entire geomechanical model was divided into three parts. The upper part is a dry zone which is saturated with air. The middle part of the model is a water-saturated zone. And the lowest part is the actual reservoir saturated with bitumen. The thickness of each part is calculated according to the hydrostatic pressure distribution.

A pressure of 3100 kPa is assumed at a depth of 422 m in the reservoir. Using the densities of bitumen and water, one can calculate the thickness of the water-saturated zone. Consequently, the remaining portion of the whole overburden is the dry zone. Figure 5-2 shows a schematic of the three zones used in the geomechanical model along with their pore pressure and total stress. The thickness of each zone and their geomechanical properties are shown in Table 5-1. The detail is given in Appendix D.

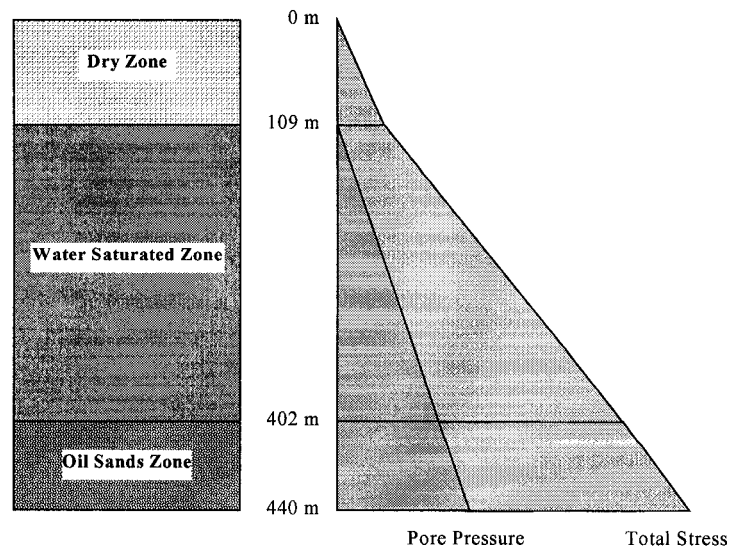


**Figure 5-2. Three Zones and Their Pore Pressure and Stress**

**Table 5-1. Geomechanical Properties**

Thermal Expansion Coefficient		2 /°C
Overburden Dry Density		$1.7 \times 10^3 \text{ kg/m}^3$
Water Saturated Zone Density		$3 \times 10^3 \text{ kg/m}^3$
Oil Sand Zone Density		$3 \times 10^3 \text{ kg/m}^3$
Poisson's Ratio $\nu$		0.3
Cohesion		0 kPa
Dilation Angle		20 °
Friction Angle		45 °
Thickness of Dry Zone		109 m
Thickness of Water Saturated Zone		293 m
Thickness of Oil Sands		38 m
$K_0 = 1$	$\sigma_x$	$-1.156 \times 10^7 \text{ Pa}$
	$\sigma_y$	$-1.156 \times 10^7 \text{ Pa}$
	$\sigma_z$	$-1.156 \times 10^7 \text{ Pa}$
$K_0 = 1.5$	$\sigma_x$	$-1.734 \times 10^7 \text{ Pa}$
	$\sigma_y$	$-1.156 \times 10^7 \text{ Pa}$
	$\sigma_z$	$-1.734 \times 10^7 \text{ Pa}$

**5.1.2 Initial Stress Condition**

Research shows that  $K_0$  ( $\sigma_h/\sigma_v$ ) is greater than 1 at a depth < 500 m, and that it approaches 1 at depths > 1 km. It is assumed that the oil sands were deposited at a shallow depth; therefore, the average horizontal stresses are significantly greater than the vertical stresses. In order to analyze the effect of different initial stress states,  $K_0 = 1$  and 1.5 were considered.

**5.1.3 Grid Development and Boundary Conditions**

To match the grid system used in the reservoir simulation, the size of the pay zone was made the same in both the reservoir and the geomechanical models. The number of layers (1 m for each layer up to 38 layers) is also the same in both models. In the x direction,

two grids in the reservoir model are combined into one grid in the stress model, except for the leftmost grid. Figure 5-3 shows this combination. Because the displacement of the matrix is negligible, it is assumed that these two grid systems totally overlap each other.

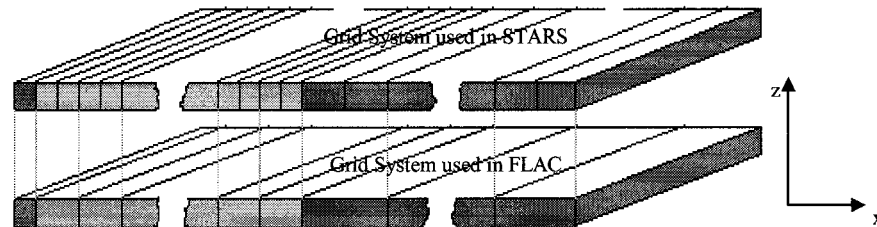


**Figure 5-3. Comparison of the Grid Systems**

For the water-saturated zone, the grid size in the  $z$  direction is increased by a ratio of 1.46, and the grid size in the  $x$  direction is identical to the reservoir zone. The dry zone is one layer, which is 109 m thick. The whole grid system for the stress model is shown in Figure 5-4.

In this model, the top surface is a free boundary and both the left and right boundaries are free to move in the  $z$  direction only. The bottom boundary is fixed in both the  $x$  and  $z$  directions. The detail is seen in Figure 5-4.

After developing grids that match both the reservoir and geomechanical simulation meshes, temperature and pressure data files from STARS are introduced into FLAC at each time step. Stress and strain profiles are computed at each time step according to the new temperature and pressure profiles.

Here only the basic SAGD and the Fast-SAGD cases, in which the offset well is started after one and three years, are studied (Cases 1, 6 and 8). It is important to note that different initial stress states ( $K_0 = 1.0$  and  $1.5$ ) are considered in these three cases.

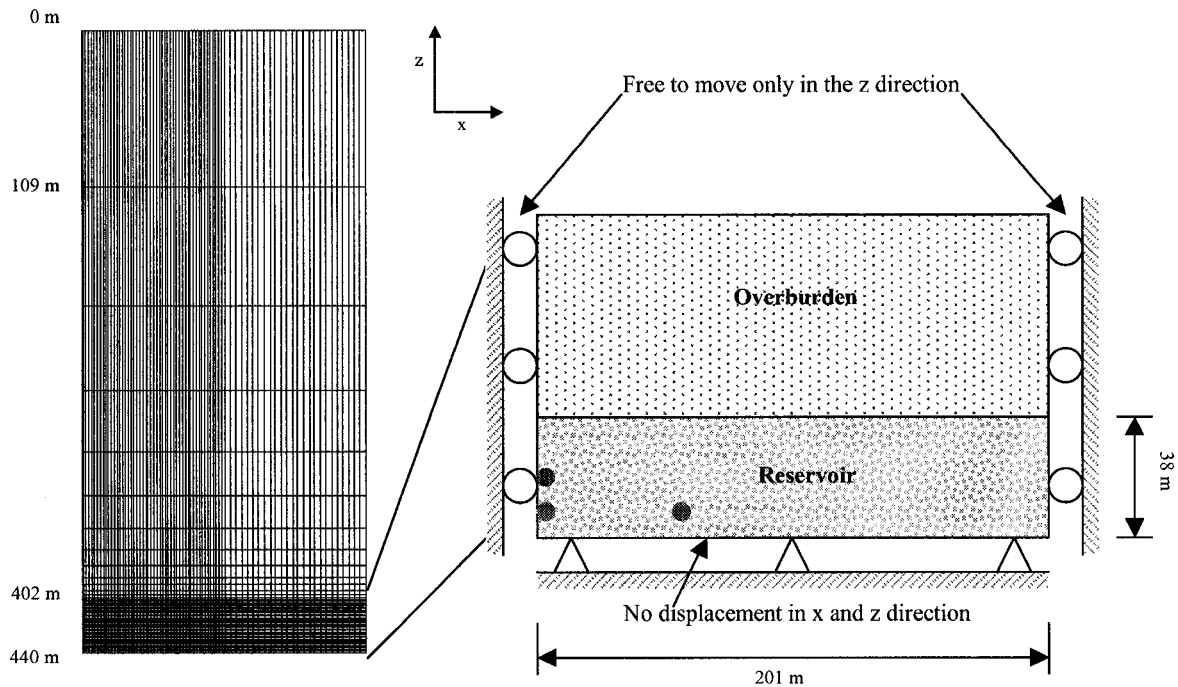


**Figure 5-4. Geomechanical Model and Boundary Conditions**

## 5.2 Geomechanical Results and Discussion

Let us consider a thermal oil recovery process in which steam is introduced into the reservoir. A high injection pressure results in a low effective confining stress of the reservoir rocks, while heat produces thermal expansion to increase the confining stress. Geomechanical issues<sup>(30,32,33,34)</sup> have been recognized as important factors in the recovery of oil. In the Fast-SAGD process, the operation of the SAGD well pair is at a pressure near the reservoir pressure with a high temperature, while the offset well is at both high pressure and temperature. Thus, geomechanical impact is an important issue in this process.

According to the characteristics of the temperature and pressure variations, three locations of the reservoir were selected for analyzing the stress-strain relationship (Figure 5-5).

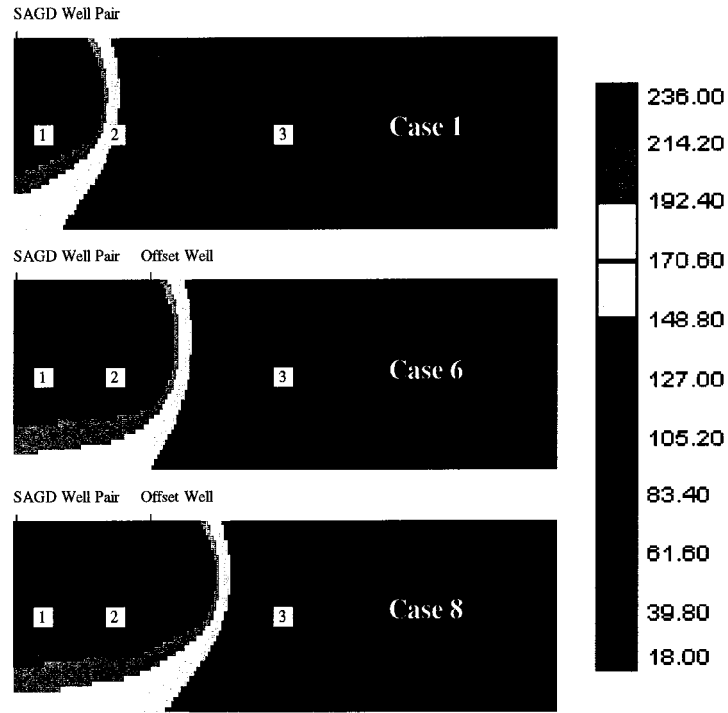


**Figure 5-5. Element Locations Used in Describing Stress Path History within Reservoir**

### 5.2.1 Initial Stress State

Generally, under the same conditions, material would fail more easily at  $K_0=1.5$  than at  $K_0=1.0$ , as indicated in Appendix E. The anisotropic stress distribution is potentially more sensitive to shear yield. As one can observe in Figures E-1 and E-2, the starting point of the stress path is much closer to the failure envelope in the case of  $K_0=1.5$  than in the case of  $K_0=1.0$ .

### 5.2.2 Stress Path and Volume Strain Increment

The stress path is used to analyze the variation of the stress state. The stress state is determined by the deviatoric ( $q'=(\sigma'_1-\sigma'_3)/2$ ) and average ( $p'=(\sigma'_1+\sigma'_3)/2$ ) stresses. A high injection pressure decreases all of the three principal effective stresses. As a result, the stress path approaches the failure envelope horizontally, when the average stress  $p'$  drops off and the deviatoric stress  $q'$  stays constant. The thermal expansion induced by

heat increases the total stress in all directions so that the stress path moves upwards towards the failure envelope. In the reservoir, it is the combination of temperature and pressure that controls the stress path, as shown in Figure 5-6. Volumetric deformations within the reservoir result from the thermally induced stresses and pore-pressure-induced stress. In the following, the stress paths in Case 8 ( $K_0=1.5$ ) are used to illustrate the stress variation in the Fast-SAGD process.

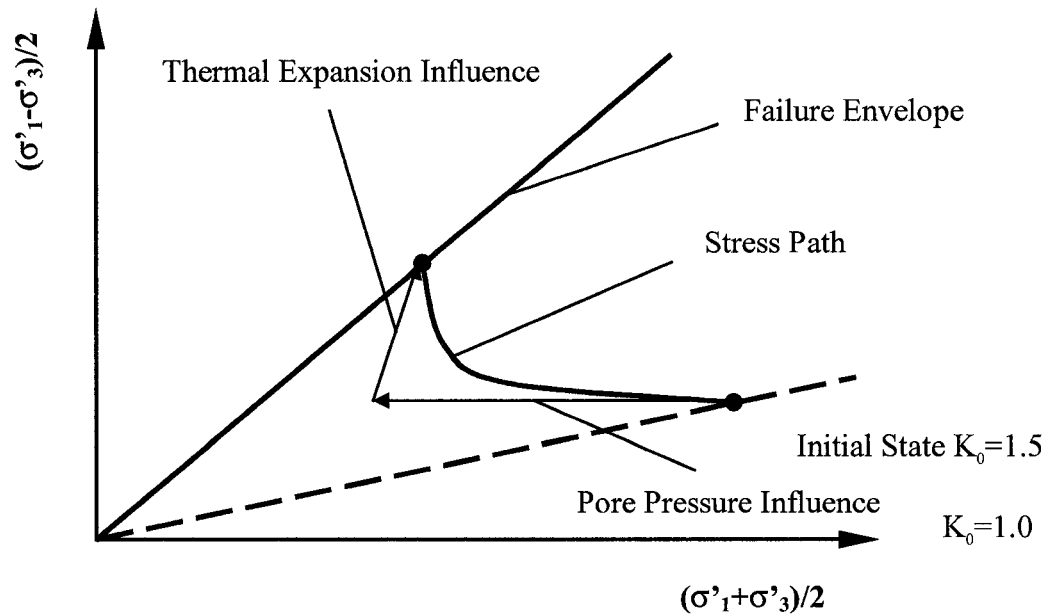


**Figure 5-6. Stress Path in Thermal Recovery Process**

#### *Elements around the SAGD well pair*

In the vicinity of the SAGD well pair, the pore pressure was less than the fracture pressure. Steam temperature was the main factor that affected the stress path. The typical stress path (Figure 5-7) in the steam chamber moved upwards but stayed below the failure envelope. The volume strain increment of the rock increased due to thermal expansion. When the offset well was operated cyclically, the stress path touched the failure envelope. During the steaming of the offset well, the volume strain decreased as it was affected by the nearby offset well (Figure 5-10). This may be a potential mechanism for the recovery of bitumen from the SAGD producer by geomechanical compaction during the CSS period, as shown by Beattie et al<sup>(17)</sup>.

#### *Elements around the offset well*

When the high-pressure steam was injected into the offset well, the pore pressure front was always ahead of the temperature front around the offset well. The effective stress was low in this relatively high pressure and low temperature area. Therefore, it was easier to shear the formation during the injection phase of the CSS process. It is observed from Figure 5-8 that the stress path touched the failure envelope during that time. This means that, during the offset well's operation, the pore volume and permeability of the porous medium around the offset well were increased before the heat invaded. Potentially, this would accelerate communication within the reservoir. Pore volume deformation, induced by loading and unloading, would be another potential mechanism for the offset well to produce the bitumen (Figure 5-11).

#### *Elements outside the steam chamber*

Outside the steam chamber, the reservoir temperature and pressure were at their initial values. However, due to the thermal expansion of adjacent regions of the reservoir, the elements in this zone have a tendency to reach shear failure. From the stress path in Figure 5-9, it is seen that, after the CSS operation, the elements in this area had reached a failure state. Such dilation, if it is located near the steam chamber, could be a significant mechanism for the recovery of oil. Laboratory tests and simulations<sup>(34,46,47)</sup> have shown that shear dilation is induced by three conditions: (i) low effective stress, (ii) a compressive strain increment in one direction, and (iii) an expansive strain increment in the other perpendicular direction. If the operating pressures were high enough, a large shear dilation would be expected and it would impact recovery.



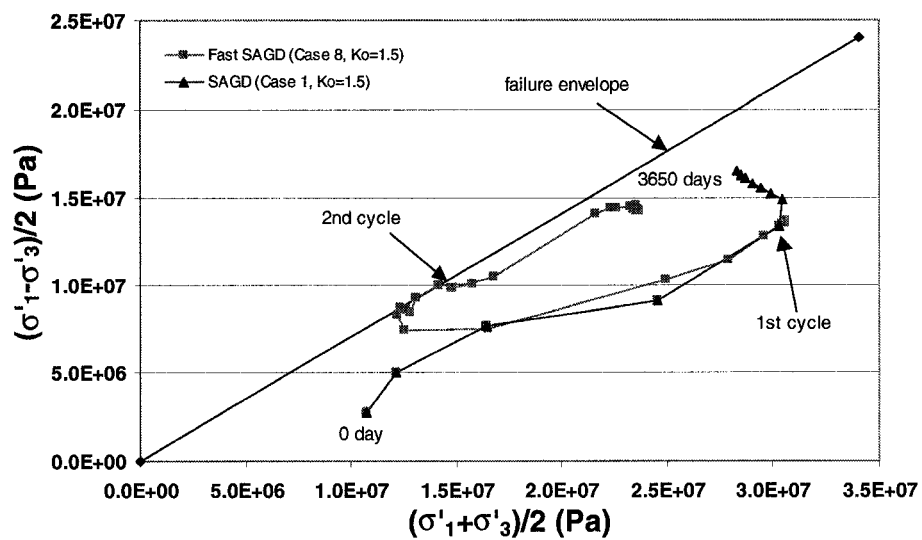


Figure 5-7. Stress Path for 1st Element

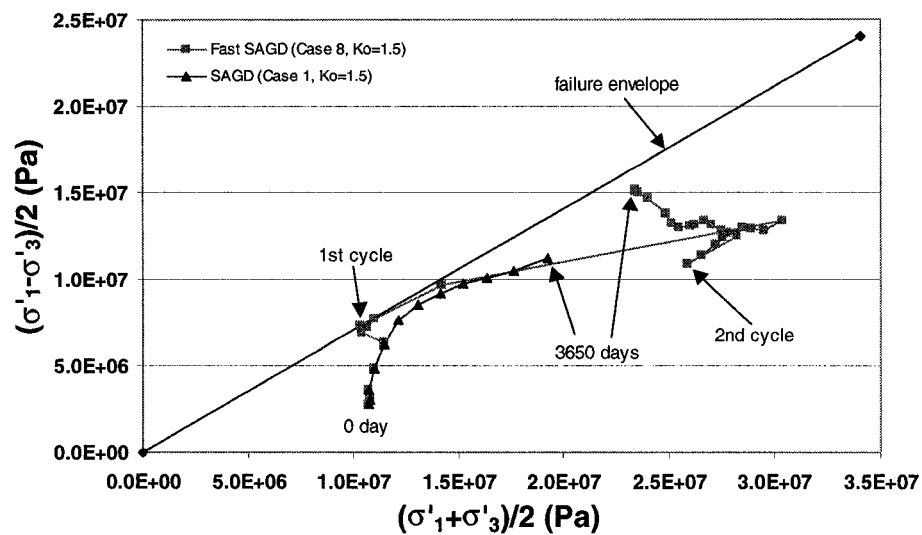


Figure 5-8. Stress Path for 2nd Element

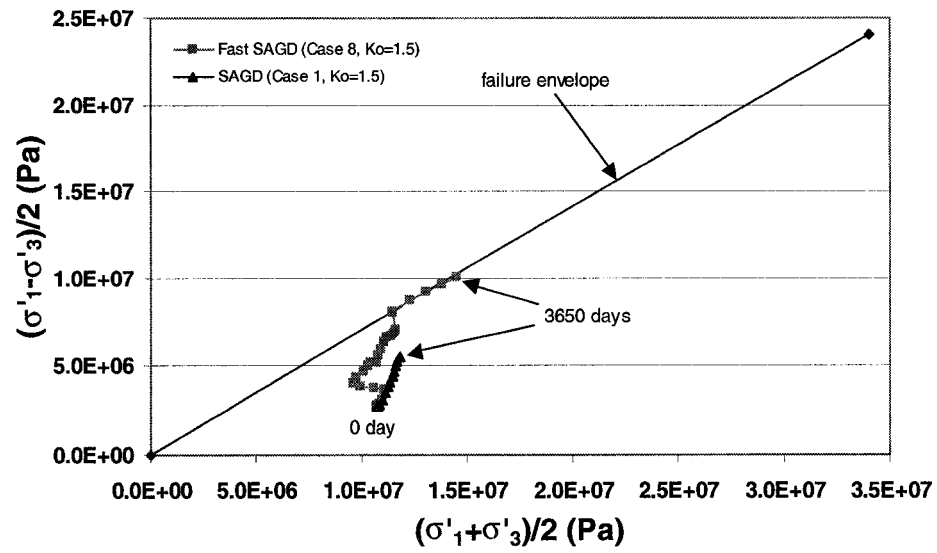


Figure 5-9. Stress Path for 3rd Element

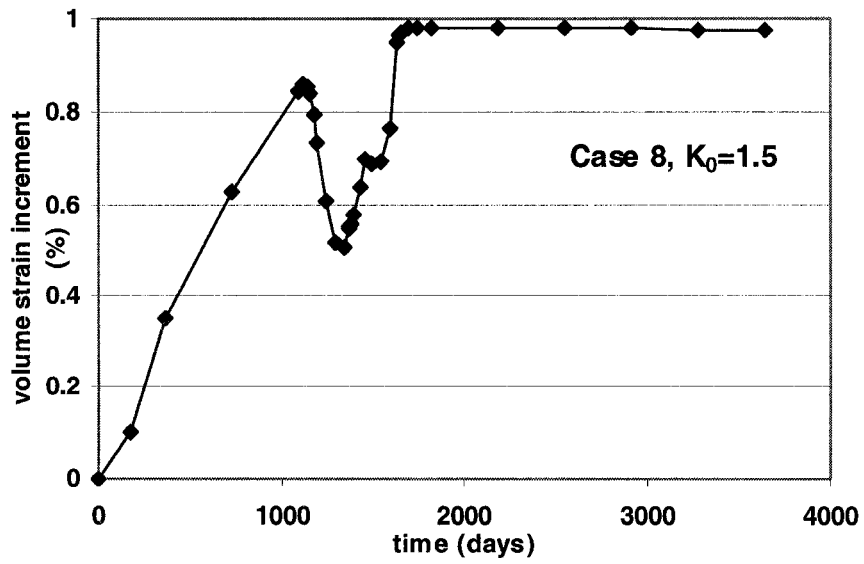
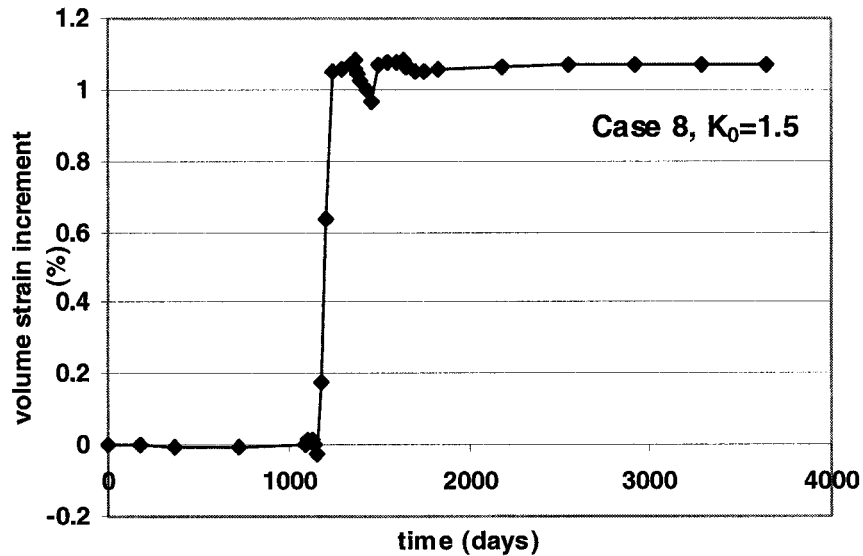


Figure 5-10. Volume Strain Increment for 1st Element



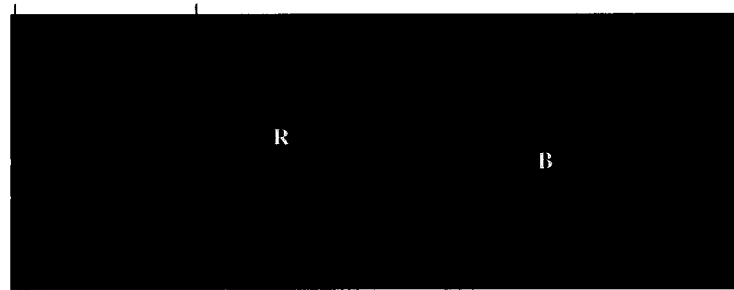
**Figure 5-11. Volume Strain Increment for 2nd Element**

Because of the different start-up times of the offset well in Cases 6 and 8, the stress path touched the failure envelope earlier in Case 6 than in Case 8. Because heat communication was developed at later times during CSS in Case 8, huge amount of steam could be injected from the offset well. Thermal expansion increases the horizontal stress more than the vertical stress and provides enough deviatoric stress to let the zone outside the steam chamber yield after the CSS. This causes the shear zone in Case 8 to be larger than that in Case 6. The complete results are given in Appendix E.

### **5.2.3 Shear Failure Zone**

Simulation results have shown that, because of the cyclic steam operation, a large shear failure zone was generated in the reservoir (Figure 5-12), while it didn't happen in the SAGD operation alone. Shear failure first appeared around the offset well, propagated to the SAGD well pair area, and finally expanded laterally in the reservoir. No tensile failure appeared in all cases studied. Complete results for all cases are given in Appendix E (Figures E-13 to E-16).

Generally, the failure zone is larger in the case of  $K_0=1.5$  than in the case of  $K_0=1.0$ . The shape of the failure zone is also different. For Case 6, CSS started one year after SAGD, and the heated zones around the wells are isolated from each other because of the lack of heat communication between the SAGD well pair and the offset well. The failure zone expands vertically and in isolation, especially at  $K_0=1.0$ . This probably increases the risk of leaking heat to the overburden as compared to Case 8. The main failure zone is generated by the CSS operation. However, in Case 8, with  $K_0=1.5$ , the failure zone expands laterally and continuously after the CSS operation.



Red – post-failure, Green – currently in failure, Blue – elastic state

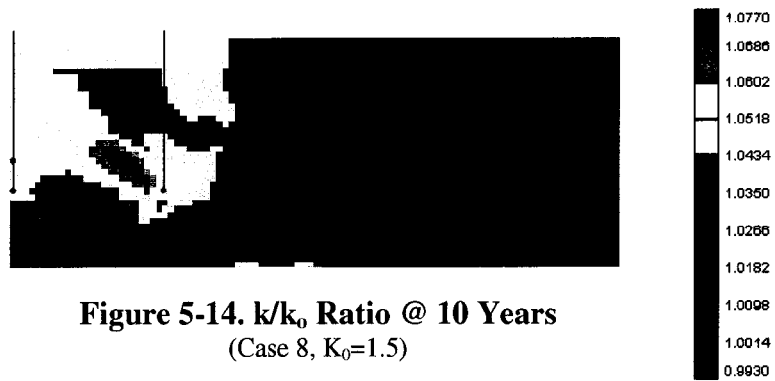
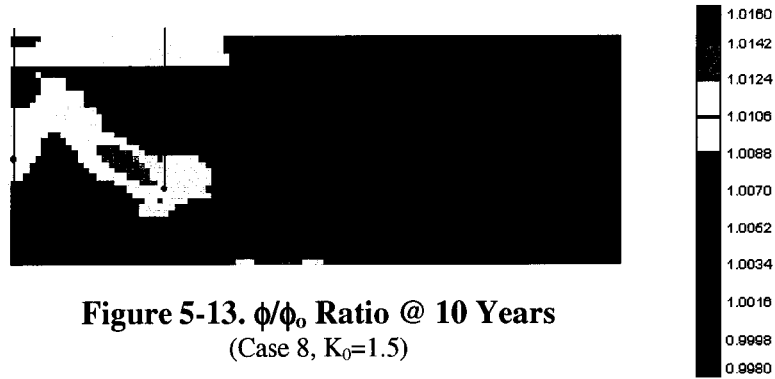
**Figure 5-12. Failure Zone @ 10 Years (Case 8,  $K_0=1.5$ )**

#### 5.2.4 Stress-Induced Porosity and Absolute Permeability Changes

The permeability and pore volume changes could be computed at the each time step. However, for this study, there was no feed-back from FLAC into STARS (decoupled model).

The equations developed by Tortike and Farouq Ali<sup>(28,29)</sup>, which are listed in Appendix D, were used to link the geomechanical and the reservoir simulations. The porosity and permeability variations at the end of the ten-year simulation are shown in Figures 5-13 and 5-14, respectively, for Case 8 at  $K_0=1.5$ . Similar results for all the other cases are given in Appendix E (Figures E-17 to E-28). In Case 1 of SAGD, the variation appeared in the steam chamber. The lower porosity zone was more sensitive to the stress variation and larger porosity and permeability improvements were observed in this zone. For the Cases 6 and 8, the largest variation appeared in the combined steam chamber. Especially in Case 8, the largest variation is observed around the offset well, which showed that heat

communication was accelerated by the offset well operation. As there was no feedback from FLAC into STARS, the variation of pore volume as well as permeability would probably be underestimated in the reservoir.



### 5.3 Summary

1. The formation yields much more easily in an anisotropic stress state.
2. For Fast-SAGD, a different type of stress path occurs in each of three parts of the reservoir.
3. Due to stress changes, the pore volume and permeability are modified.
4. Shear failure appears when CSS is conducted at the offset well.
5. Due to the operating pressure and the corresponding high temperature, thermal expansion is the main factor affecting the geomechanical response in the case studied.

## 6.0 CONCLUSIONS AND FUTURE WORK

The results presented in this study show that Fast-SAGD is a feasible thermal oil recovery process, both from a reservoir and a geomechanics perspective. The following conclusions can be drawn from this work:

- Compared to SAGD, Fast-SAGD generates a much larger steam chamber, resulting in 94% incremental cumulative production.
- The cumulative SOR for Fast-SAGD stays at the same level as that of SAGD.
- Lateral heat communication of the steam chamber is a significant factor in making the Fast-SAGD process more efficient.
- Besides helping the steam chamber expand down the reservoir, the offset well induces a pressure drive for producing additional bitumen from the SAGD producer during CSS.
- Shear failure and pore volume deformation are the additional mechanisms in this recovery process.
- Given the operating pressure of the process being near the reservoir pressure, thermal expansion is the main factor affecting the geomechanical response. However, at high injection pressures, or in shallow reservoirs, shear dilation is expected to be another important factor.

In this study, the Fast-SAGD process was not optimized. The following future work is recommended:

- Laboratory verification of the numerical findings by conducting Fast-SAGD experiments.
- Development of fully coupled reservoir-geomechanics models in order to predict the history accurately.
- Study of reservoirs deposited at different depths to analyze the role of geomechanical factors on the Fast-SAGD process.
- Development of an operating strategy for subsequent equidistant offset wells.

## 7.0 REFERENCES

- 1 Butler, R. M., McNab, G. S. and Lo, H. Y., "Theoretical Studies on the Gravity Drainage of Heavy Oil During In-Situ Steam Heating", presented at the 29<sup>th</sup> Canadian Chemical Engineering Conference, Sarnia, Ontario, October 1-3, 1979; Canadian Journal of Chemical Engineering, Vol. 59, August 1981.
- 2 Edmunds, N. R., Haston, J. A. and Best, D. A., "Analysis and Implementation of the Steam Assisted Gravity Drainage Process at the AOSTRA UTF", paper No. 125 presented at the 4<sup>th</sup> UNITAR/UNDP International Conference on Heavy Crude and Tar Sands, Edmonton, August 7-12, 1988.
- 3 Polikar, M., Cyr, T. J. and Coates, R. M., "Fast-SAGD: Half the Wells and 30% Less Steam", paper SPE 65509 presented at the 2000 SPE/Petroleum Society of CIM International Conference on Horizontal Well Technology, Calgary, Alberta, Canada, November 6-8, 2000.
- 4 Butler, R. M. and Stephens, D. J., "The Gravity Drainage of Steam-Heated Heavy Oil to Parallel Horizontal Wells", Journal of Canadian Petroleum Technology, Vol. 20, No. 2, April-June, 1981.
- 5 Butler, R. M., "Thermal Recovery of Oil and Bitumen", published by Prentice-Hall Inc. 1997.
- 6 Butler, R. M., "A New Approach to the modelling of Steam-Assisted Gravity Drainage", Journal of Canadian Petroleum Technology, Vol. 24, No. 3, May-June, 1985.
- 7 Scott Ferguson, F. R. and Butler, R. M., "Steam-Assisted Gravity Drainage Model Incorporating Energy Recovery From A Cooling Steam Chamber", Journal of Canadian Petroleum Technology, Vol. 27, No. 5, September-October 1998.
- 8 Chung, K. H. and Butler, R. M., "In Situ Emulsification by The Condensation of Steam in Contact with Bitumen", Journal of Canadian Petroleum Technology, Vol. 28, No. 1, January-February 1989.

- 9 Sugianto, S. and Butler, R. M., "The Production of Conventional Heavy Oil Reservoirs with Bottom Water Using Steam-Assisted Gravity Drainage", *Journal of Canadian Petroleum Technology*, Vol. 29, No. 2, March-April 1990.
- 10 Yang, G. and Butler, R. M., "Effects of Reservoir Heterogeneities on Heavy Oil Recovery by Steam-Assisted Gravity Drainage", *Journal of Canadian Petroleum Technology*, Vol. 31, No. 8, October 1992.
- 11 Sawhney, G. S., Liebe, H. and Butler, R. M., "Vertical Injection Wells for SAGD: A Practical Option or Not?", *Journal of Canadian Petroleum Technology*, Vol. 34, No. 1, January 1995.
- 12 Chow, L. and Butler, R. M., "Numerical Simulation of the Steam-Assisted Gravity Drainage Process (SAGD)", *Journal of Canadian Petroleum Technology*, Vol. 35, No. 6, June 1996.
- 13 Oballa, V. and Buchanan, W. L., "Single Horizontal Well in Thermal Recovery Process", Paper SPE 37115 presented at the 1996 SPE International Conferences on Horizontal Well Technology, Calgary, Canada, 18-20 November 1996.
- 14 Shen, C., "Numerical Investigation of SAGD Process Using s Single Horizontal Well", *Journal of Canadian Petroleum Technology*, Vol. 39, No. 3, March 2000.
- 15 Sasaki, K., Akibayashi, S., Doan, Q. and Farouq Ali, S. M., "Experimental Modelling of the SAGD Process – Enhancing SAGD Performance with Periodic Stimulation of the Horizontal Producer", paper SPE 56544 presented at the 1999 Annual Technical Conference and Exhibition held in Houston, Texas, 3-6 October 1999.
- 16 Denbina, E. S., Boberg, T. C. and Rotter, M. B., "Evaluation of Key Reservoir Drive Mechanisms in the Early Cycles of Steam Stimulation at Cold Lake", *SPE Reservoir Engineering*, Vol. 6, No. 2, May 1991.
- 17 Beattie, C. I., Boberg, T. C. and McNab, G. S., "Reservoir Simulation of Cyclic Steam Stimulation in the Cold Lake Oil Sands", *SPE Reservoir Engineering*, Vol. 6, No. 2, May 1991.
- 18 Vittoratos, E., Scott, G. R. and Beattie, C. I., "Cold Lake Cyclic Steam Stimulation: A Multiwell Process", *SPE Reservoir Engineering*, Vol. 5, No. 1, February 1990.



- 19 Walters, D. A., Settari, A. and Kry, P. R., "Poroelastic Effects of Cyclic Steam Stimulation in the Cold Lake Reservoir", paper SPE 62590 presented at the 2000 SPE/AAPG Western Regional Meeting, Long Beach, California, June 19-23, 2000.
- 20 Gutierrez, M., Lewis, R. W. and Masters, I., "Petroleum Reservoir Simulation Coupling Fluid Flow and Geomechanics", SPE Reservoir Evaluation & Engineering, Vol. 4, No. 3, June 2001.
- 21 Settari, A. and Walters, D. A., "Advances in Coupled Geomechanical and Reservoir Modelling with Applications to Reservoir Compaction", paper SPE 51927 presented at the 1999 SPE Reservoir Simulation Symposium, Houston, Texas, February 14-17, 1999.
- 22 Geertsma, J., "The Effect of Fluid Pressure Decline on Volumetric Changes of Porous Rocks", Trans. AIME, Vol. 210. 1957.
- 23 Settari, A., "Physics and Modeling of Thermal Flow and Soil Mechanics in Unconsolidated Porous Media", SPE Production Engineering, Vol. 7, No. 1, February 1992.
- 24 Settari, A. and Mourits, F. M., "Coupling of Geomechanics and Reservoir Simulation Models", published in Computer Methods and Advances in Geomechanics, Vol. 3, Netherlands, 1994.
- 25 Settari, A. and Mourits, F. M., "A Coupled Reservoir and Geomechanical Simulation System", SPE Journal, Vol. 3, No. 3, September 1998.
- 26 Fung, L. S. -K. and Buchanan, L., "Coupled Geomechanical-thermal Simulation for Deforming Heavy-oil Reservoir", Journal of Canadian Petroleum Technology, Vol. 33, No. 4, April 1994.
- 27 Fung, L. S. -K., "A Coupled Geomechanic-Multiphase Flow Model for Analysis of In Situ Recovery in Cohesionless Oil Sands", Journal of Canadian Petroleum Technology, Vol. 31, No. 6, June 1992.
- 28 Tortike, W. S. and Farouq Ali, S. M., "Prediction of Oil Sand Failure due to Steam-Induced Stresses", Journal of Canadian Petroleum Technology, Vol. 30, No. 1, January-February 1991.

- 29 Tortike, W. S. and Farouq Ali, S. M., "Reservoir Simulation Integrated with Geomechanics", Journal of Canadian Petroleum Technology, Vol. 32, No. 5, May 1993.
- 30 Chalaturnyk, R. J. and Scott, D. J., "Geomechanics Issues of Steam Assisted Gravity Drainage", paper SPE 30280 presented at the International Heavy Oil Symposium, Calgary, Alberta, Canada, June 19-21, 1995.
- 31 Chalaturnyk, R. J., Geomechanics of SAGD in Heavy Oil Reservoirs. Ph. D thesis, Department of Civil and Environmental Engineering, University of Alberta, 1996.
- 32 Chalaturnyk, R. and Scott, D. J., "Geomechanical Response of Heavy Oil Reservoirs to the Steam Assisted Gravity Drainage Process", paper SPE 37569 presented at the 1997 SPE International Thermal Operations and Heavy Oil Symposium, Bakersfield, California, USA, 10-12 February 1997.
- 33 Ito, Y. and Suzuki S., "Numerical Simulation of the SAGD Process in the Hangingstone Oil Sands Reservoir", Journal of Canadian Petroleum Technology, Vol. 38, No. 9, September 1999.
- 34 Chalaturnyk, R. J. and Li, P., "When is it Important to Consider Geomechanics in SAGD Operations?", Paper 2001-46 presented at the Petroleum Society's Canadian International Petroleum Conference 2001, Calgary, Alberta, Canada, 12-14 June 2001.
- 35 Cyr, T. J., Coates, R. M. and Polikar, M., "Steam-Assisted Gravity Drainage Heavy Oil Recovery Process", patent No. US 6,257,334, 13 pp. July 10, 2001.
- 36 Farouq Ali, S. M., "CSS – Canada's Super Strategy for Oil Sands", Journal of Canadian Petroleum Technology, Vol. 33, No. 9, November 1994.
- 37 O'Rourke, J. C., Chambers, J. I., Suggett, J. C. and Good, W. K., "UTF Project Status and Commercial Potential – An Update, May 1994", paper No. 94-90 presented at the 48<sup>th</sup> Annual Technical Meeting of CIM/AOSTAR, Calgary, Alberta, June 12-15, 1994.
- 38 Butler, R. M. and Yee, C. T., "Progress in the In Situ Recovery of Heavy Oils and Bitumen", Journal of Canadian Petroleum Technology, Vol. 41, No. 1, January 2002.

- 39 Computer Modelling Group Ltd., 2000, STARS user's guide.
- 40 Kisman, K. E. and Yeung, K. C., "Numerical Study of the SAGD Process in the Burnt Lake Oil Sands Lease", paper SPE 30276, Presented at the International Heavy Oil Symposium held in Calgary, Alberta, Canada, June, 1995.
- 41 Donnelly, J. K., "Application of Steam Assisted Gravity Drainage (SAGD) to Cold Lake", Presented at the Joint SPE-Petroleum Society of CIM 6<sup>th</sup> One-Day Conference on Horizontal Well Technology, November, 1997.
- 42 Donnelly, J. K., "Hilda Lake a Gravity Drainage Success", paper SPE 54093 presented at the 1999 SPE International Operations and Heavy Oil Symposium, Bakersfield, California, March 17-19, 1999.
- 43 Donnelly, J. K., "The Best Process for Cold Lake: CSS vs. SAGD", Journal of Canadian Petroleum Technology, Vol. 39, No. 8, August 2000.
- 44 Edmunds, N. and Chhina, H., "Economic Optimum Operating Pressure for SAGD Projects in Alberta", Journal of Canadian Petroleum Technology, Vol. 40, No. 12, December 2001.
- 45 Itasca, 1995, FLAC: Fast Lagrangian Analysis of Continua. Volume I, User's Manual.
- 46 Scott, J. D., Proskin, S. A., and Adhikary, D. P., "Volume and Permeability Changes Associated with Steam Stimulation in an Oil Sands Reservoir", Journal of Canadian Petroleum Technology, Vol. 33, No. 7, September 1994.
- 47 Wong, R. C. K., "Stress-strain Response of Cold Lake Oil Sands", Canadian Geotechnical Journal, Vol. 30, 1993.
- 48 Vermeer, P. A. and de Borst, R., "Non-Associated Plasticity for Soils", Concrete and Rock, HERON, Vol. 29, No. 3, 63 P, 1984.

## Appendix A: Fluid and Rock Properties

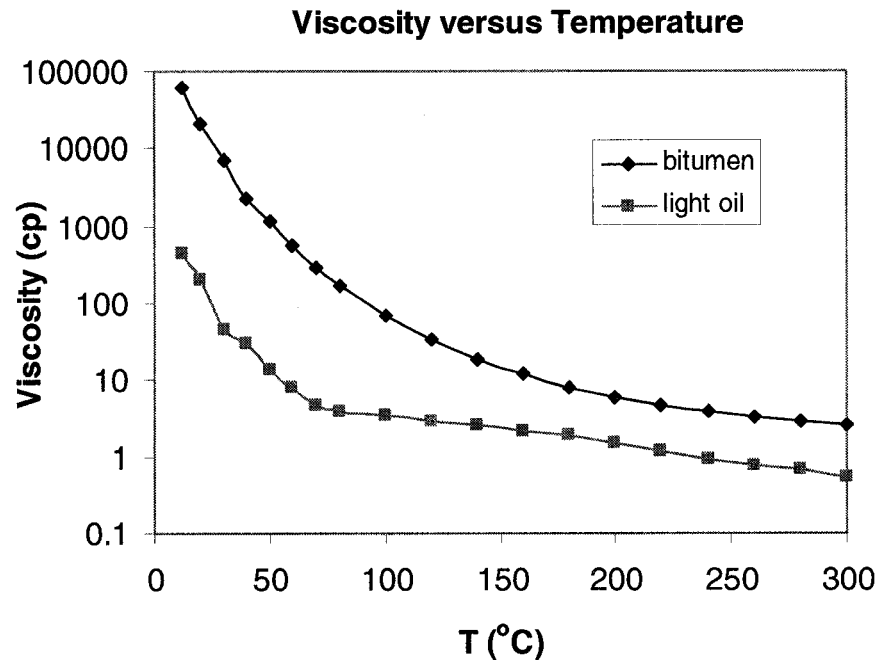


Figure A-1. Bitumen Viscosity

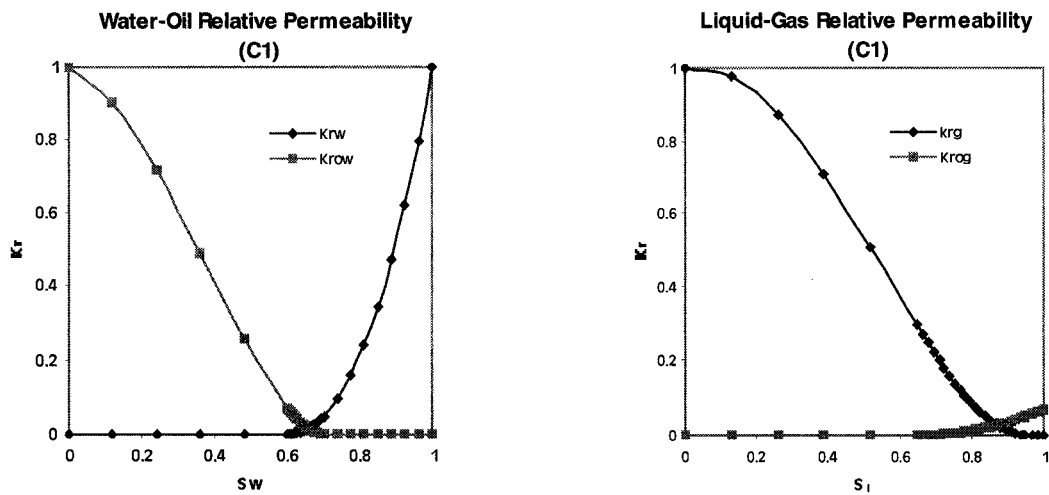
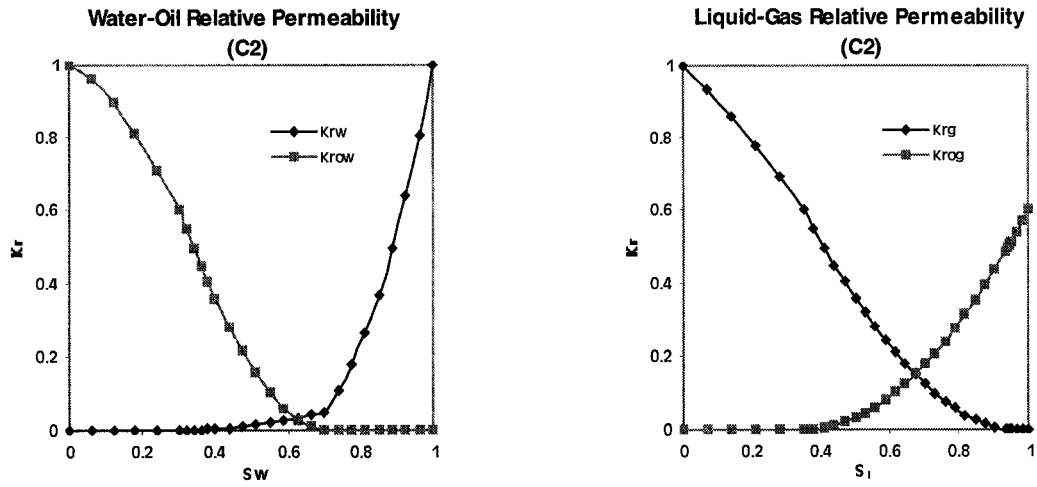
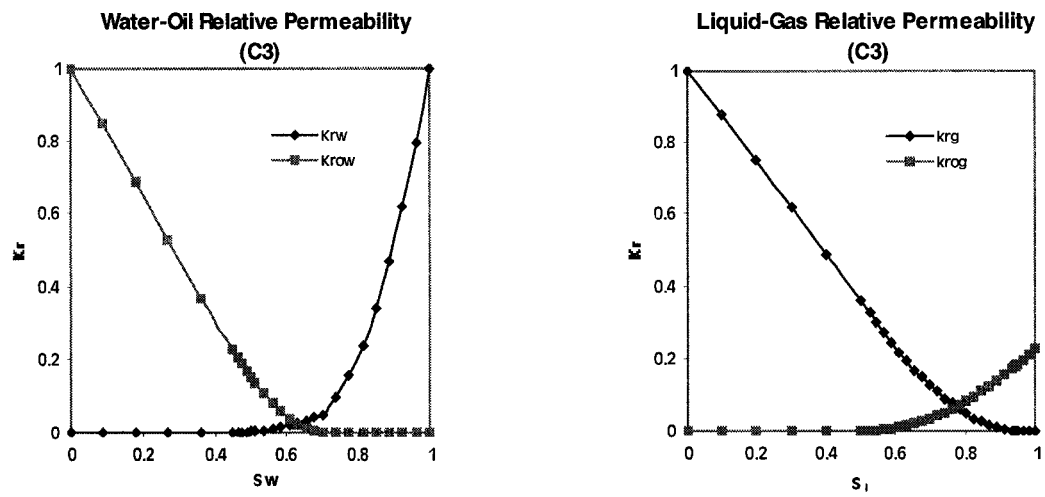


Figure A-2. Relative Permeability Curves for C1



**Figure A-3. Relative Permeability Curves for C2**



**Figure A-4. Relative Permeability Curves for C3**

## **Appendix B: Impact of Hydrostatic Pressure on SAGD Operation**

In thermal oil recovery simulations, normally constant pressure was assumed in the reservoir. However, when the simulation was run, the reservoir pore pressure would reach the hydrostatic equilibrium pressure due to the effect of gravity during the early stages of the simulation. Because SAGD is a gentle process with low-pressure drops, the resulting production may be different when comparing simulation and actual field results.

A numerical simulation is developed to study the effect of hydrostatic pressure in the SAGD process. An obvious difference is observed between the hydrostatic pressure case and the constant pressure case. The study addressed the effect of hydrostatic reservoir pressure in the operating strategy of the SAGD process. The numerical simulation results indicate that, in order to predict the production correctly, the hydrostatic pressure naturally occurring in the reservoir should be considered in the thermal simulation. Otherwise, actual oil production is over-predicted when considering a constant pressure reservoir. This difference becomes larger as the pay zone thickness increases.

### **Numerical Model**

The SAGD simulation used for this study is a homogeneous model with a width of 200 m and a length of 900 m. The depth of the formation is approximately 400 m, with a thickness varying from 30 to 60 m. In this study, reservoir properties are considered constant. The SAGD wells are located at the base of the pay zone, with the injector placed 5 m above the producer. For all the simulations, the length of the horizontal wells is 900 m. All simulations are performed for a ten-year duration. The production well is operated by steam trap control at the local reservoir pressure. The rate of the SAGD injector is selected as 400 m<sup>3</sup>/d of CWE steam. The injection pressure was set 10 KPa higher than the production pressure. Reservoir initial conditions and petrophysical properties are given in Table B-1.

**Table B-1. Initial Conditions and Reservoir Properties.**

Reservoir Pressure	3100 kPa
Reservoir Temperature	18 °C
Oil Saturation	0.70
Water Saturation	0.30
Porosity	0.35
$k_v$	1.25 D
$k_h$	2.5 D
Reference Pressure	101.3 kPa
Reference Temperature	20 °C
Capillary Pressure	0
Formation Heat Capacity	2350 kJ/m <sup>3</sup> -°K
Rock Compressibility	$9.6 \times 10^{-6}$ kPa <sup>-1</sup>
Rock Thermal Conductivity	$6.6 \times 10^5$ J/m-d-°C
Oil Thermal Conductivity	$1.15 \times 10^4$ J/m-d-°C
Water Thermal Conductivity	$5.35 \times 10^4$ J/m-d-°C
Gas Thermal Conductivity	$1.4 \times 10^2$ J/m-d-°C
Dead Oil Viscosity @ 20°C	21,500 cp

Four numerical simulations were run. Two different thickness reservoir models were considered. Figures B-1 (151×30) and B-2 (151×60) present the x-z cross section of the grid system. In the z direction there are 30 - 60 zones, each 1 m thick, and in the y direction there is only one zone with a length of 900 m. In the x direction, the first 101-m zone is divided into 101 blocks, each 1 m wide, and the next 100-m zone is divided into 50 zones, each 2 m wide. A symmetry boundary condition is used for the left side and a no flow boundary for right side. Also both the upper and the lower boundary is a no flow boundary. In the models studied, dead oil was used. And both a constant and a hydrostatic pressure was considered in each case. However, the average pressure was still 3100 kPa. The injector pressure is 10 kPa higher than the production pressure. Table B-2 shows the details.

### **Results and Discussion**

The predicted cumulative bitumen production and SOR are listed in Table B-3 and shown in Figures B-3 & B-4.

**Table B-2. Simulation Sets of Cases A to D**

Case	A	B	C	D
Thickness (m)	30	30	60	60
CH <sub>4</sub> (mole%)	0	0	0	0
Reservoir Pressure (kPa)	constant	hydrostatic	constant	hydrostatic
Production Pressure (kPa)	3100	3231.8	3100	3368.2
Injection Pressure (kPa)	3110	3241.8	3110	3378.2
Block Pressure At Injector (kPa)	3100	3186.4	3100	3322.8

**Table B-3: Simulation Results of Cases A to D**

Case	A	B	C	D
Cum. Bitumen (m <sup>3</sup> )	174254	170521	193170	185143
Cum. Inj. Water (m <sup>3</sup> )	709458	710771	709468	711175
Cum. SOR	4.07	4.17	3.67	3.84

As can be seen from Figure B-3, when using dead oil, the cumulative oil production in the constant pressure case is larger than that in the hydrostatic pressure case. But the cumulative SOR of the first case is less than that of the second case. This difference becomes larger as the pay zone thickness increases. Due to the hydrostatic equilibrium process during the early stages (about one year), reservoir energy by itself contributes the extra oil production (Figures B-5 and B-6). It is noted that the differential pressure, 55.4 kPa, between the injection pressure and the local pore pressure of the block in the hydrostatic pressure case is larger than that (10 kPa) in the constant pressure case. So steam can be injected easily. Also due to the lower production pressure with respect to the reservoir pressure in the constant pressure case, the cumulative oil production is larger than that in the hydrostatic pressure case. The study demonstrated that the operating strategy of the SAGD process in different cases causes the obviously different cumulative oil productions and SORs.



For the thicker case (Figures B-4, B-7 and B-8), it can be seen also that the cumulative bitumen production in the constant pressure case is larger than that in the hydrostatic pressure case and that the cumulative SOR is less. The thicker the pay zone is, the larger the difference is. It was concluded, that in thick reservoirs, in order to predict the production correctly, the impact of hydrostatic pressure should be considered in the thermal oil recovery simulation.

## **Conclusions**

Four numerical simulations were performed to demonstrate the impact of hydrostatic pressure in reservoir simulation. The following conclusions can be drawn from this study.

- The impact of hydrostatic pressure on the SAGD process simulation was demonstrated.
- The thicker the reservoir is, the larger the impact of hydrostatic pressure is.
- The cumulative oil production in the constant pressure case is larger than that in the hydrostatic pressure case
- The cumulative SOR in the hydrostatic pressure case is larger than that in the constant pressure case.

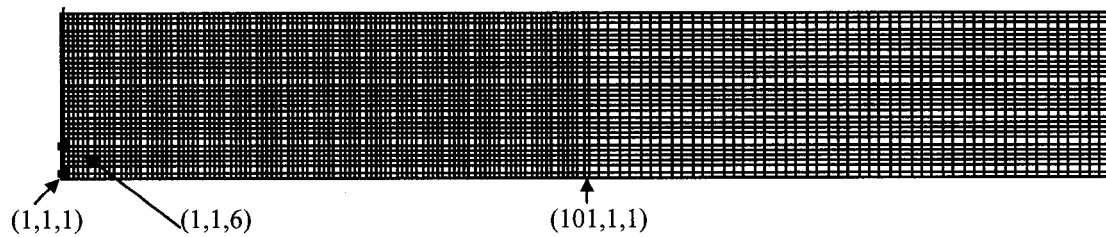


**Figure B-1. Grid System of 30 m Pay Zone Reservoir Model**

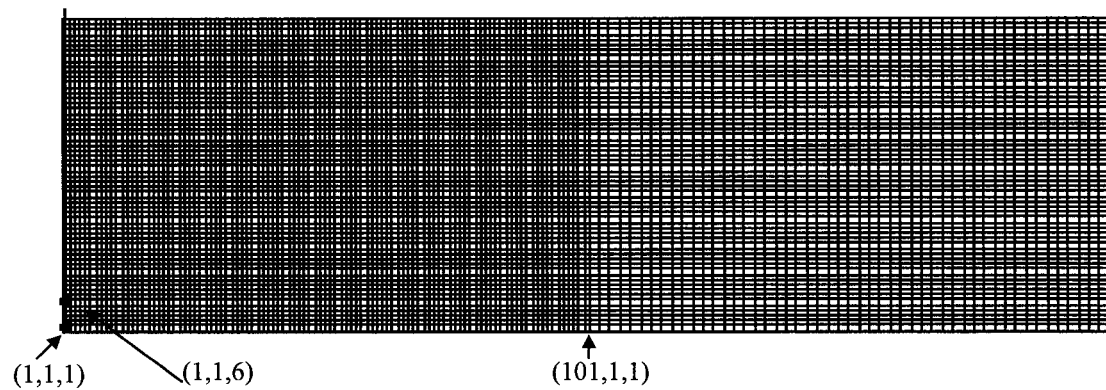


**Figure B-2. Grid System of 60 m Pay Zone Reservoir Model**

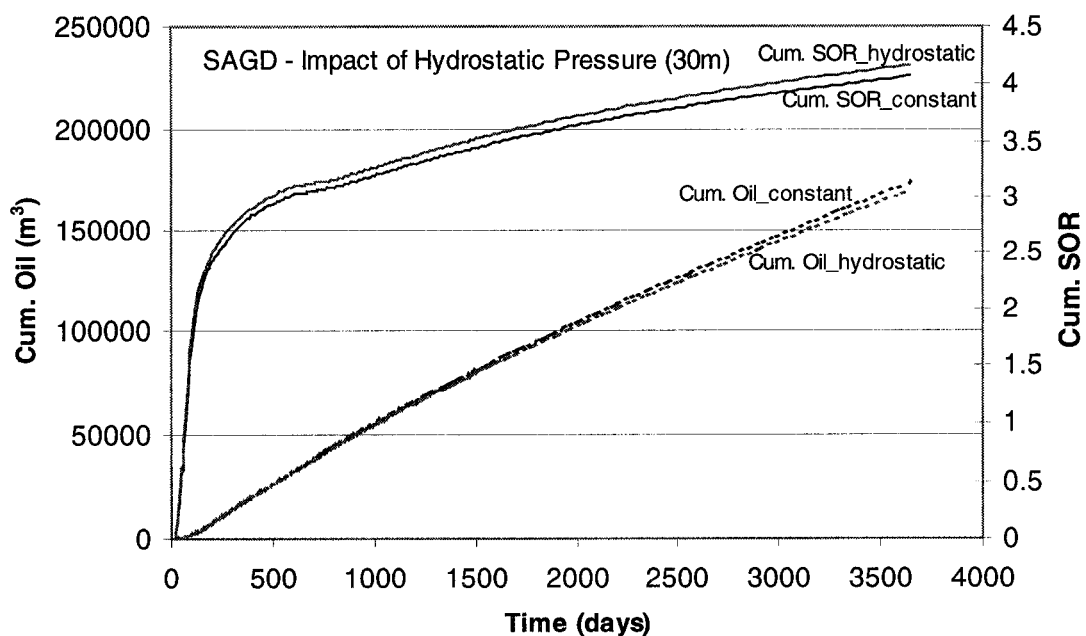


**Figure B-3. Comparison of Cumulative Oil and SOR (30m)**

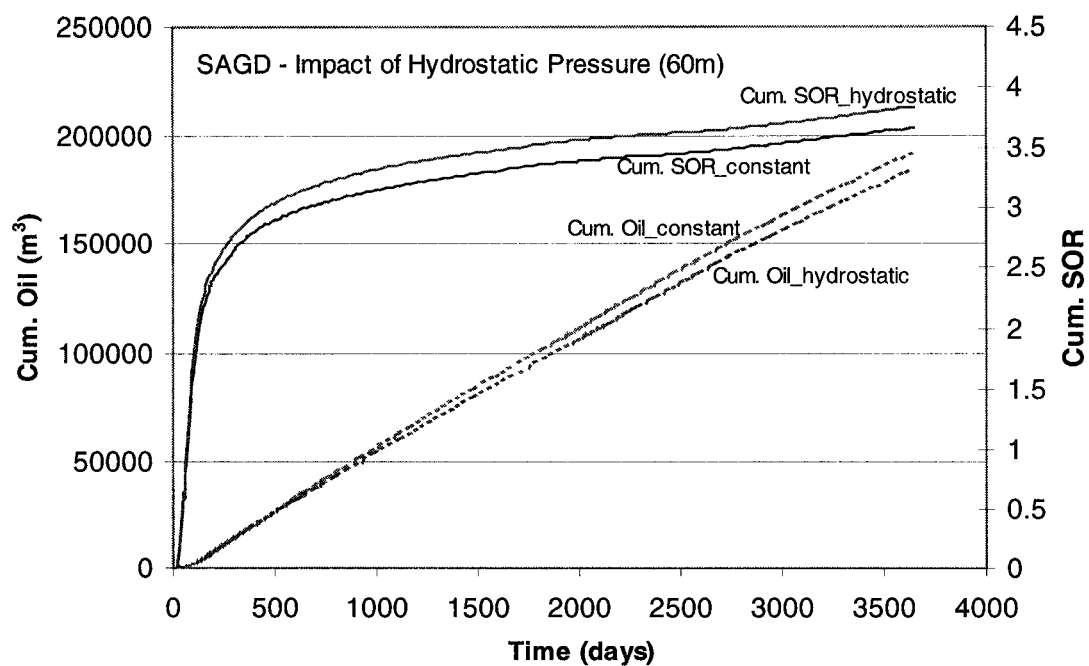
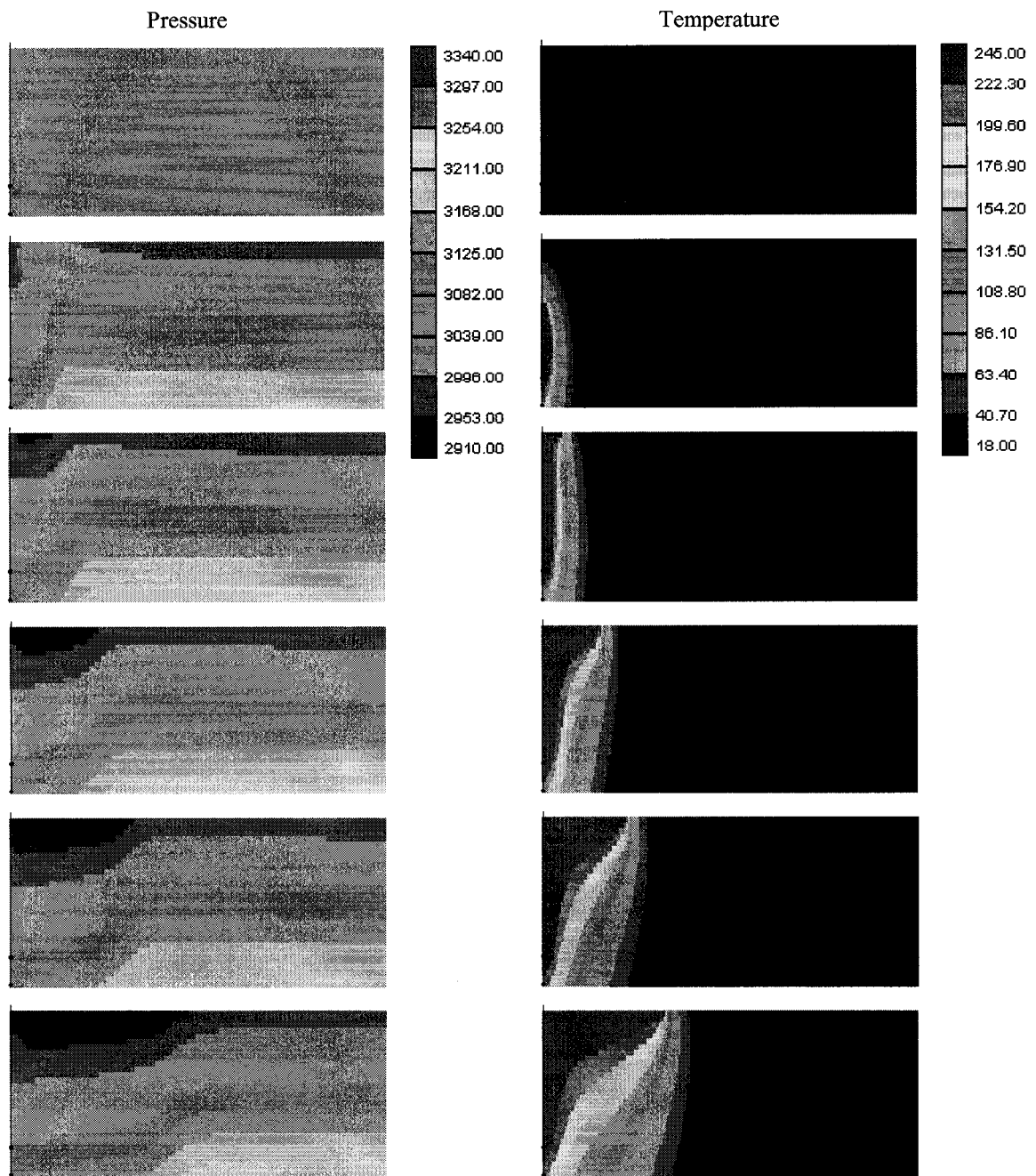
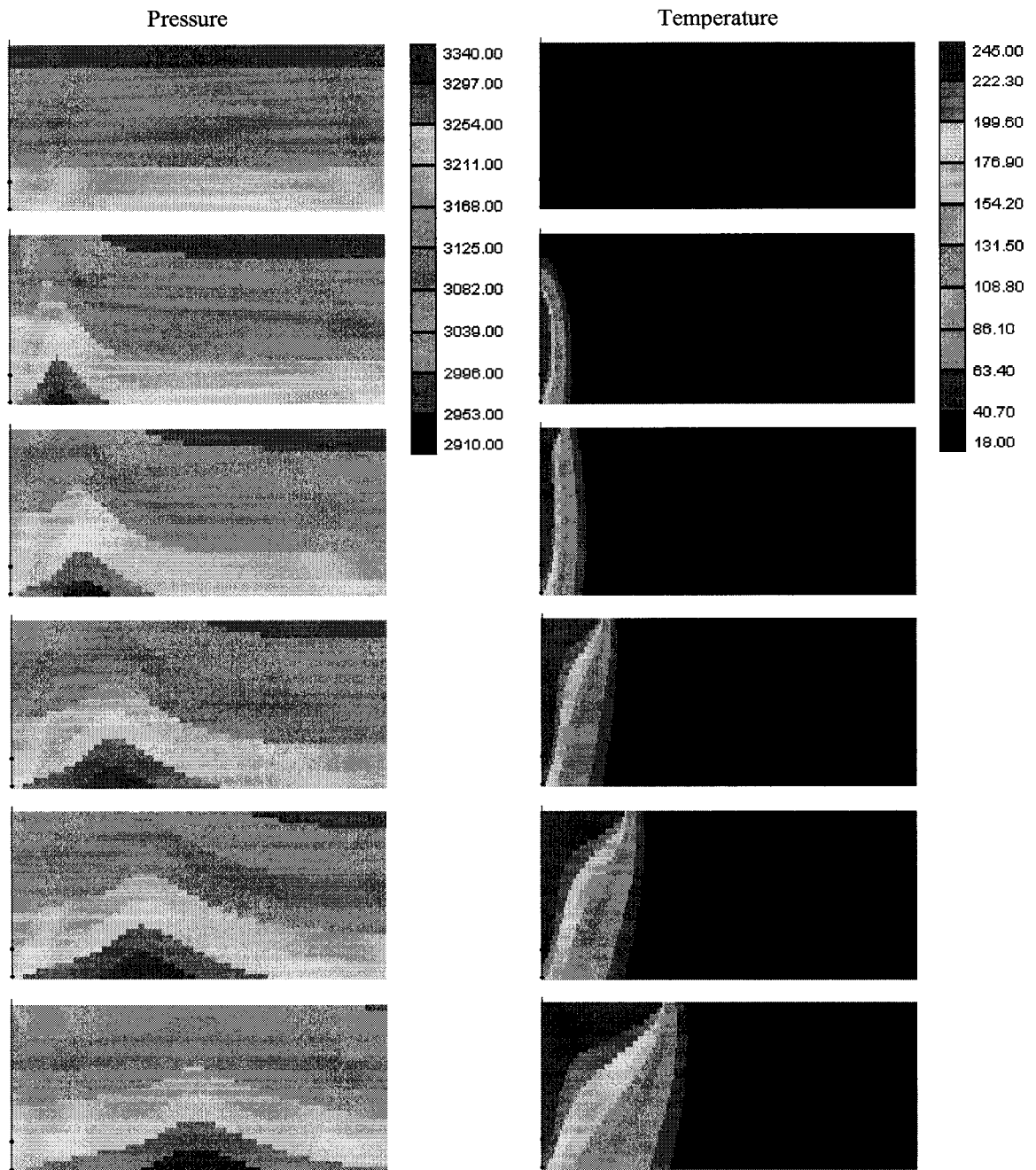


**Figure B-4. Comparison of Cumulative Oil and SOR (60m)**



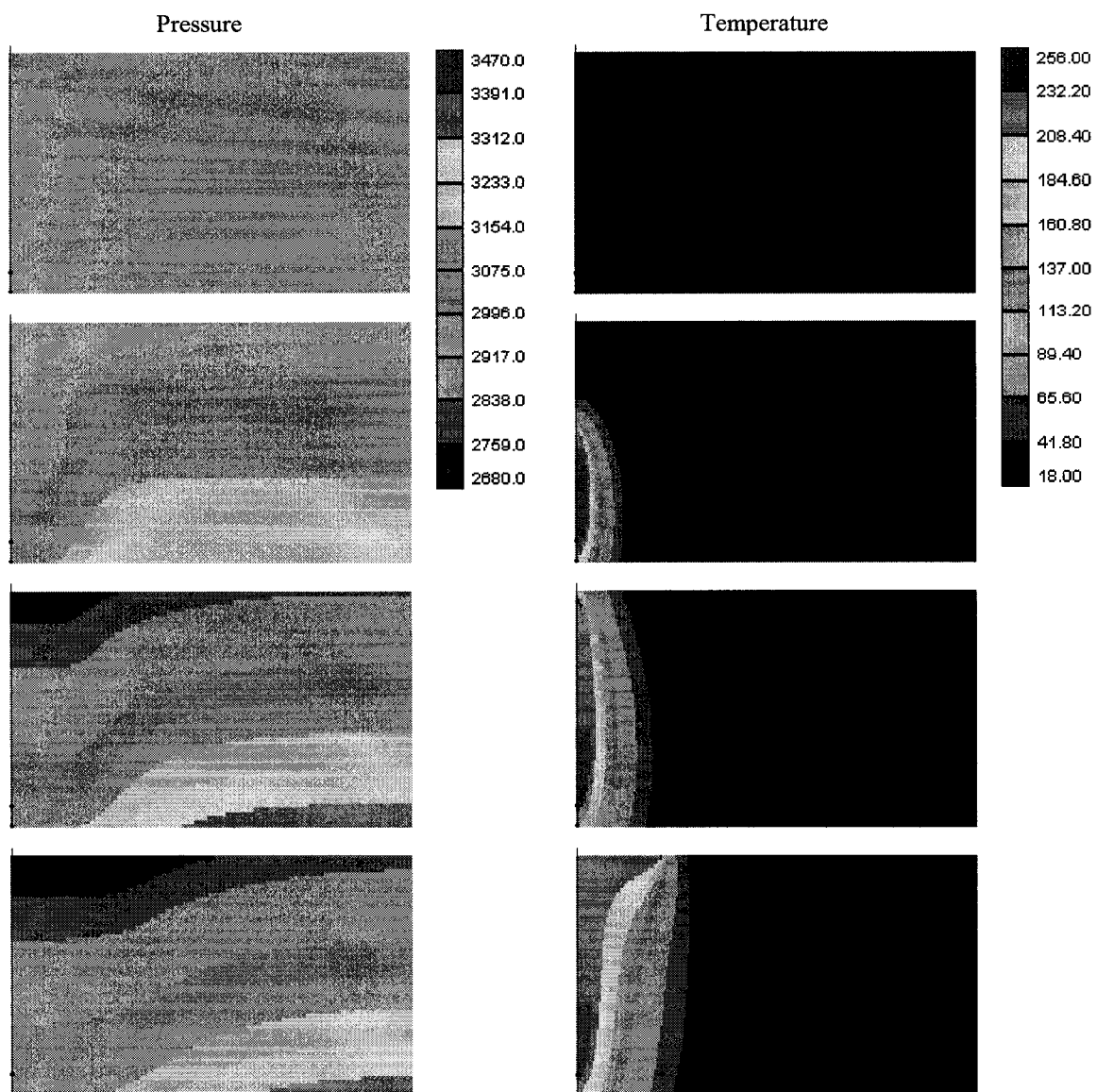
Note: dead oil; 30 m pay zone; constant pressure; z:x ratio = 3:1  
0, 1, 2, 4, 6, and 10 year's profiles

**Figure B-5. Pressure and Temperature Profiles (Constant Pressure; 30m)**



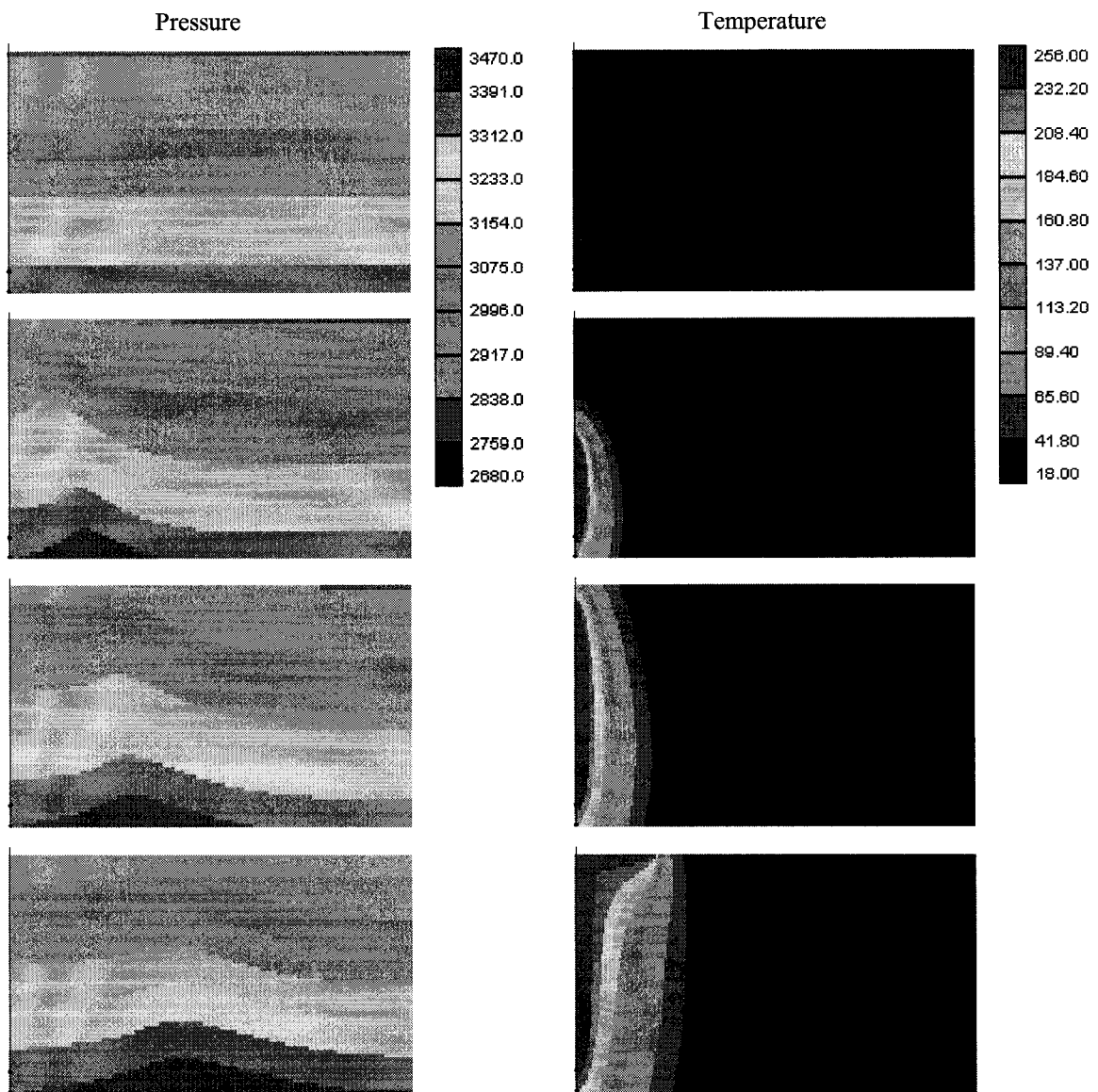
Note: dead oil; 30 m pay zone; hydrostatic pressure; z:x ratio = 3:1  
0, 1, 2, 4, 6, and 10 year's profiles

**Figure B-6. Pressure and Temperature Profiles (Hydrostatic Pressure; 30m)**



Note: dead oil; 60 m pay zone; constant pressure; z:x ratio = 2:1  
0, 2, 5, and 10 year's profiles

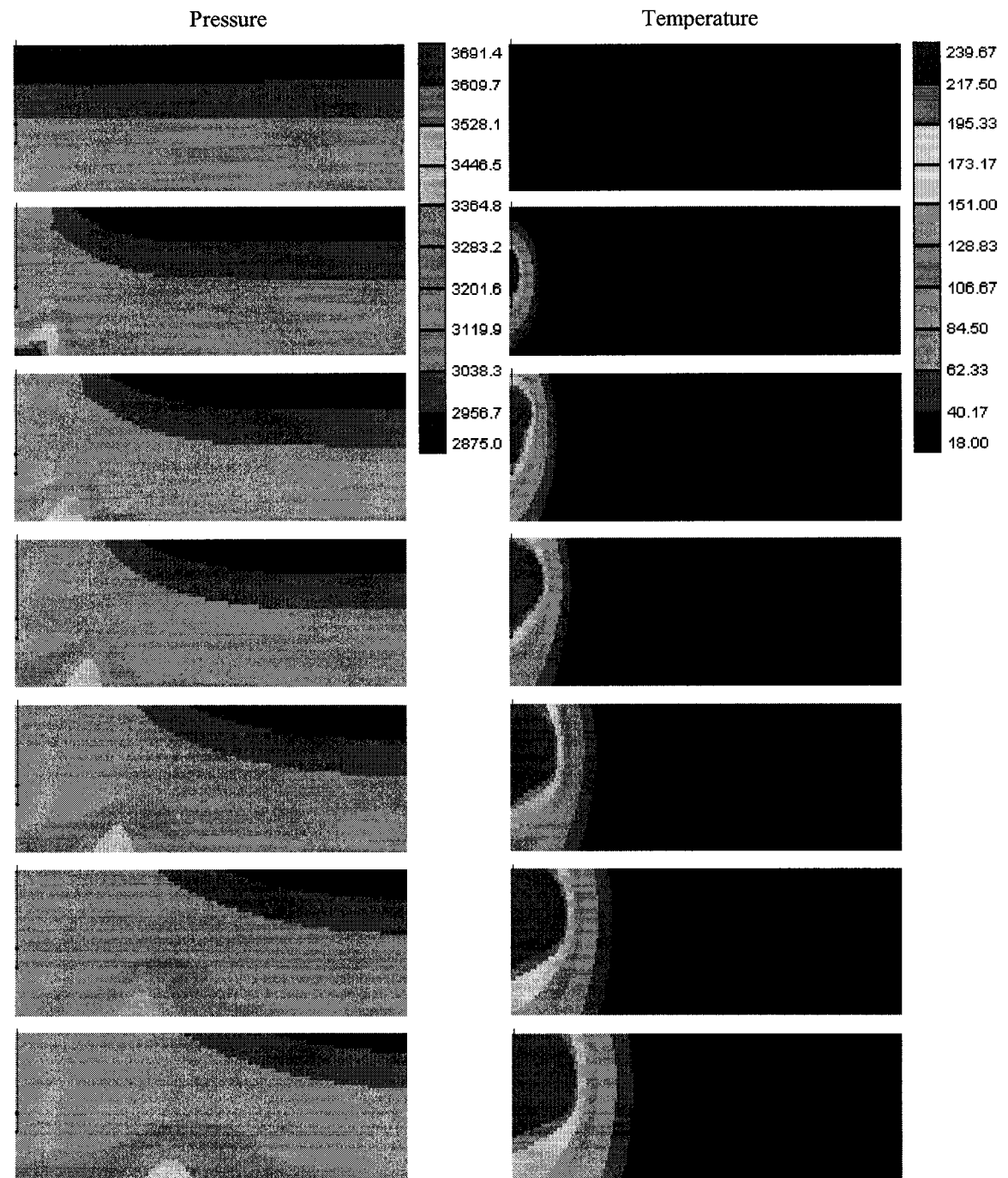
**Figure B-7. Pressure and Temperature Profiles (Constant Pressure; 60m)**



Note: dead oil; 60 m pay zone; hydrostatic pressure; z:x ratio = 2:1  
0, 2, 5, and 10 year's profiles

**Figure B-8. Pressure and Temperature Profiles (Hydrostatic Pressure; 60m)**

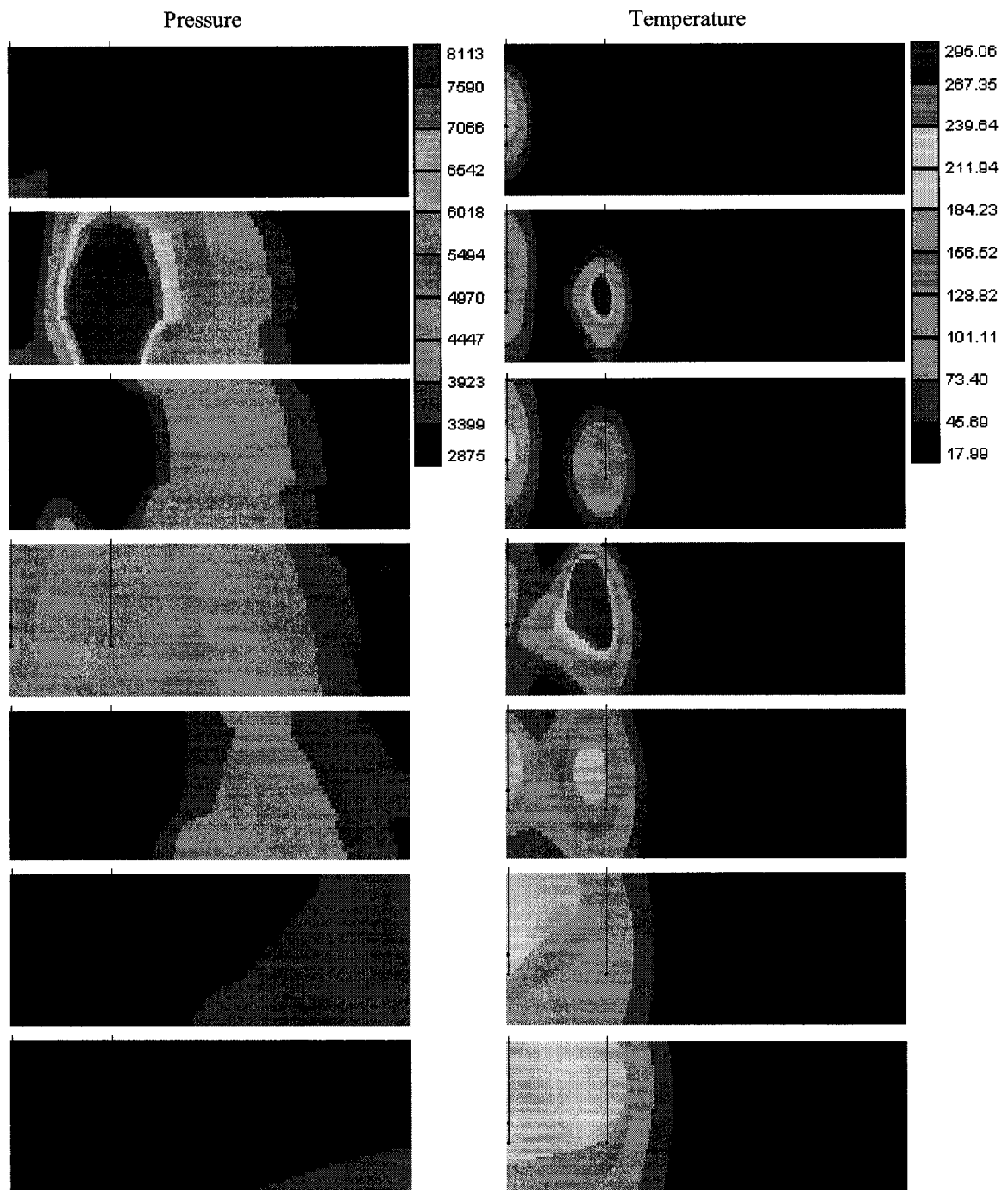
# **APPENDIX C: RESERVOIR SIMULATION RESULTS** **FOR CASES 1-9**



Note: Case 1; 0, 1, 2, 3, 5, 7, 10 year's profiles

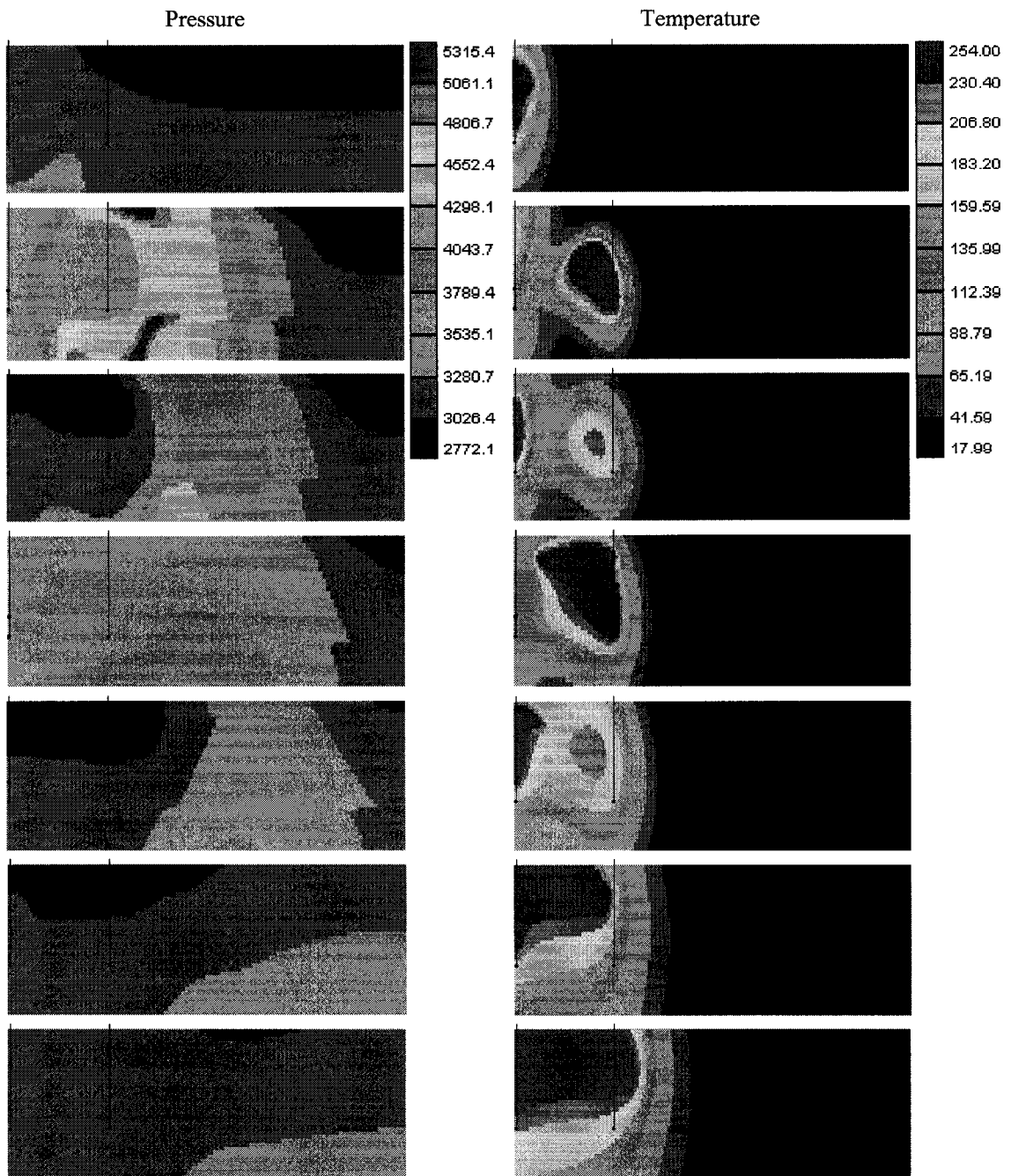
**Figure C-1. Pressure and Temperature Profiles for Case 1**





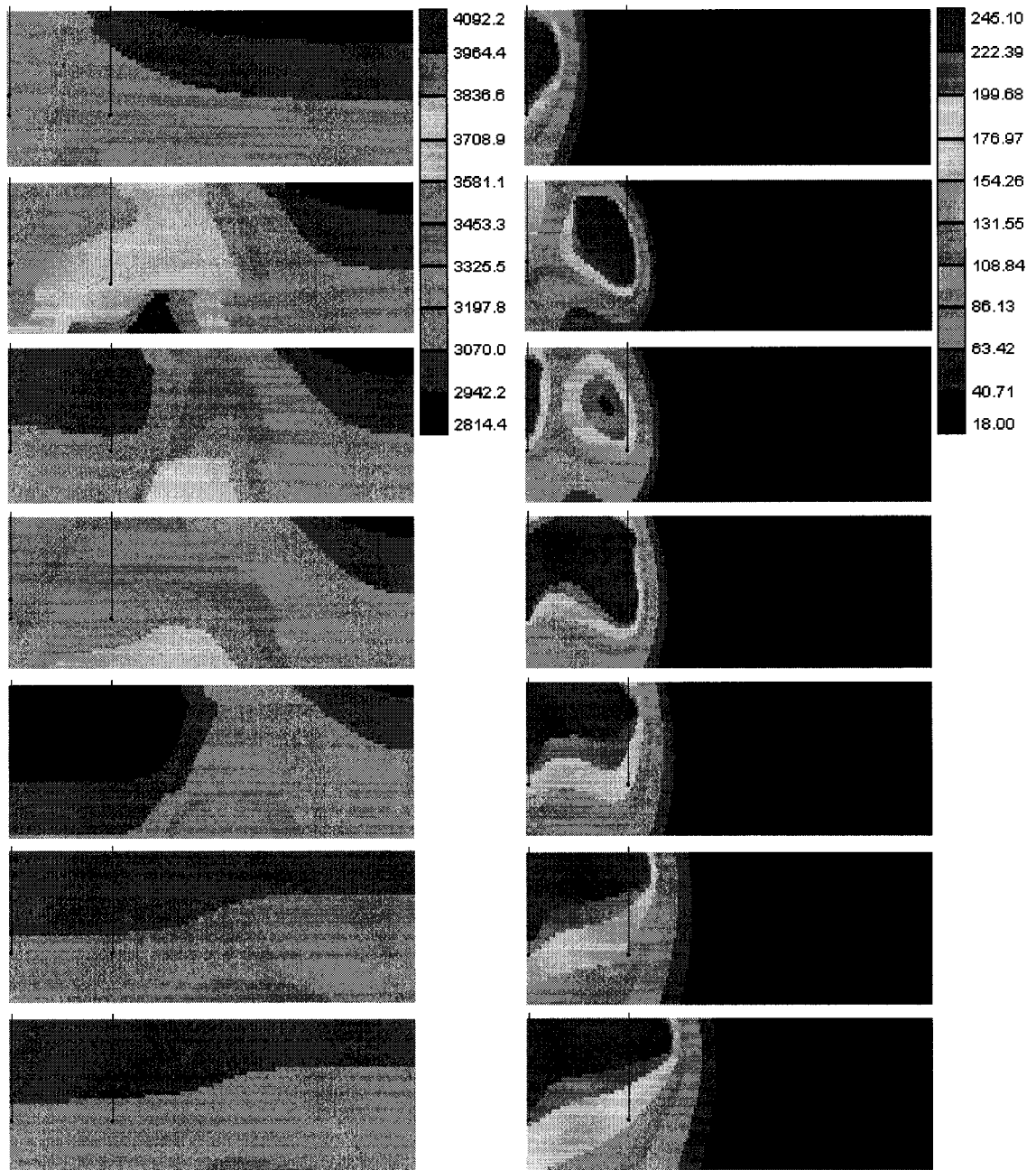
Note: Case 2; 1, 1+9months, 2, 2+6months, 3, 5, 10 year's profiles

**Figure C-2. Pressure and Temperature Profiles for Case 2**



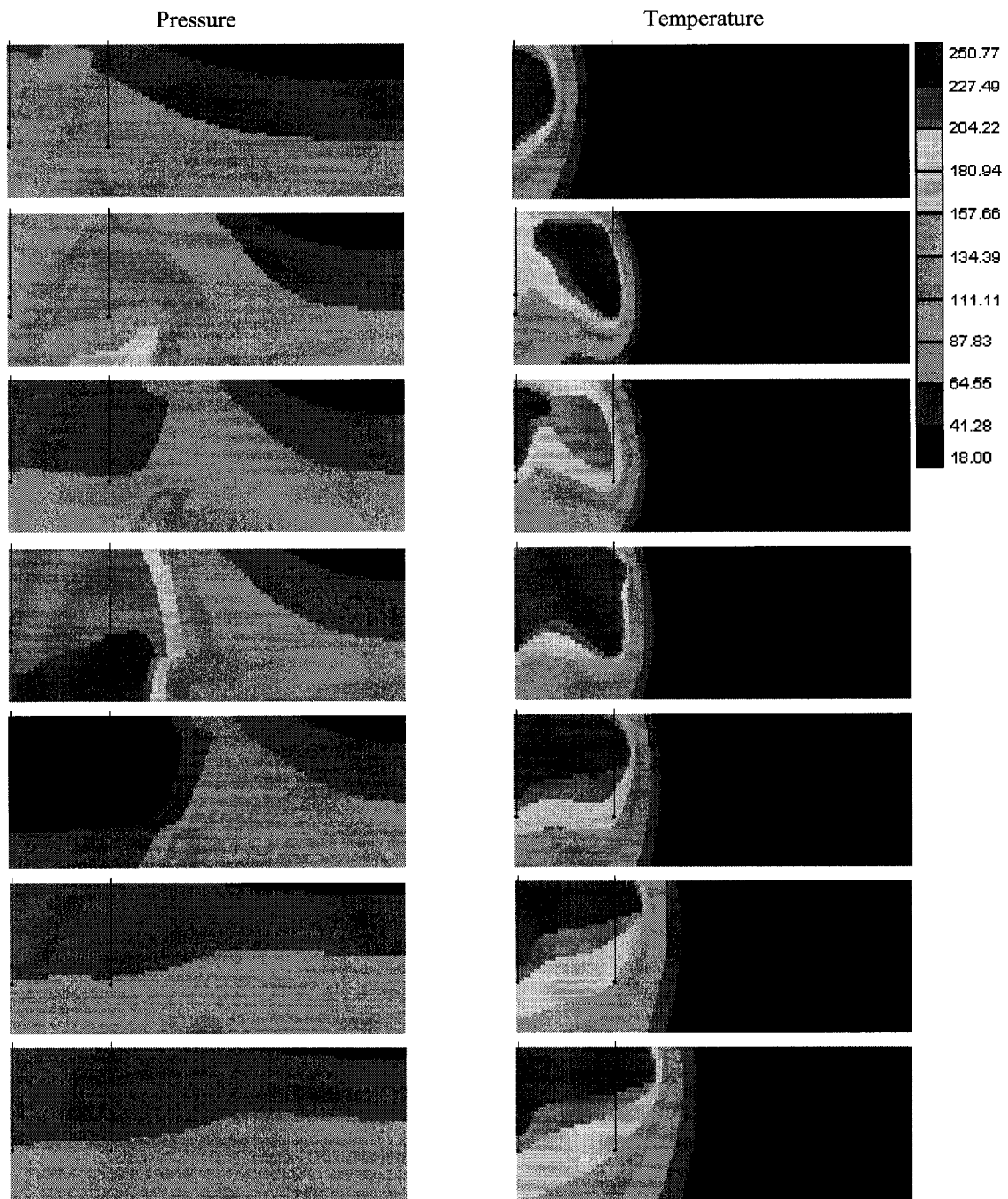
Note: Case 3; 2, 2+9months, 3, 3+6months, 4, 6, 10 year's profiles

**Figure C-3. Pressure and Temperature Profiles for Case 3**



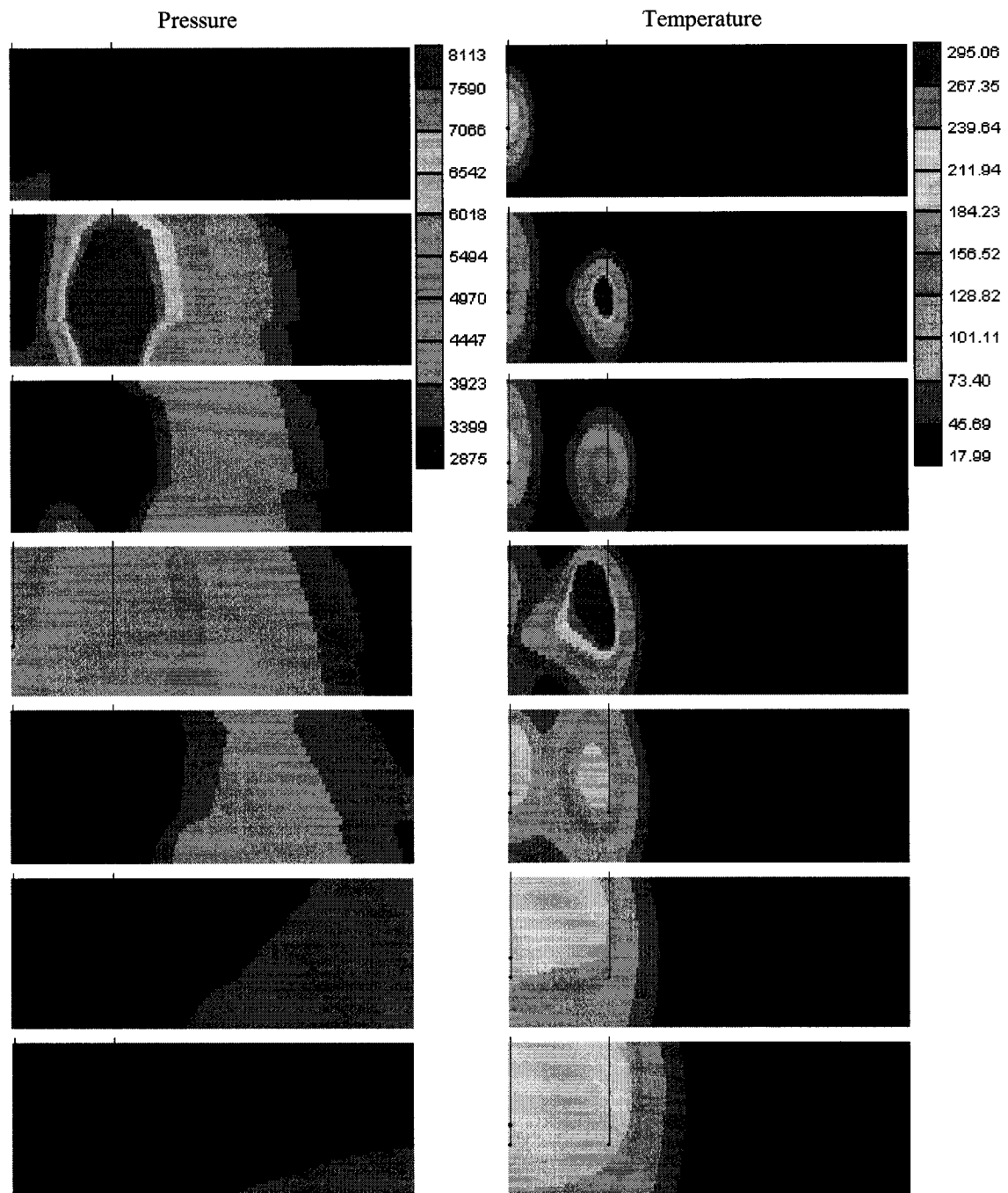
Note: Case 4; 3, 3+9months, 4, 4+6months, 5, 7, 10 year's profiles

**Figure C-4. Pressure and Temperature Profiles for Case 4**



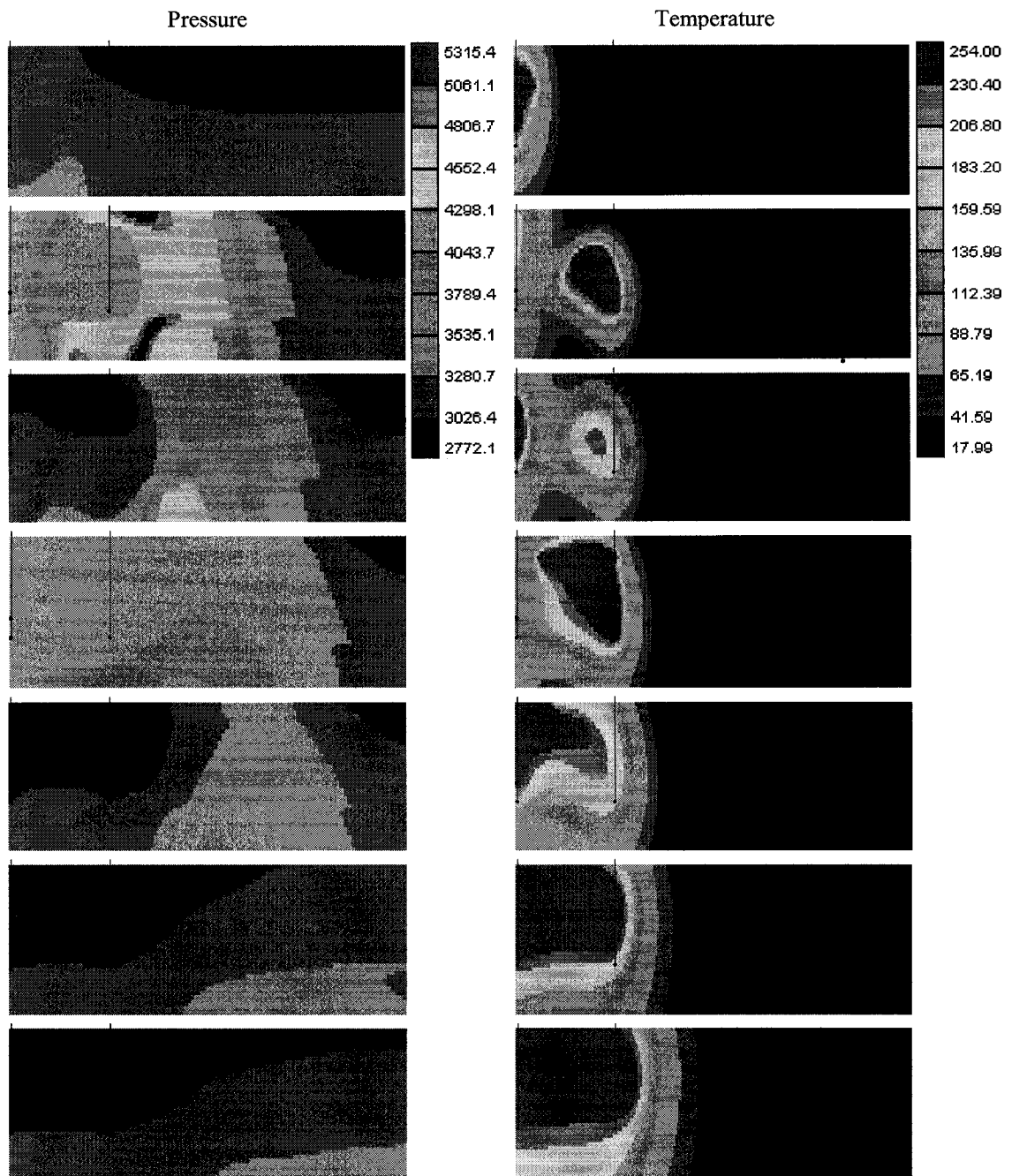
Note: Case 5; 4, 4+9months, 5, 5+6months, 6, 8, 10 year's profiles

**Figure C-5. Pressure and Temperature Profiles for Case 5**



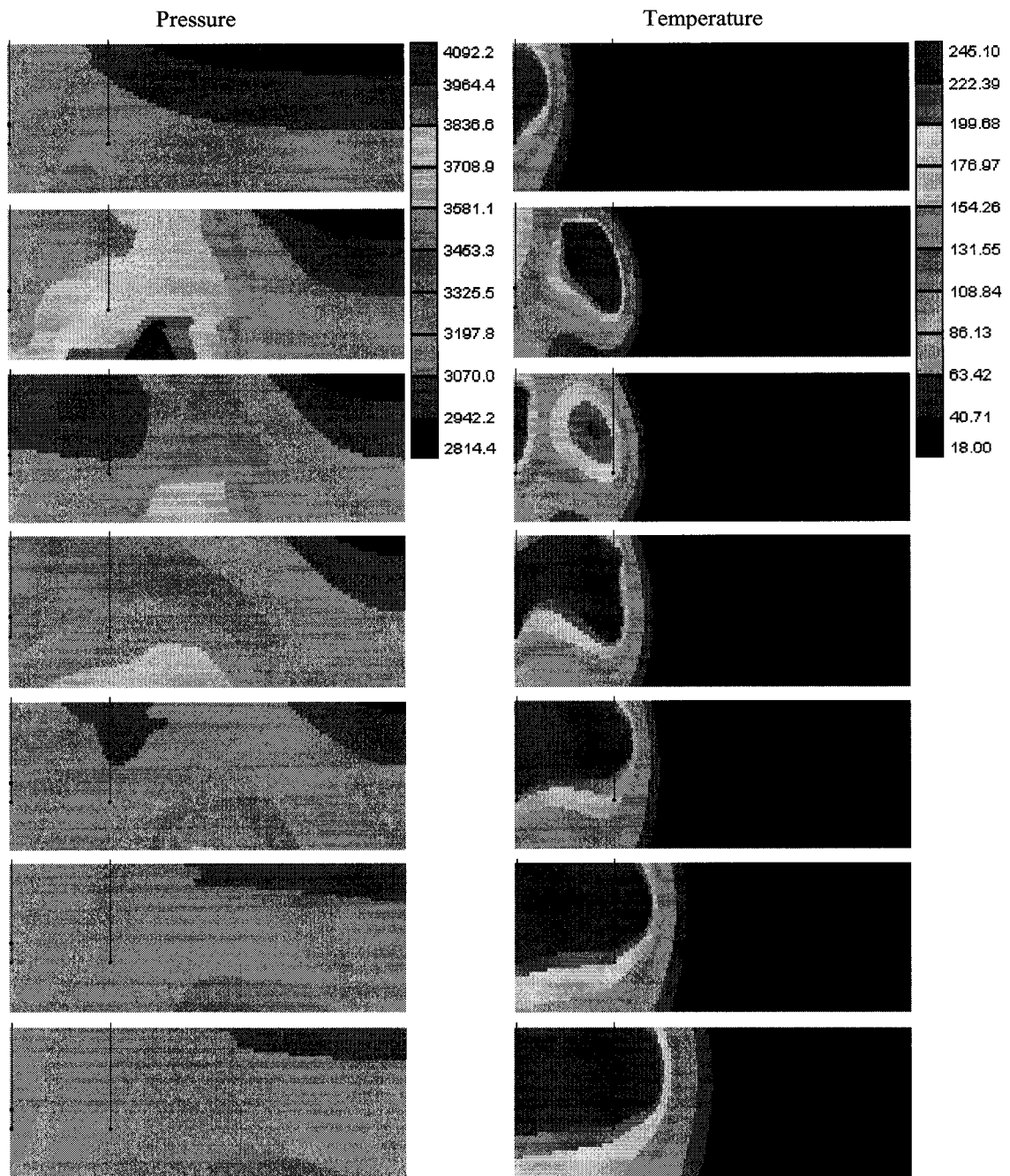
Note: Case 6; 1, 1+9months, 2, 2+6months, 3, 5, 10 year's profiles

**Figure C-6. Pressure and Temperature Profiles for Case 5**



Note: Case 7; 2, 2+9months, 3 3+6months, 4, 6, 10 year's profiles

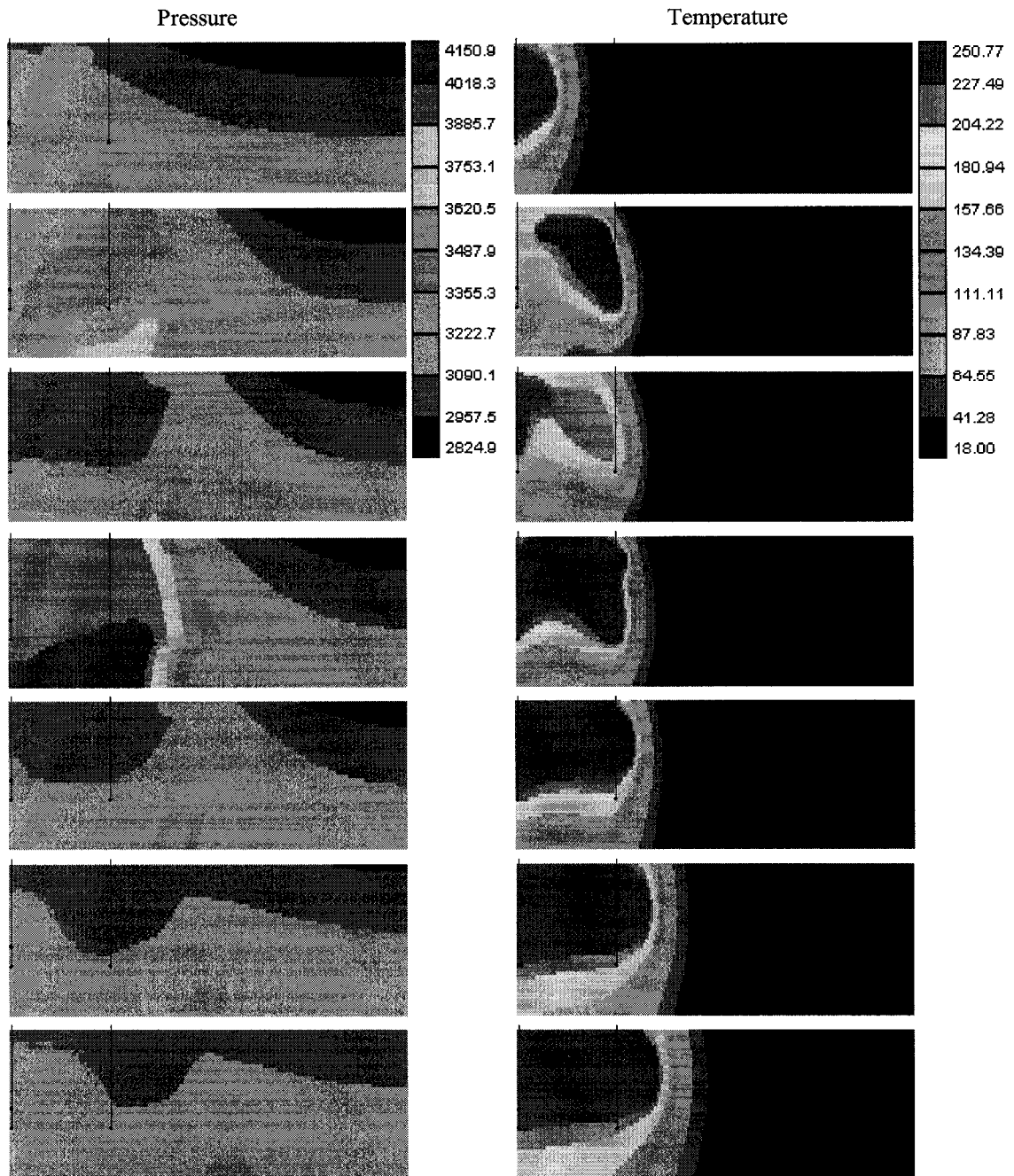
**Figure C-7. Pressure and Temperature Profiles for Case 7**



Note: Case 8; 3, 3+9months, 4 4+6months, 5, 7, 10 year's profiles

**Figure C-8. Pressure and Temperature Profiles for Case 8**

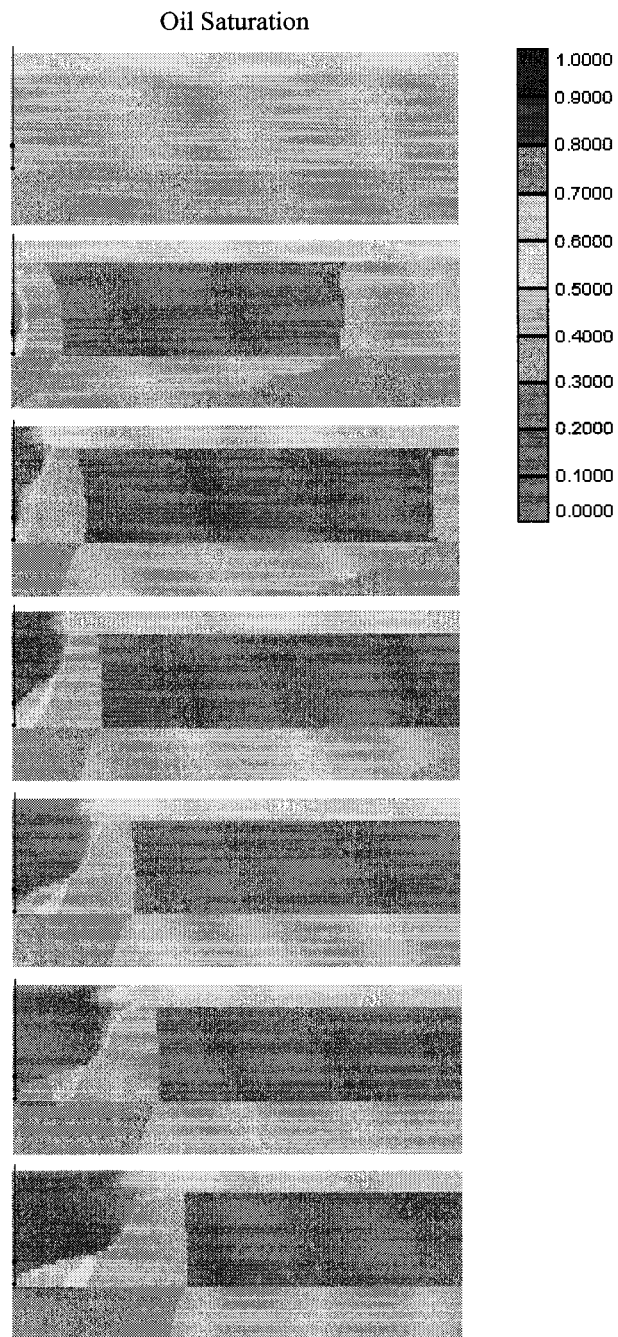




Note: Case 9; 4, 4+9months, 5, 5+6months, 6, 8, 10 year's profiles

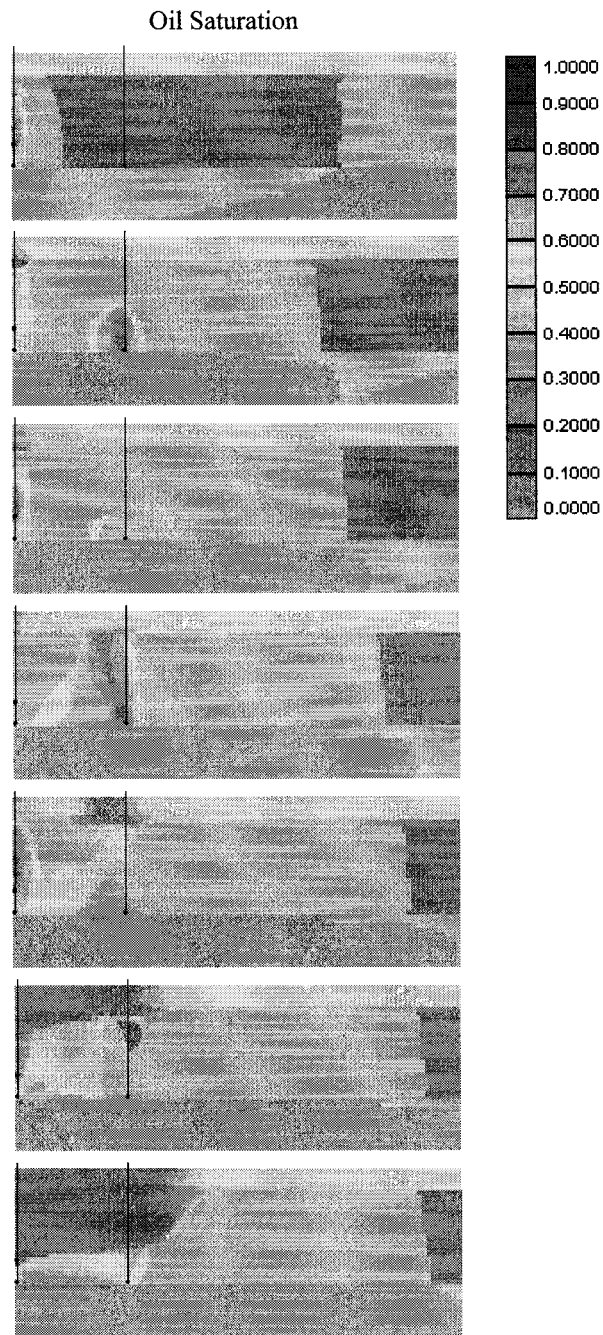
**Figure C-9. Pressure and Temperature Profiles for Case 9**





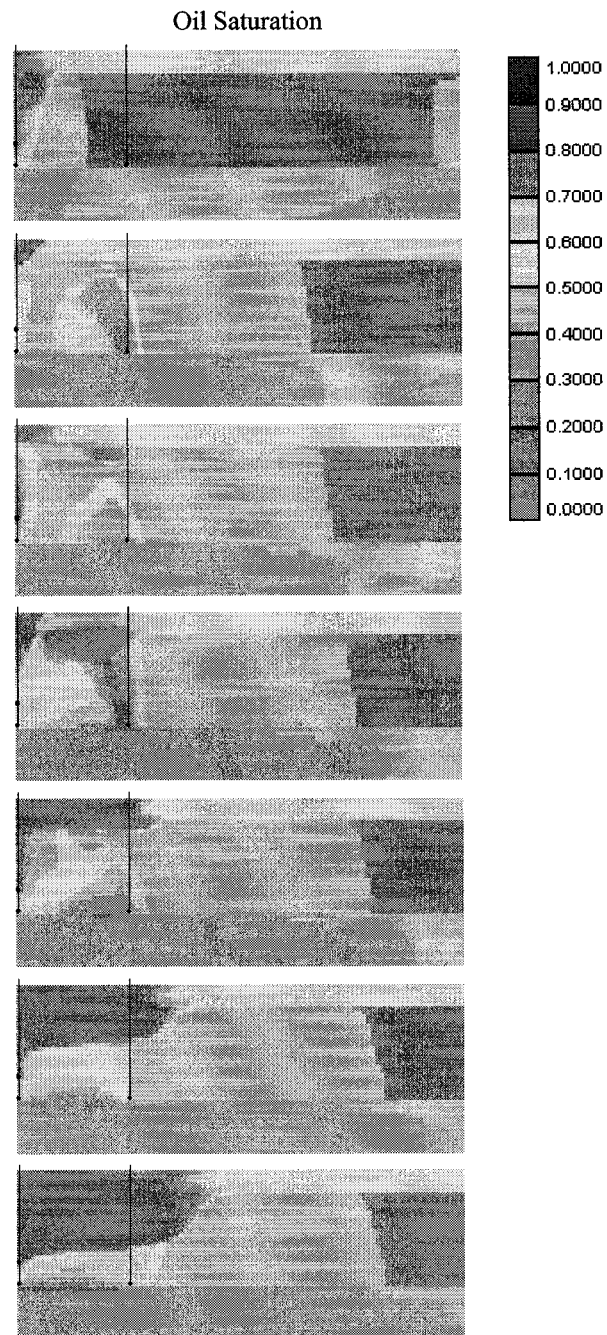
Note: Case 1; 0, 1, 2, 3, 5, 7, 10 year's profiles

**Figure C-10. Oil Saturation Profiles for Case 1**



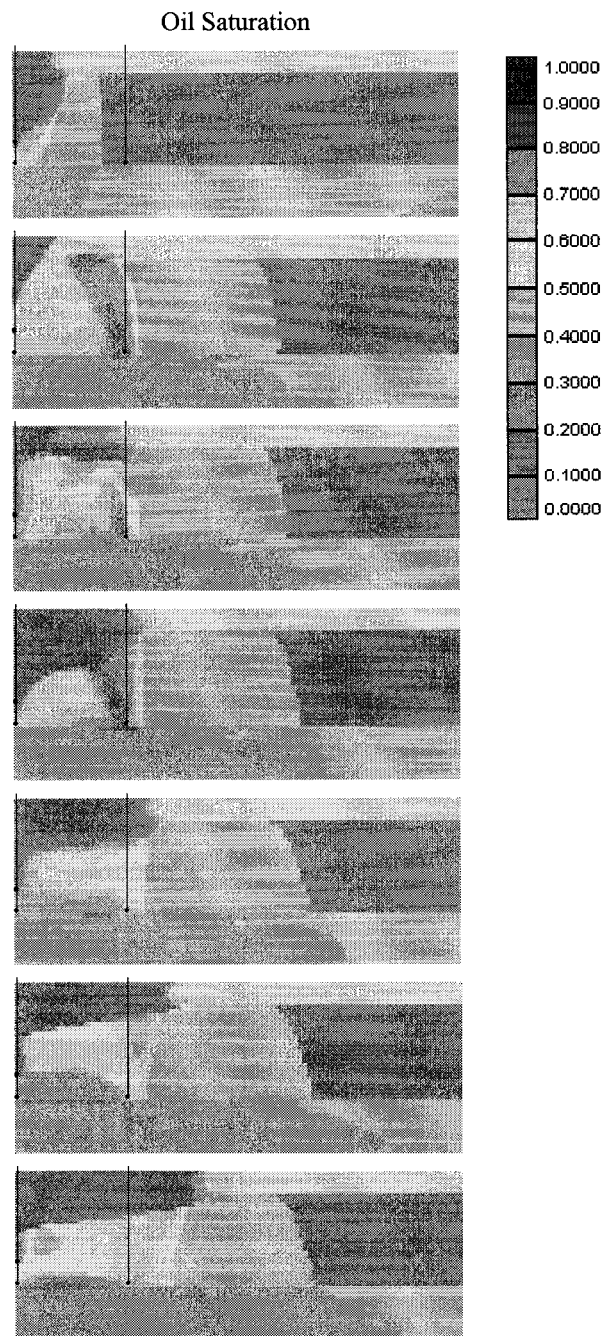
Note: Case 2; 1, 1+9months, 2, 2+6months, 3, 5, 10 year's

**Figure C-11. Oil Saturation Profiles for Case 2**



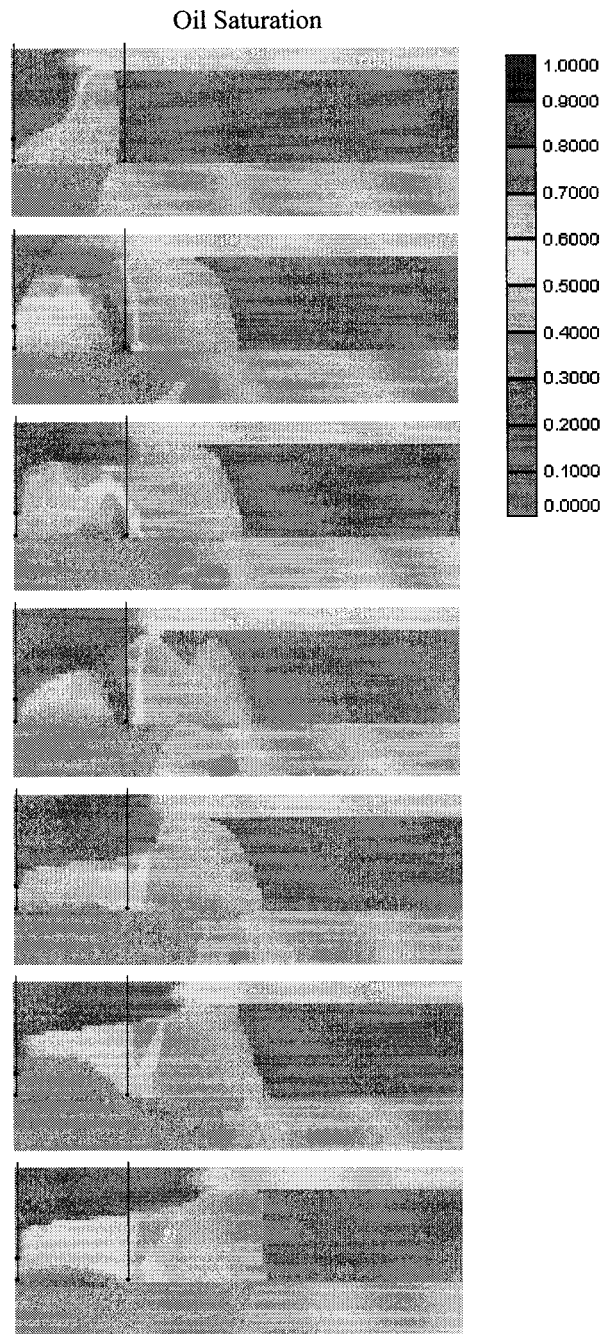
Note: Case 3; 2, 2+9months, 3, 3+6months, 4, 6, 10 year's

**Figure C-12. Oil Saturation Profiles for Case 3**



Note: Case 4; 1, 1+9months, 2, 2+6months, 3, 5, 10 year's profiles

**Figure C-13. Oil Saturation Profiles for Case 4**



Note: Case 5; 4, 4+9months, 5, 5+6months, 6, 8, 10 year's profiles

**Figure C-14. Oil Saturation Profiles for Case 5**

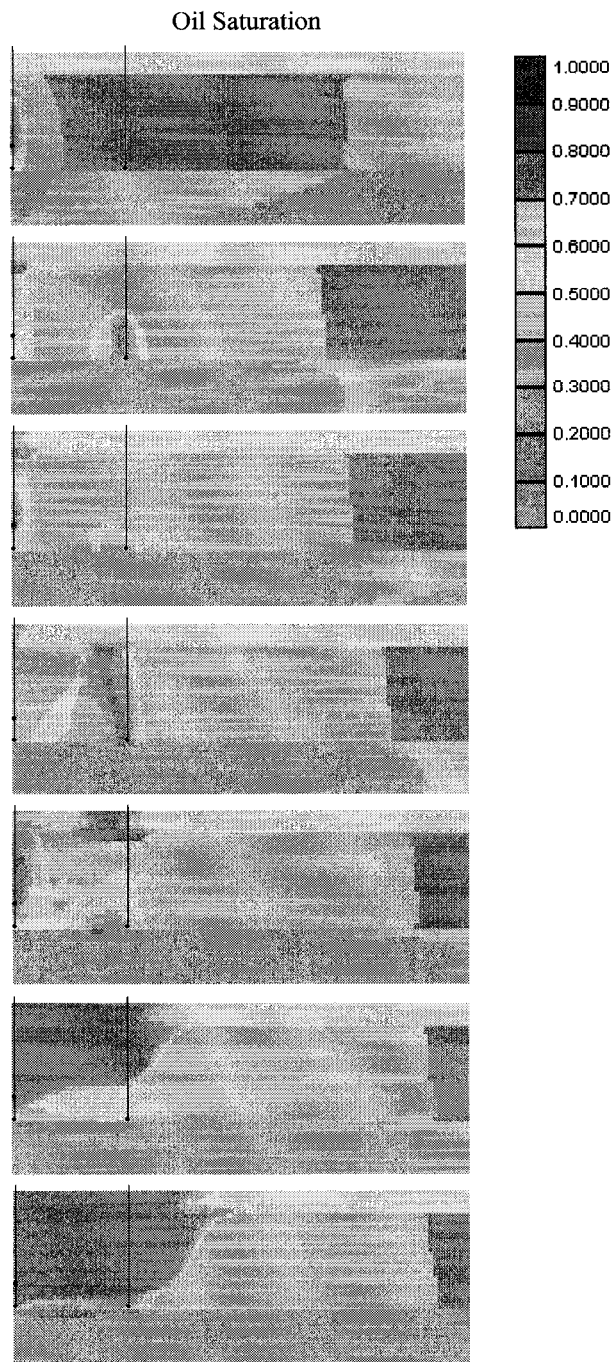
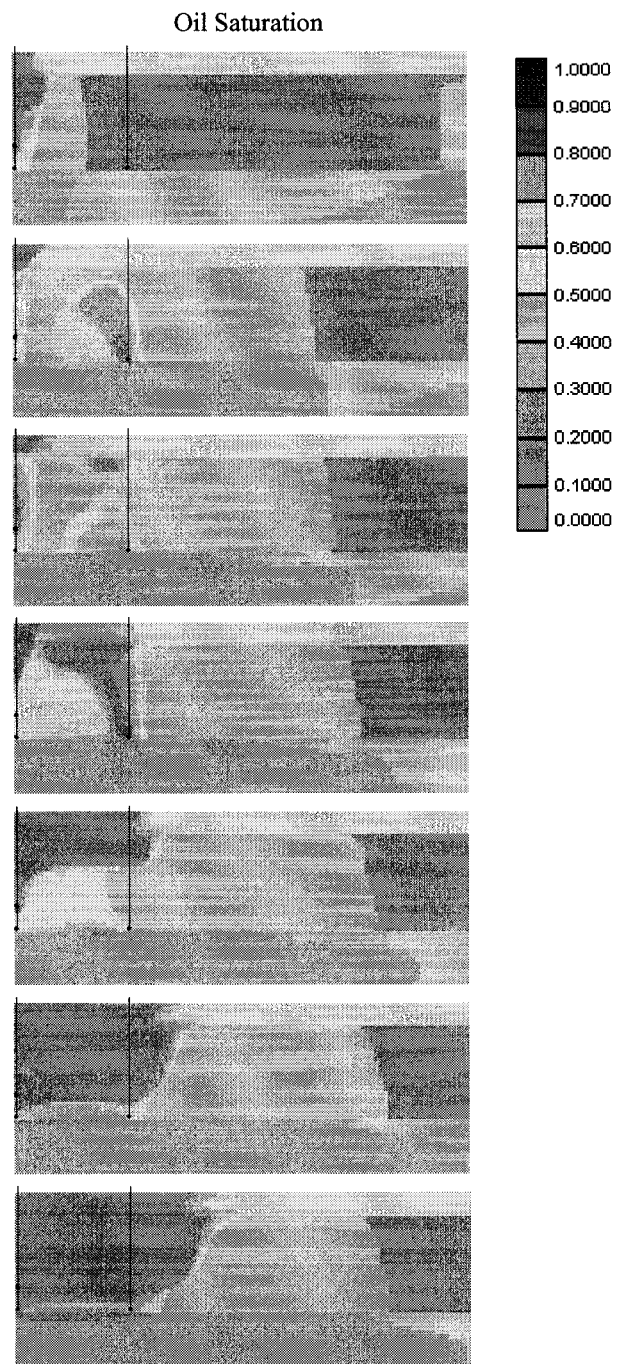


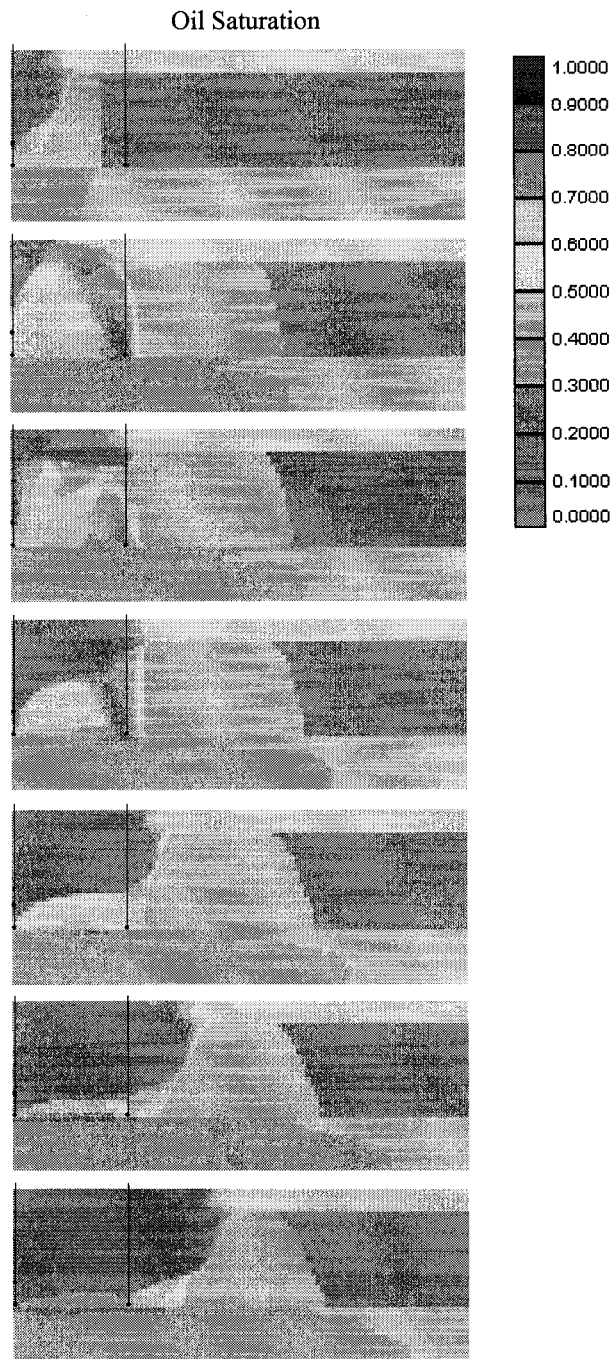
**Figure C-15. Oil Saturation Profiles for Case 6**



Note: Case 7; 2, 2+9months, 3, 3+6months, 4, 6, 10 year's profiles

**Figure C-16. Oil Saturation Profiles for Case 7**

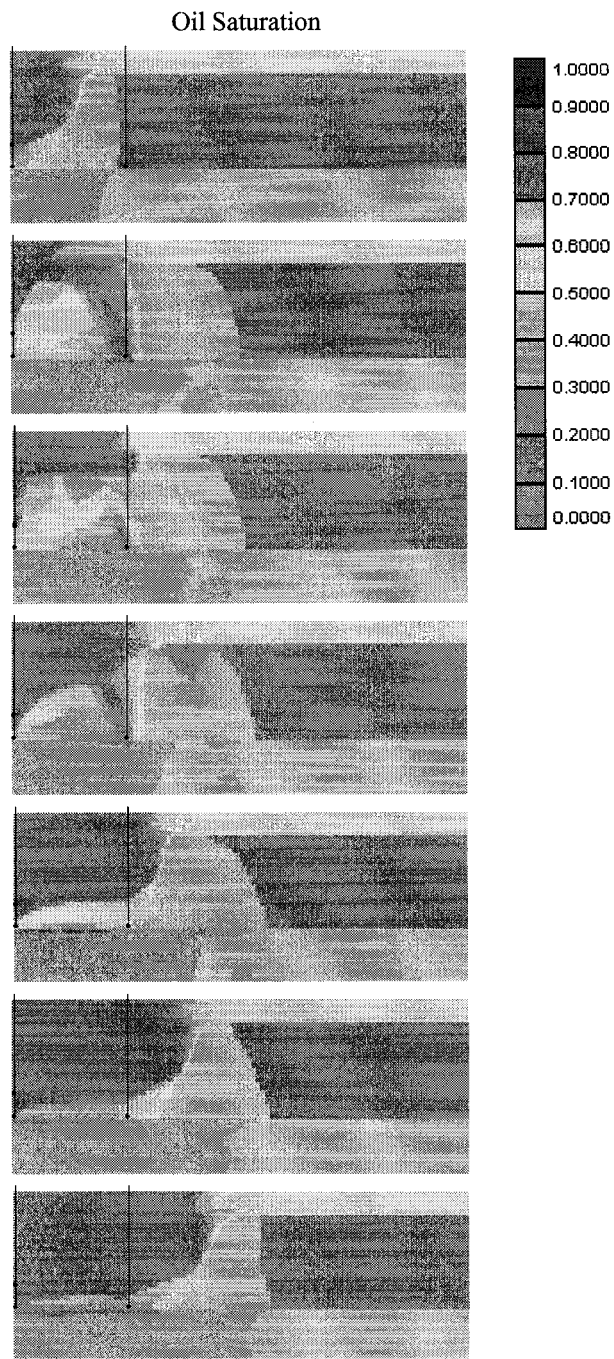




Note: Case 8; 1, 1+9months, 2, 2+6months, 3, 5, 10 year's profiles

**Figure C-17. Oil Saturation Profiles for Case 8**





Note: Case 9; 4, 4+9months, 5, 5+6months, 6, 8, 10 year's profiles

**Figure C-18. Oil Saturation Profiles for Case 9**

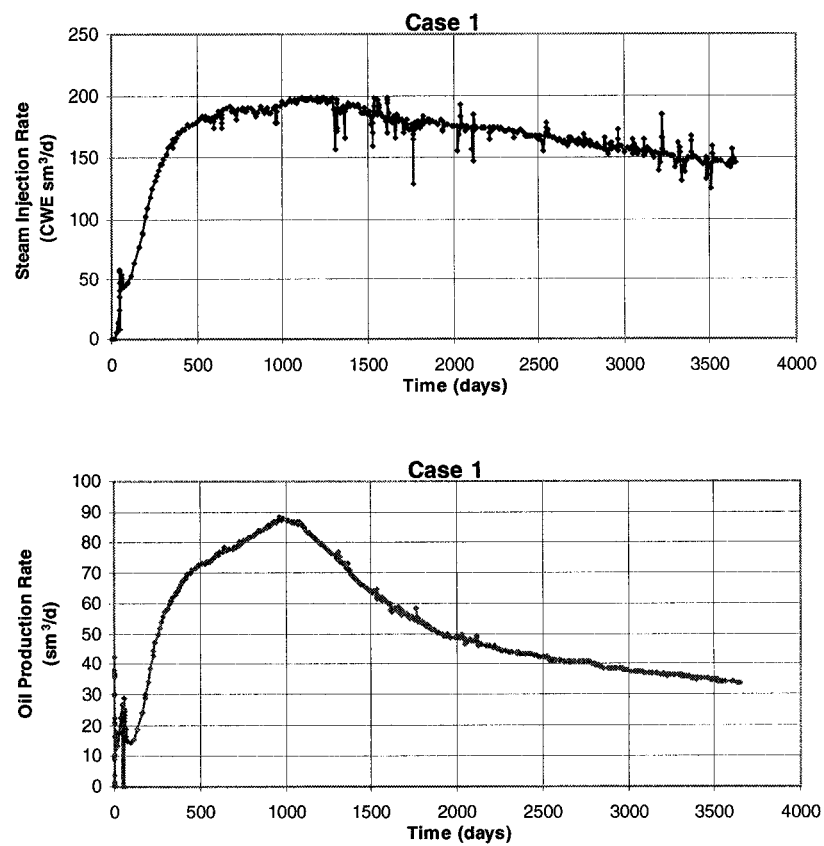


**Figure C-19. Injection and Production Rate for Case 1**

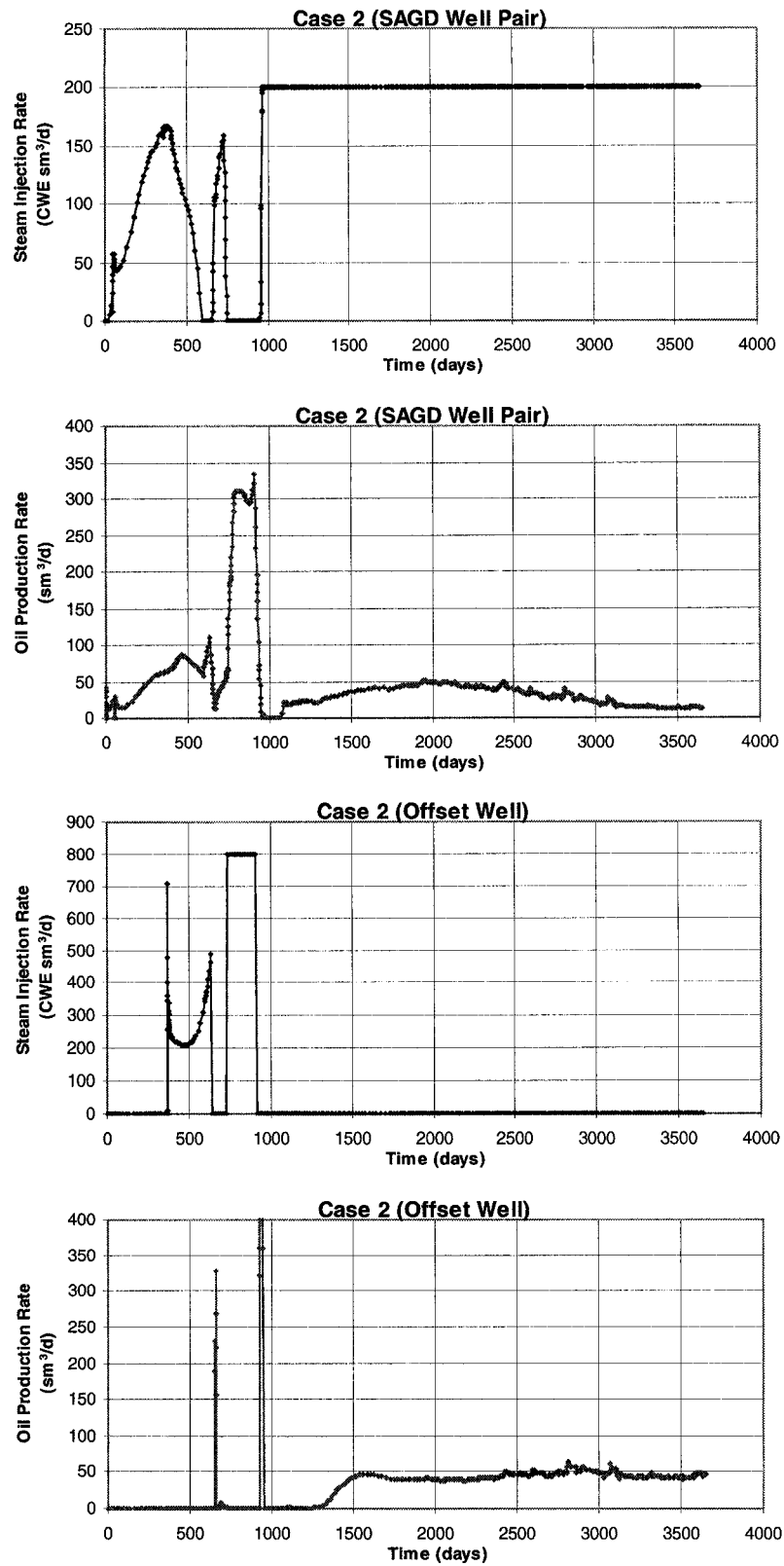


**Figure C-20. Injection and Production Rate for Case 2**

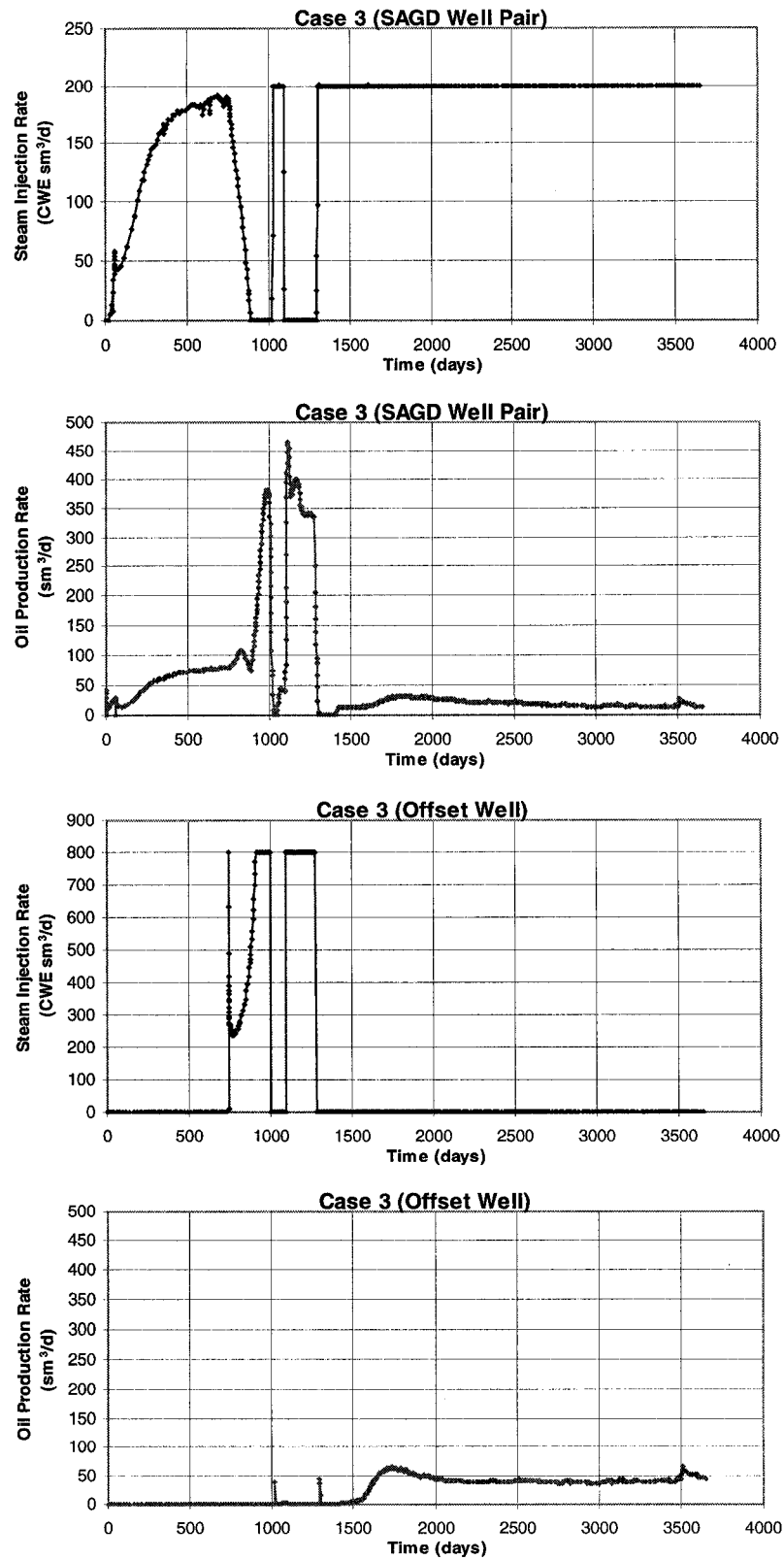


**Figure C-21. Injection and Production Rate for Case 3**

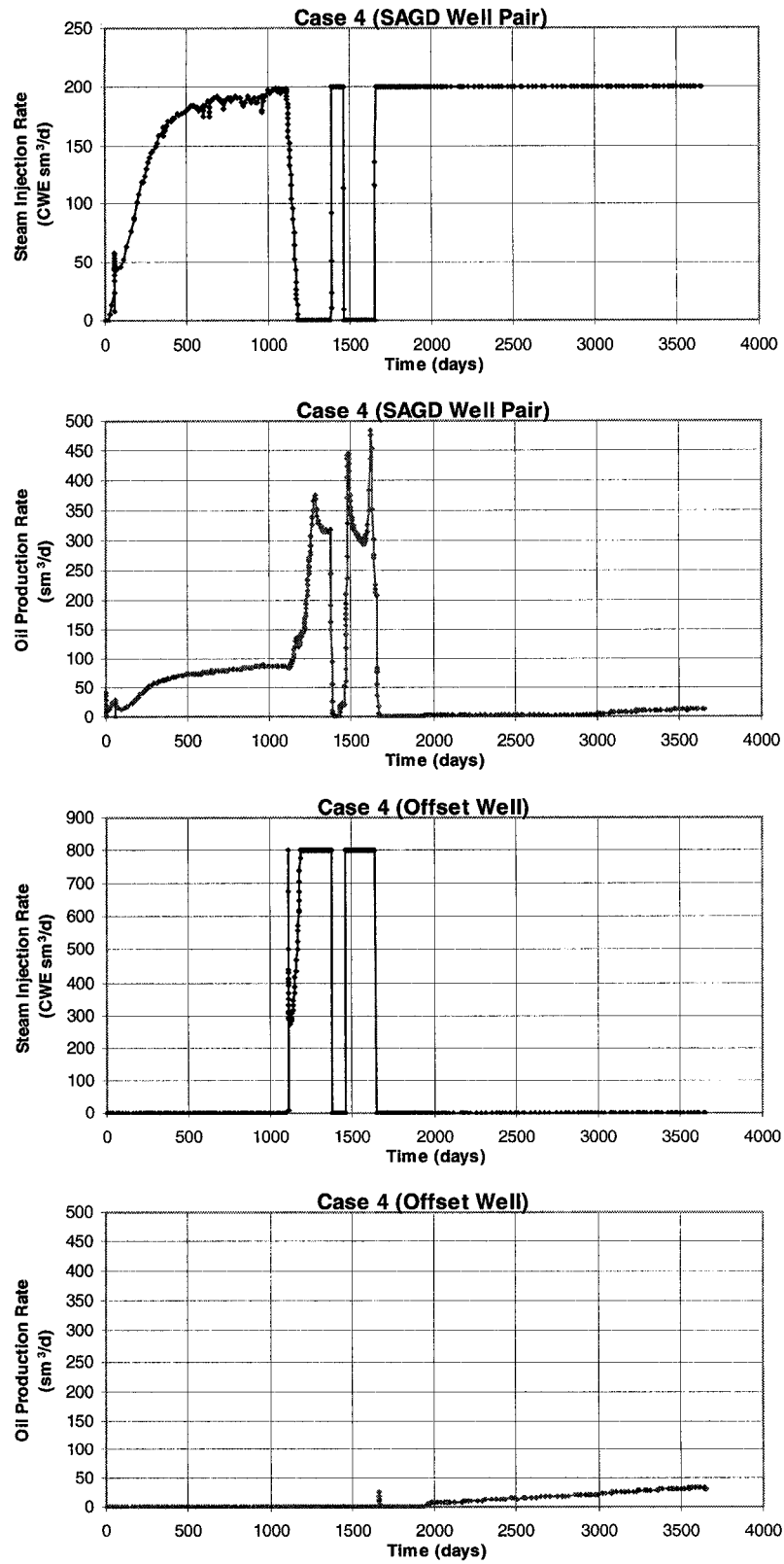


**Figure C-22. Injection and Production Rate for Case 4**

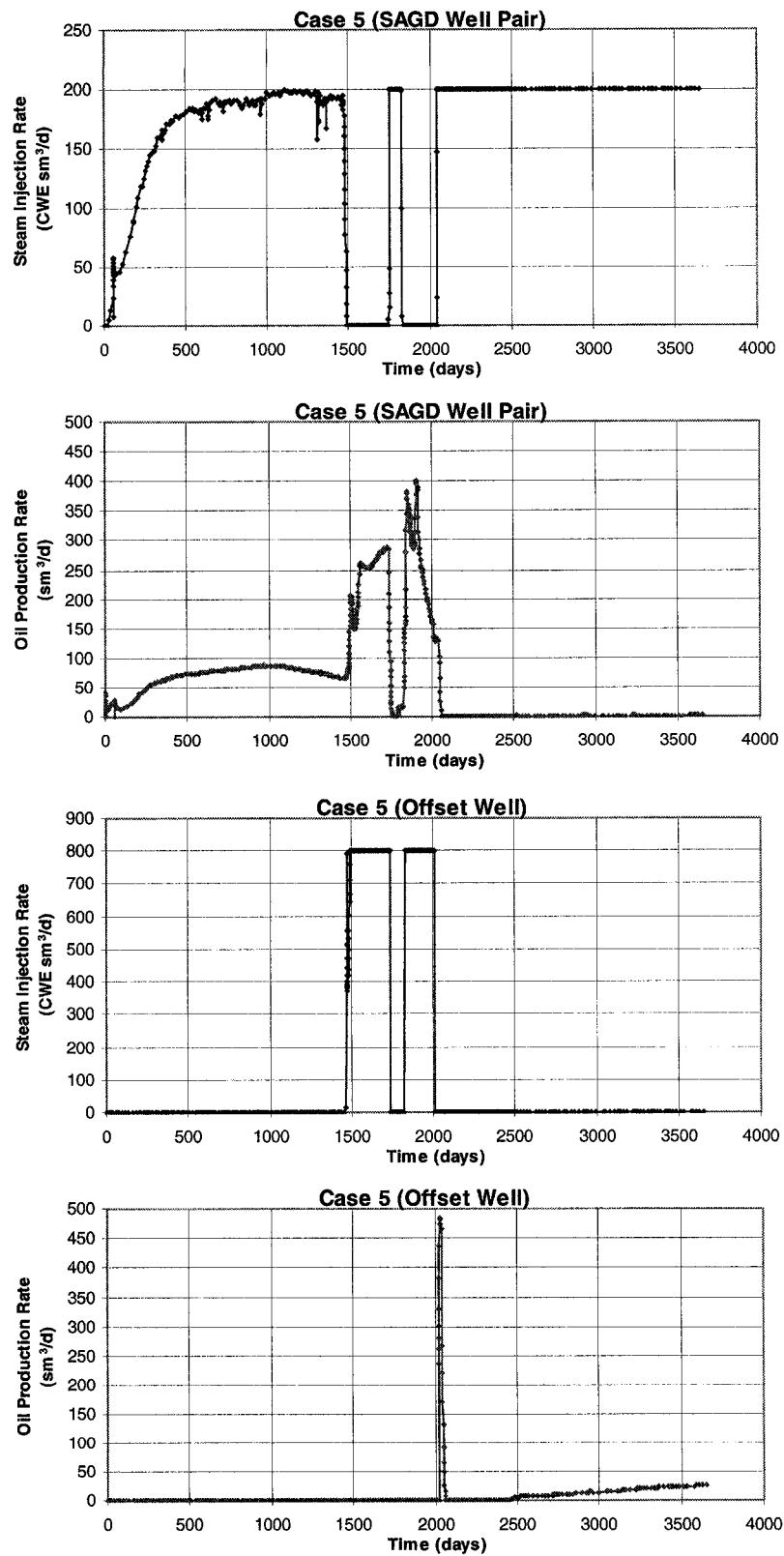


**Figure C-23. Injection and Production Rate for Case 5**

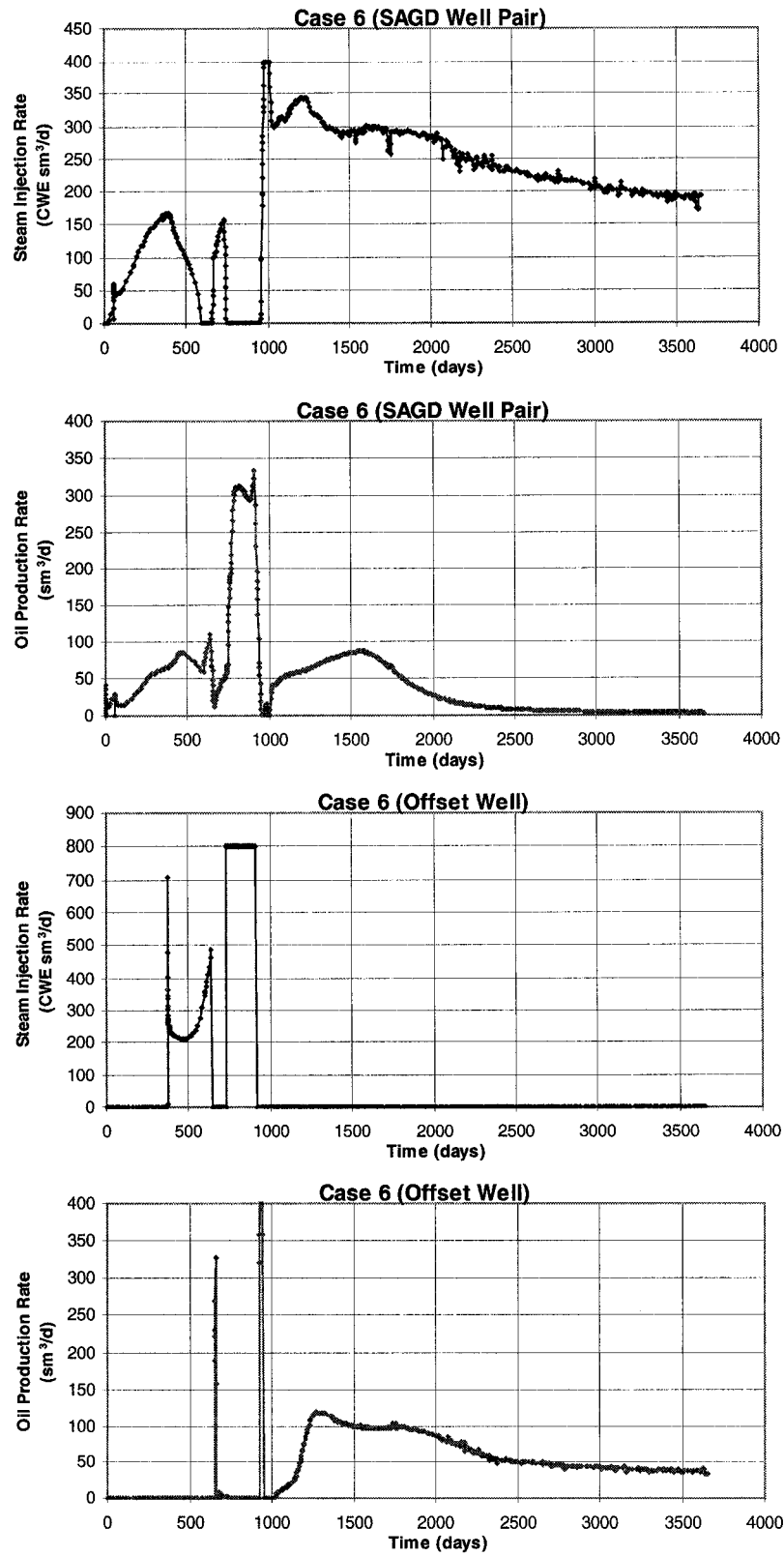


**Figure C-24. Injection and Production Rate for Case 6**

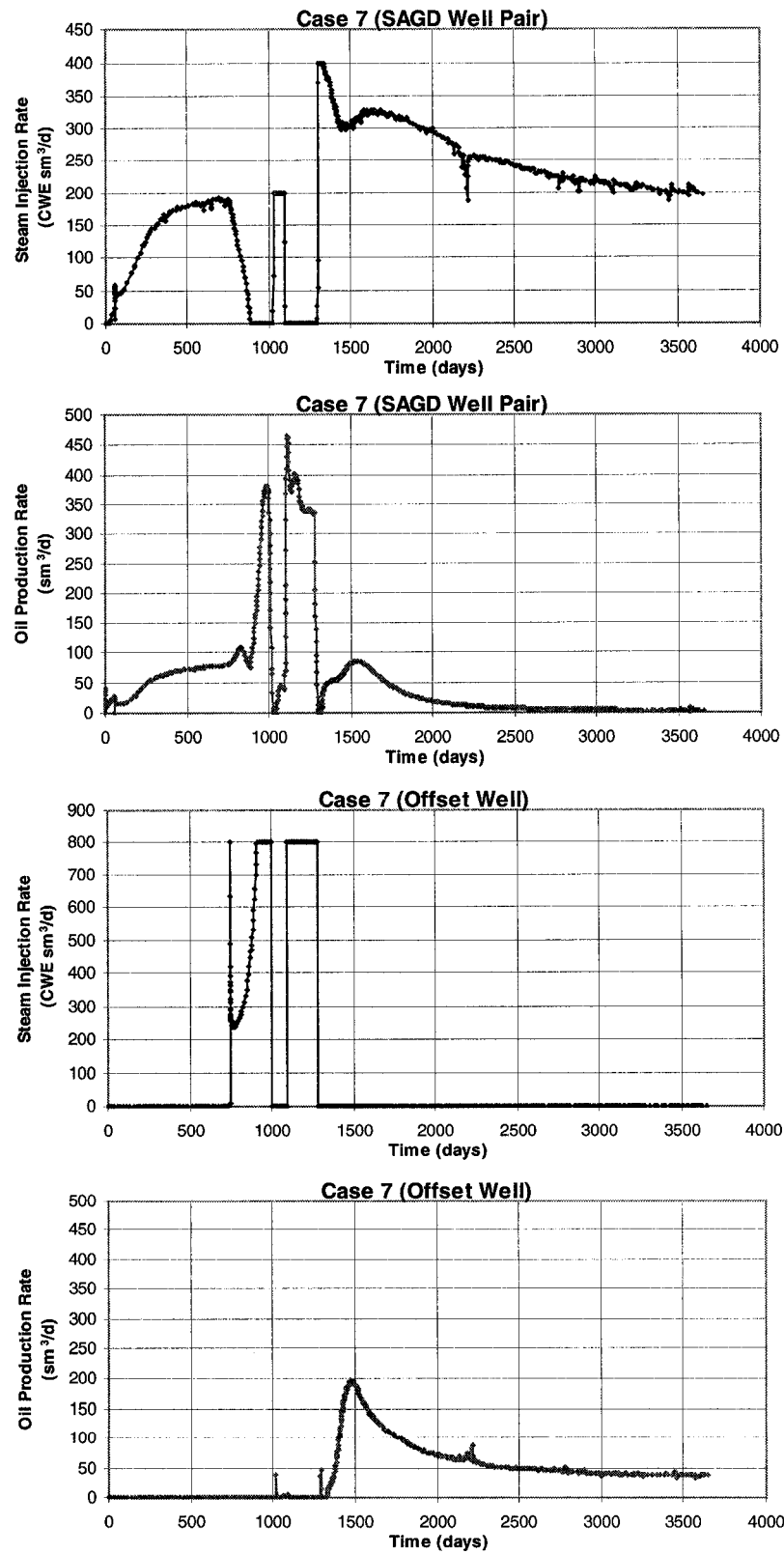


**Figure C-25. Injection and Production Rate for Case 7**



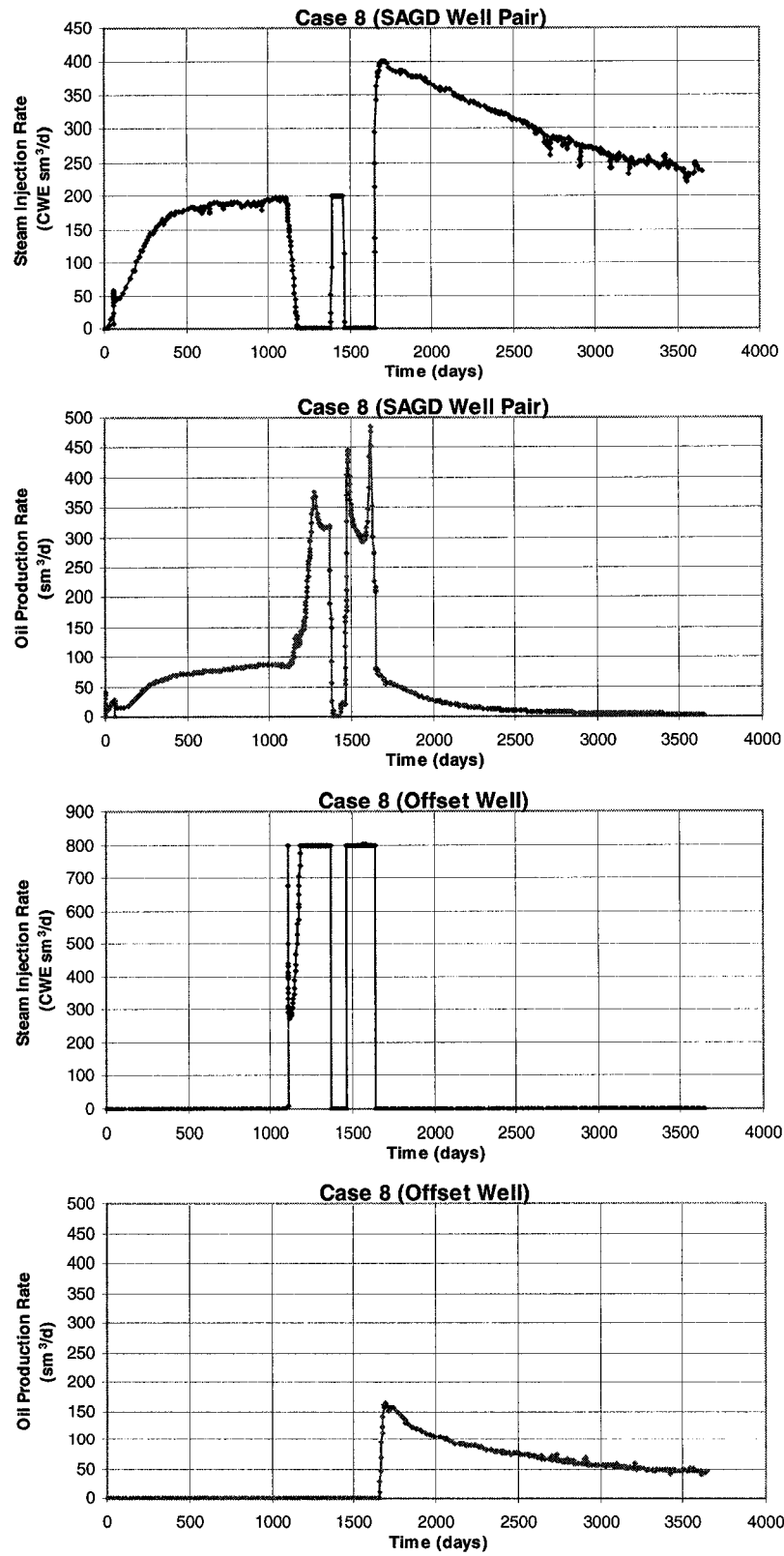


**Figure C-26. Injection and Production Rate for Case 8**

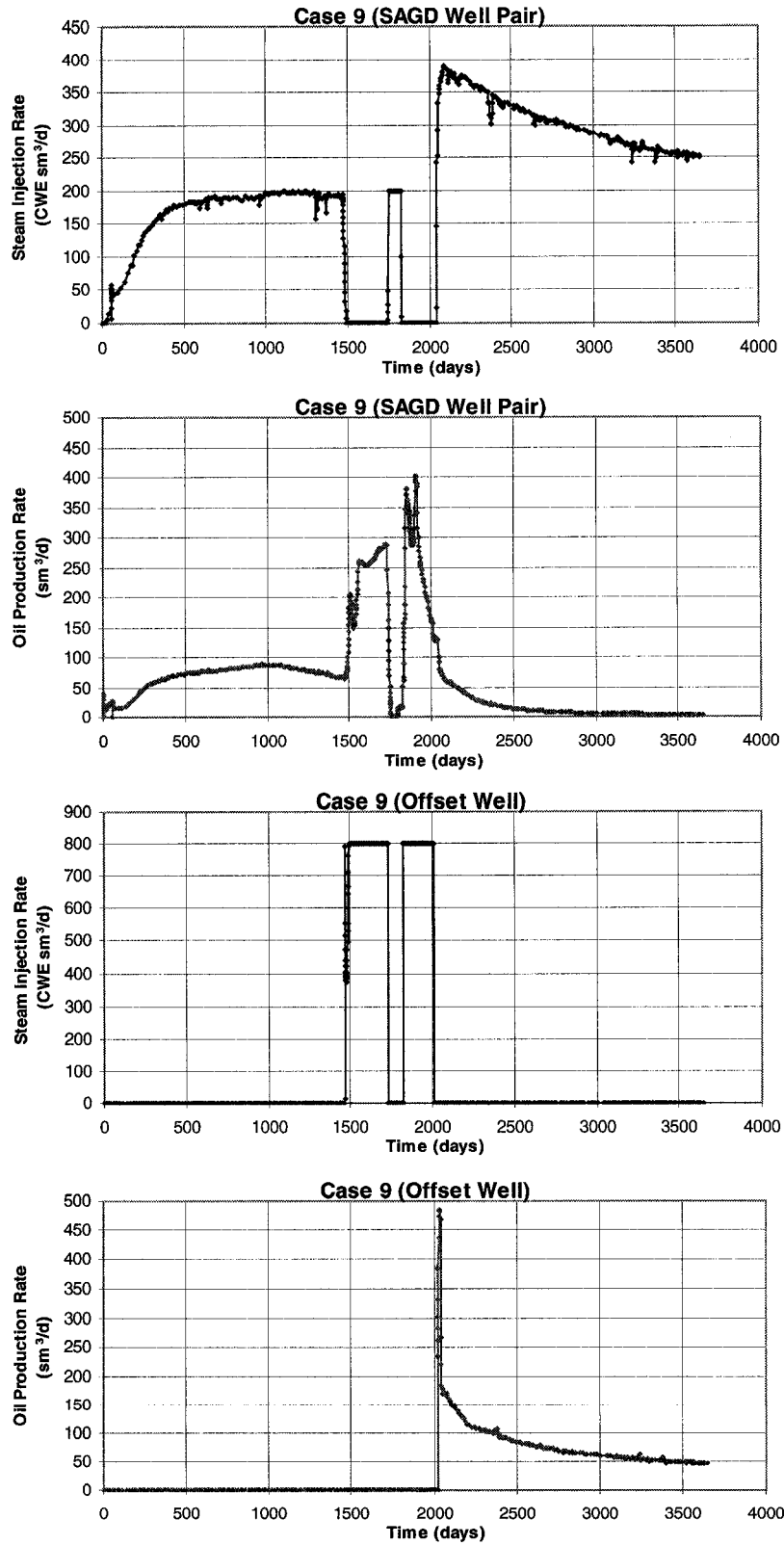


**Figure C-27. Injection and Production Rate for Case 9**

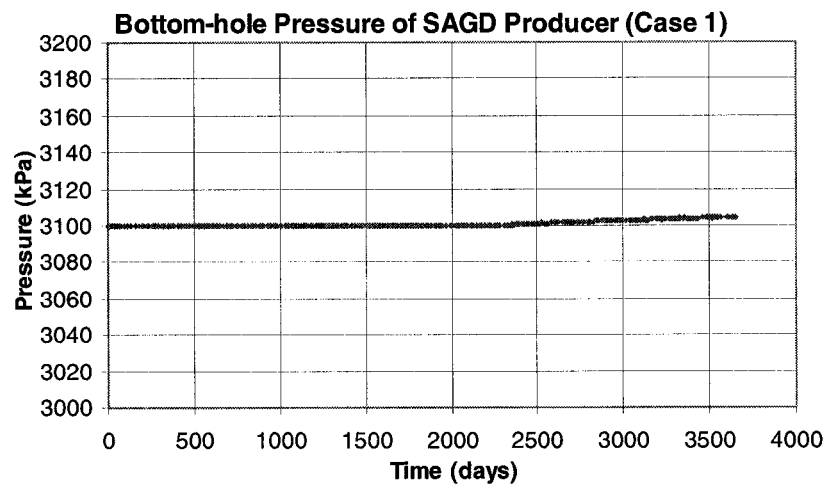
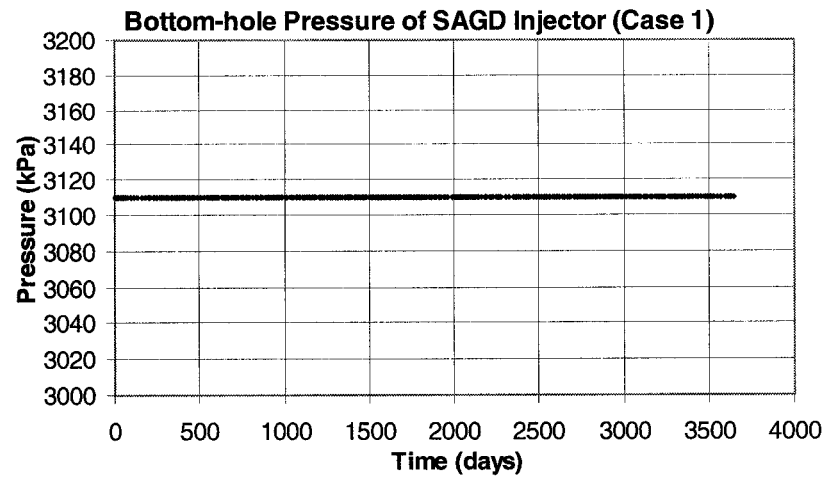


**Figure C-28. Bottom-hole Pressure of Wells for Case 1**

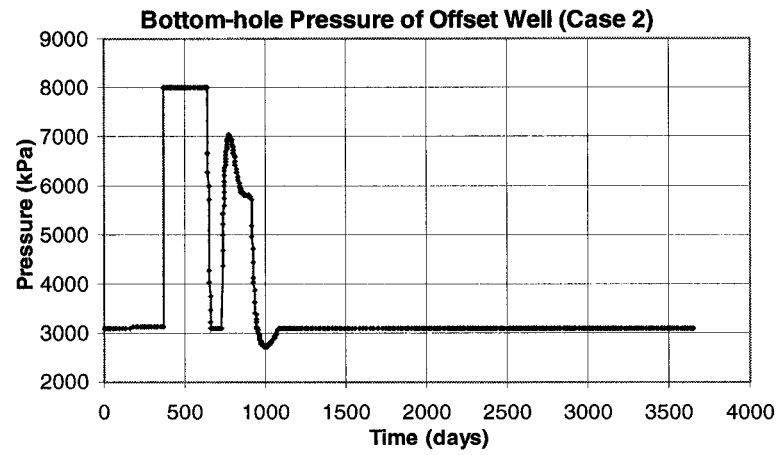
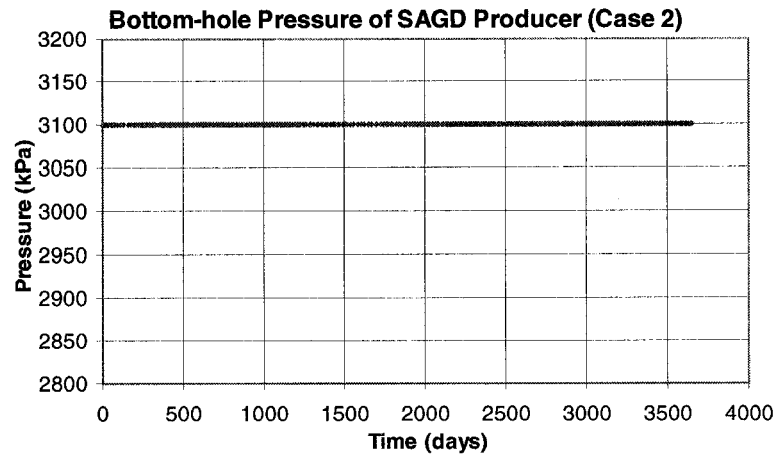
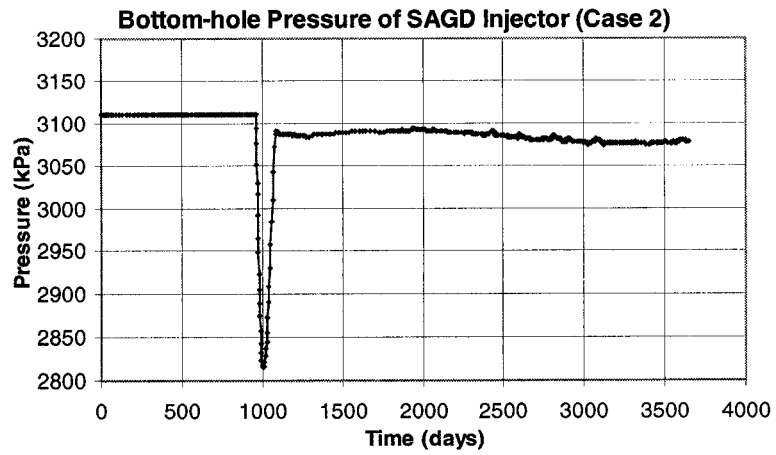


**Figure C-29. Bottom-hole Pressure of Wells for Case 2**

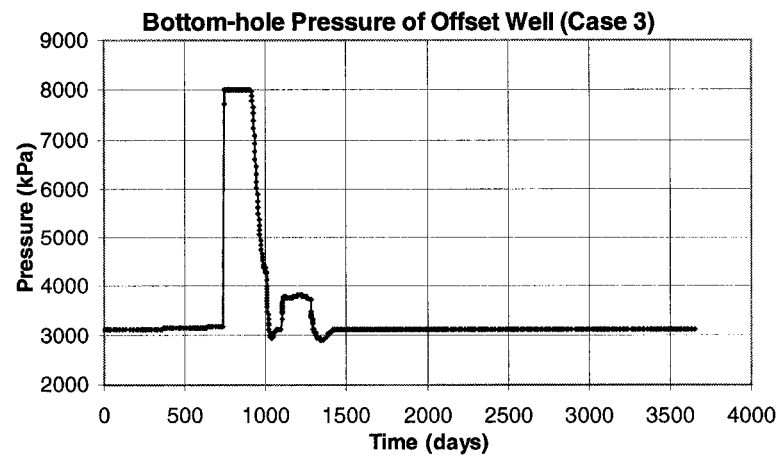
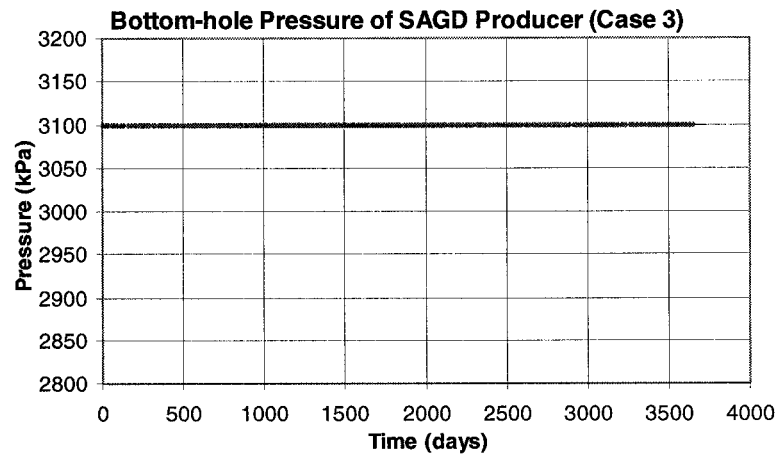
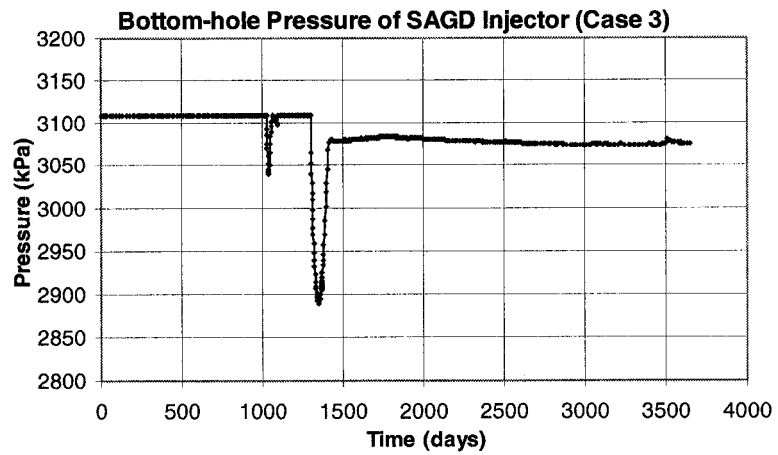


**Figure C-30. Bottom-hole Pressure of Wells for Case 3**

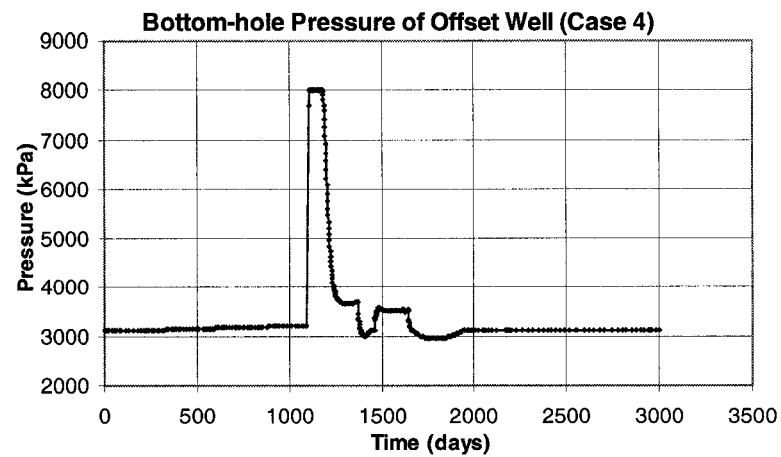
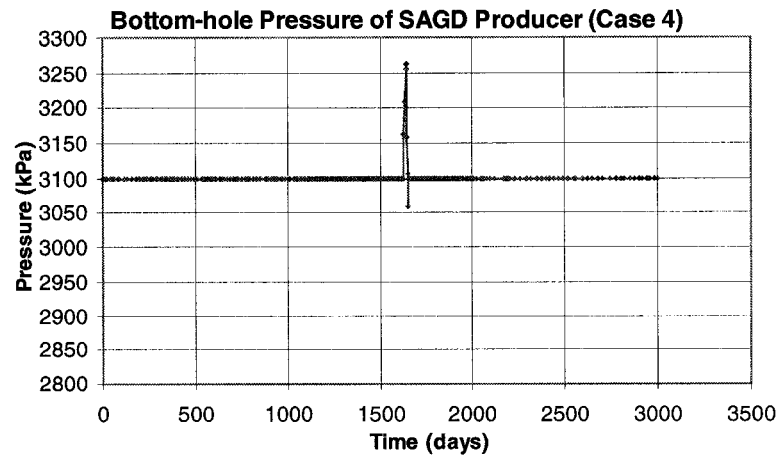
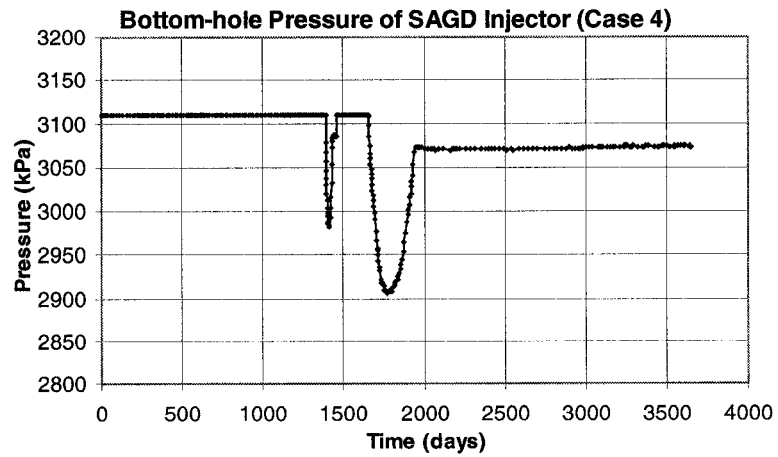


**Figure C-31. Bottom-hole Pressure of Wells for Case 4**

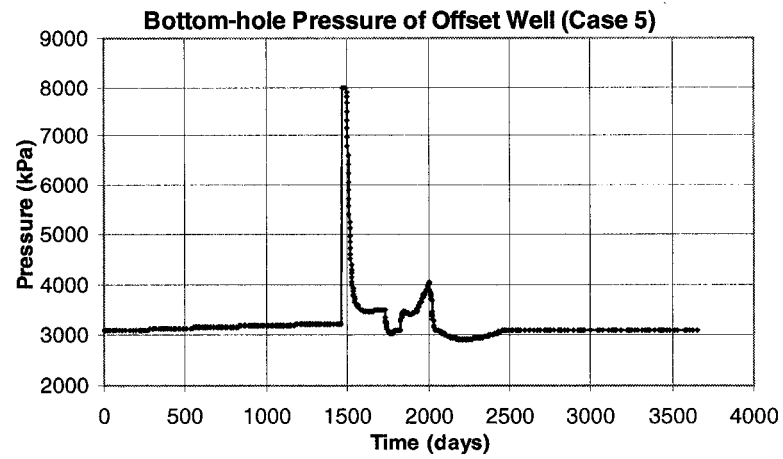
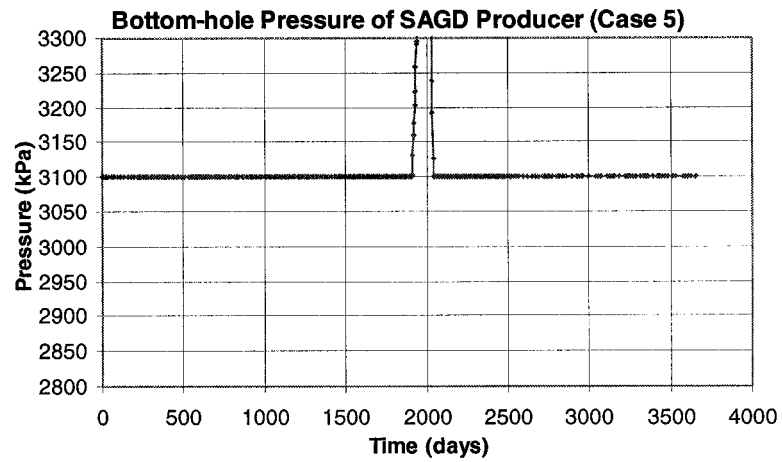
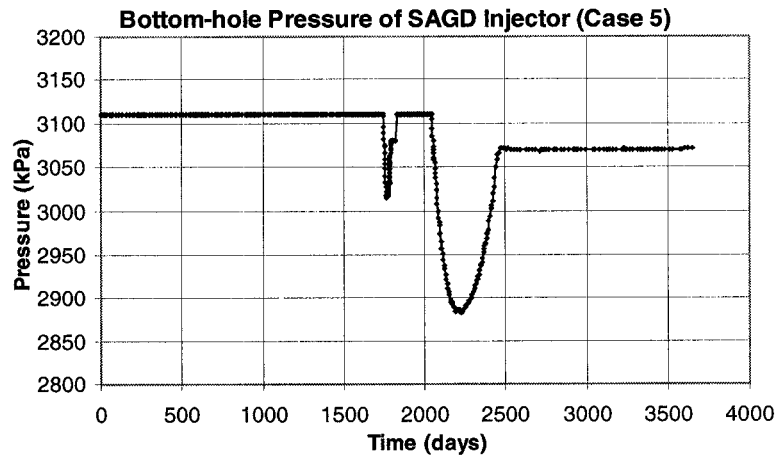


**Figure C-32. Bottom-hole Pressure of Wells for Case 5**

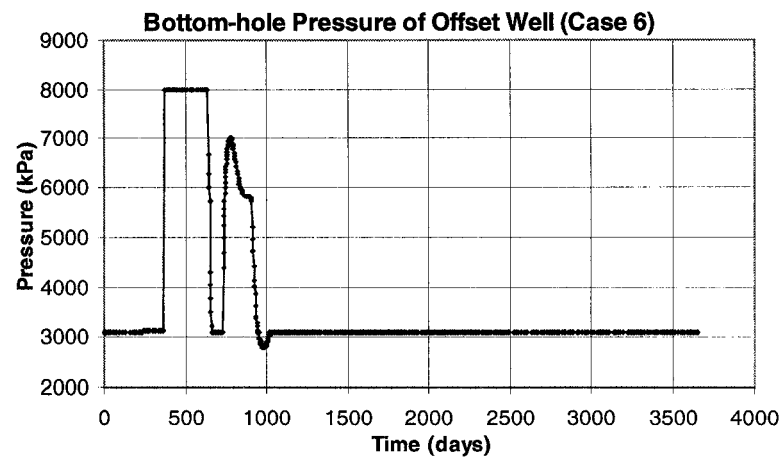
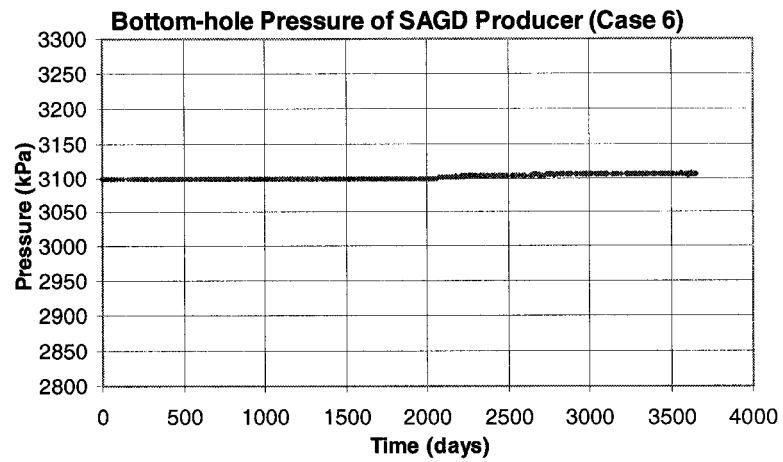
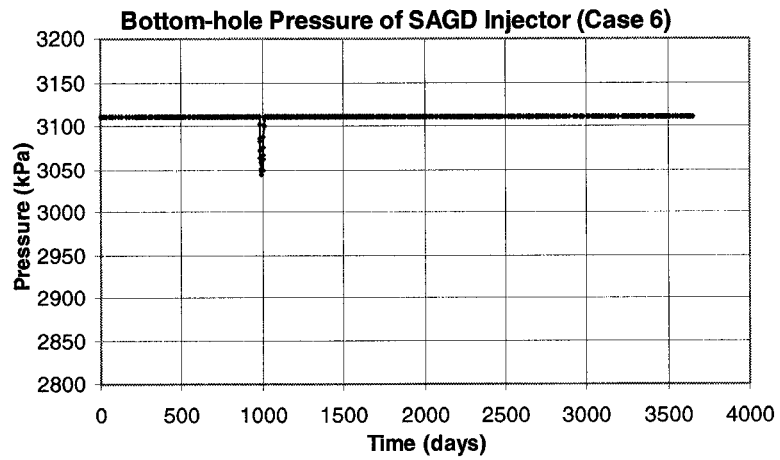


**Figure C-33. Bottom-hole Pressure of Wells for Case 6**



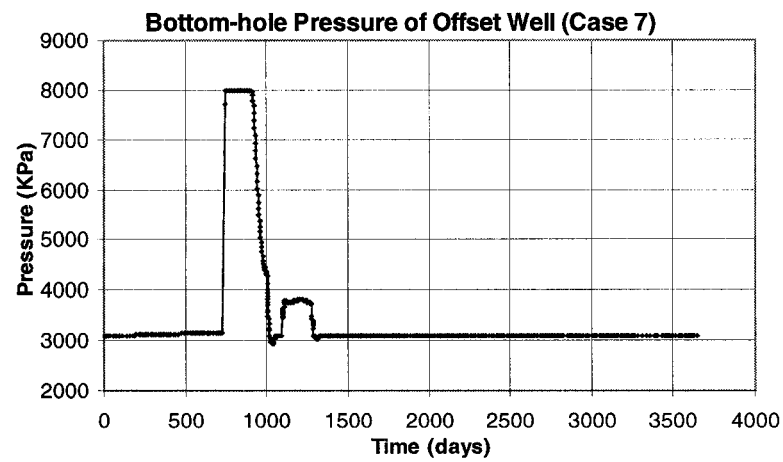
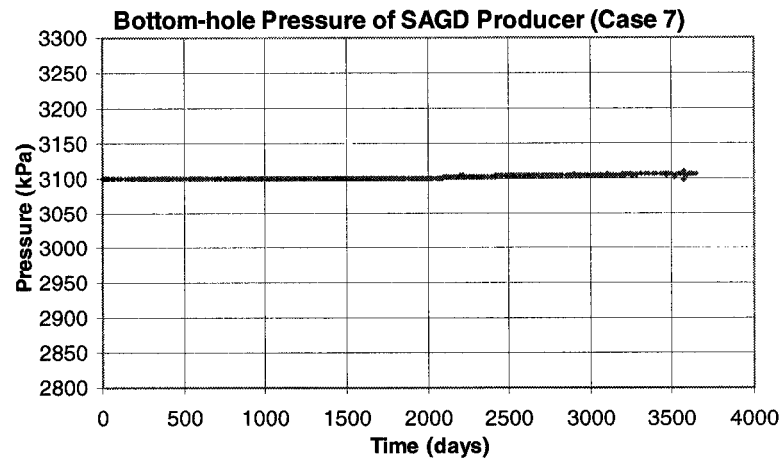
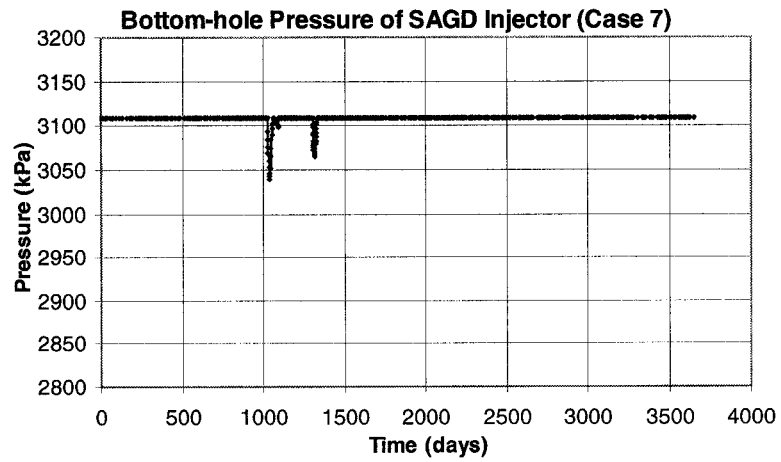


**Figure C-34. Bottom-hole Pressure of Wells for Case 7**

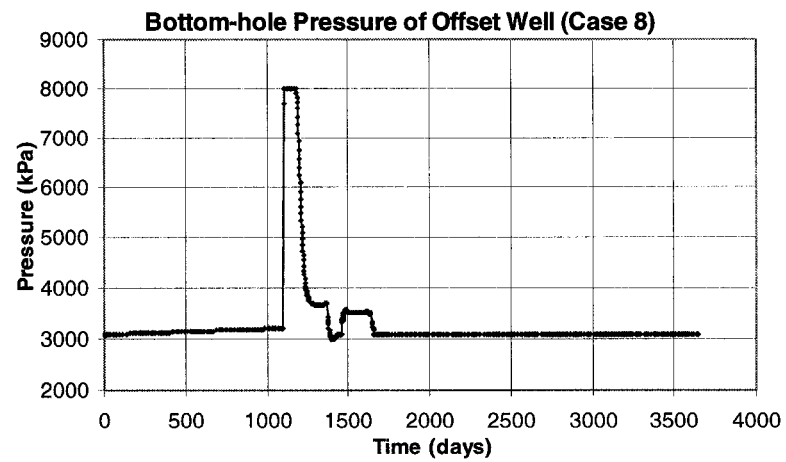
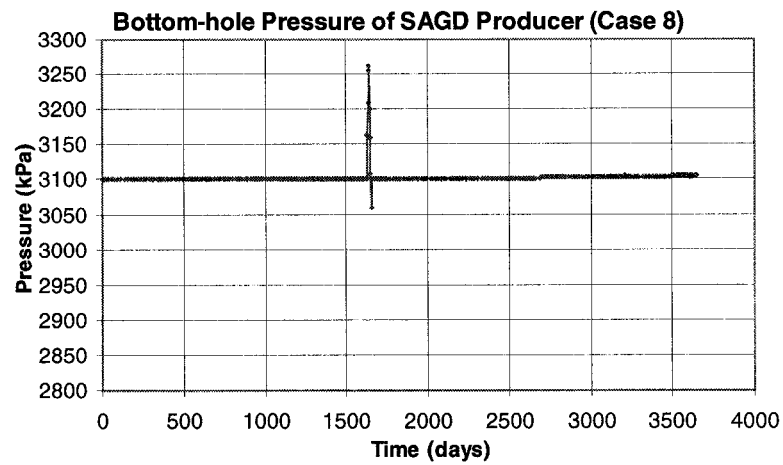
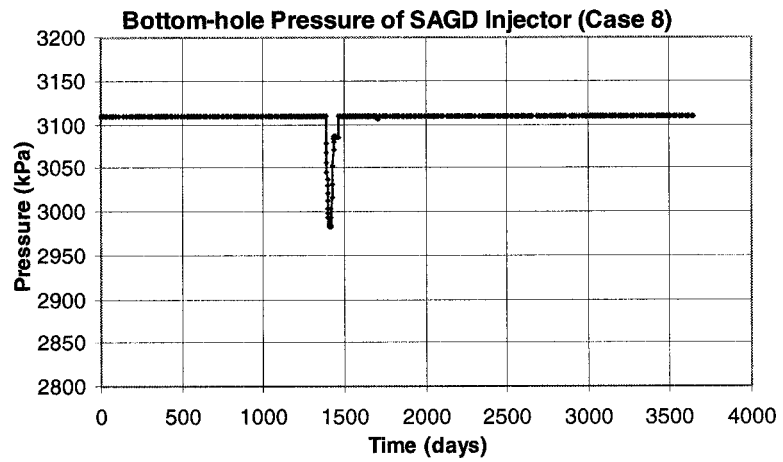


**Figure C-35. Bottom-hole Pressure of Wells for Case 8**

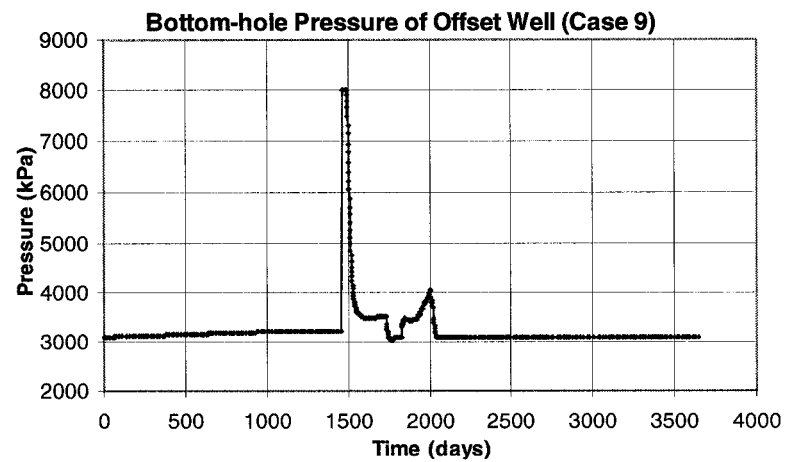
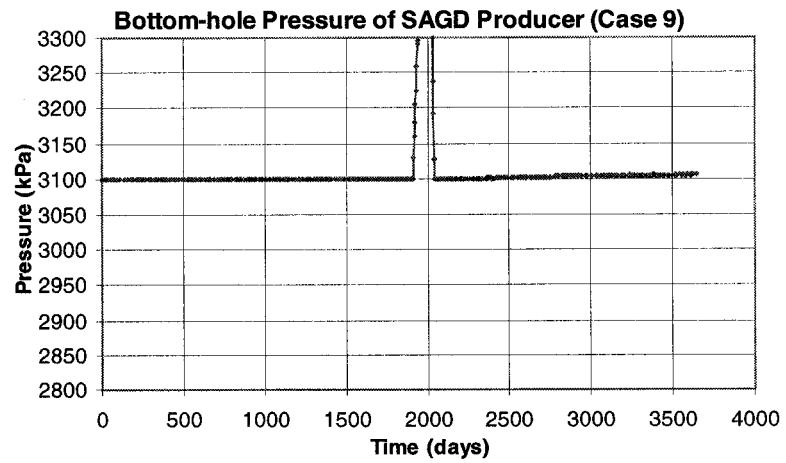
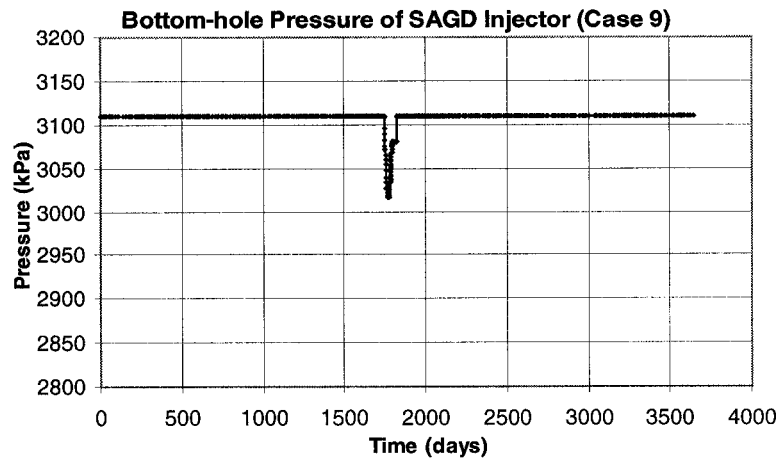


**Figure C-36. Bottom-hole Pressure of Wells for Case 9**

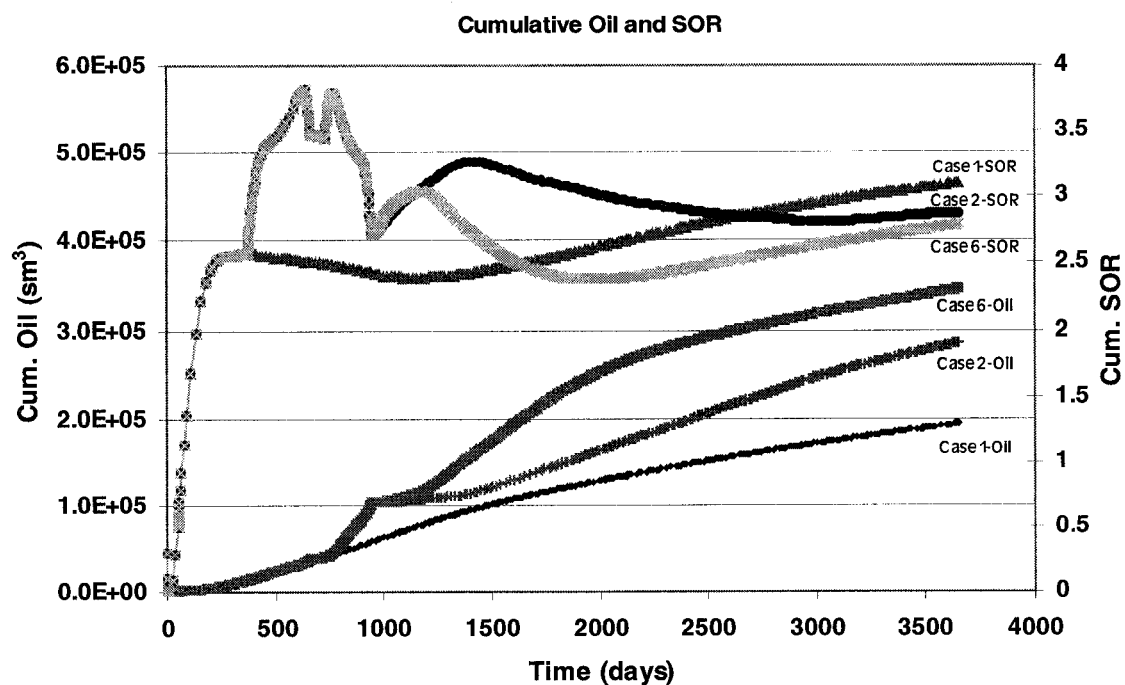


**Figure C-37. Cumulative Oil and SOR Curves for Cases 2 and 6**

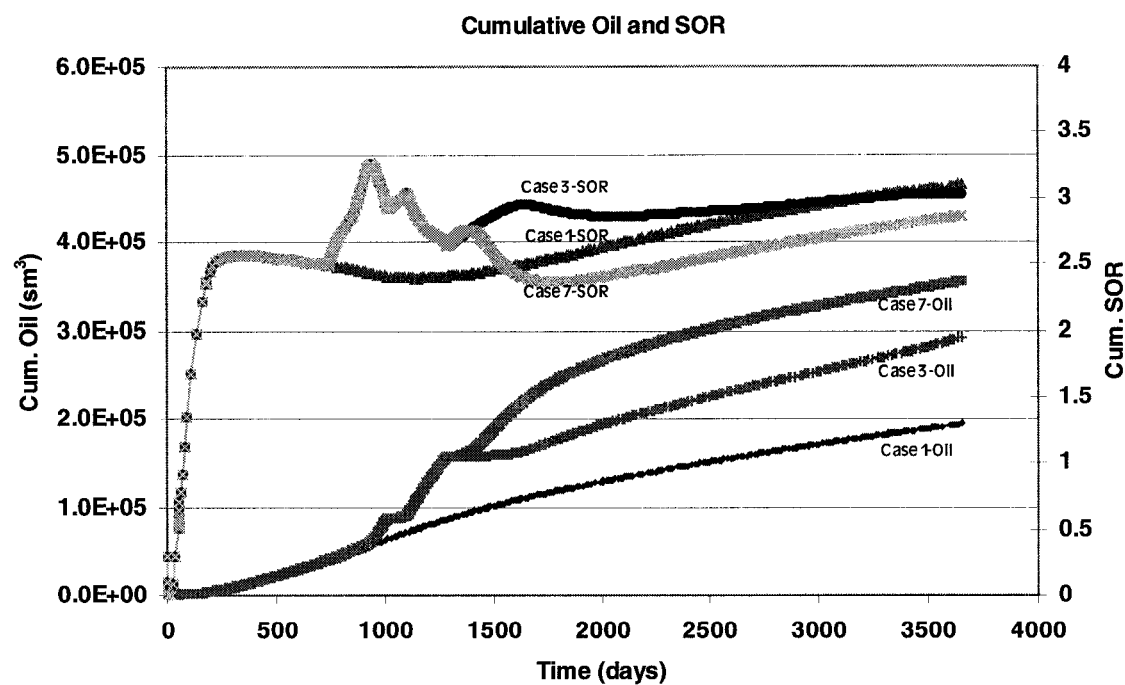


**Figure C-38. Cumulative Oil and SOR Curves for Cases 3 and 7**

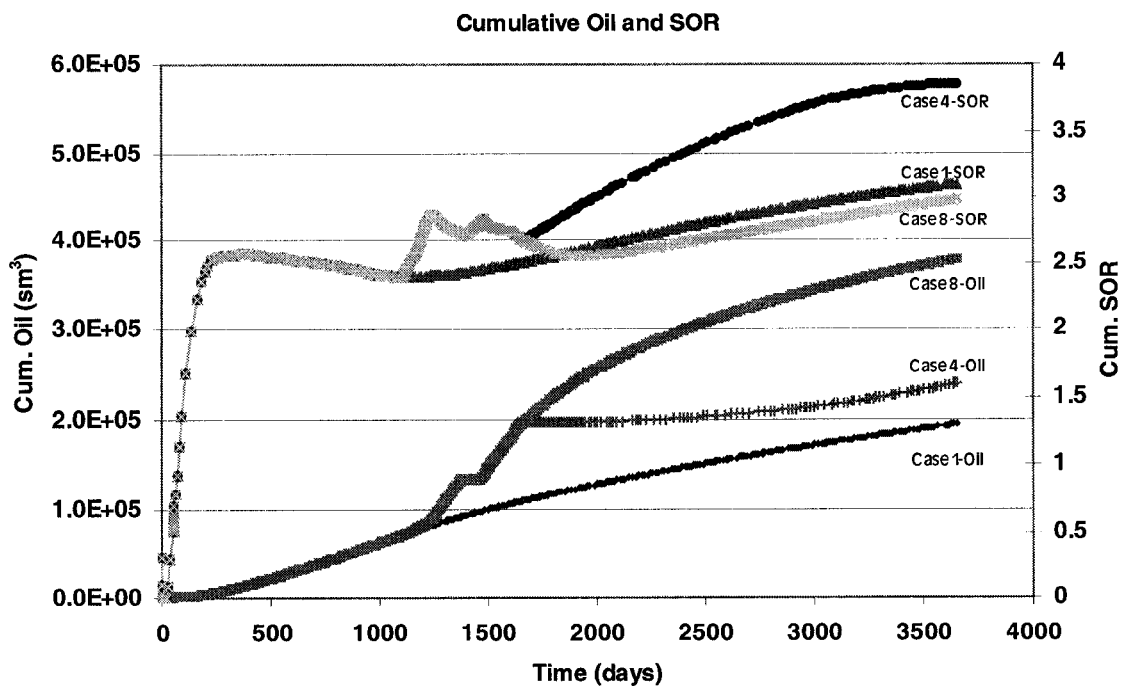


Figure C-39. Cumulative Oil and SOR Curves for Cases 4 and 8

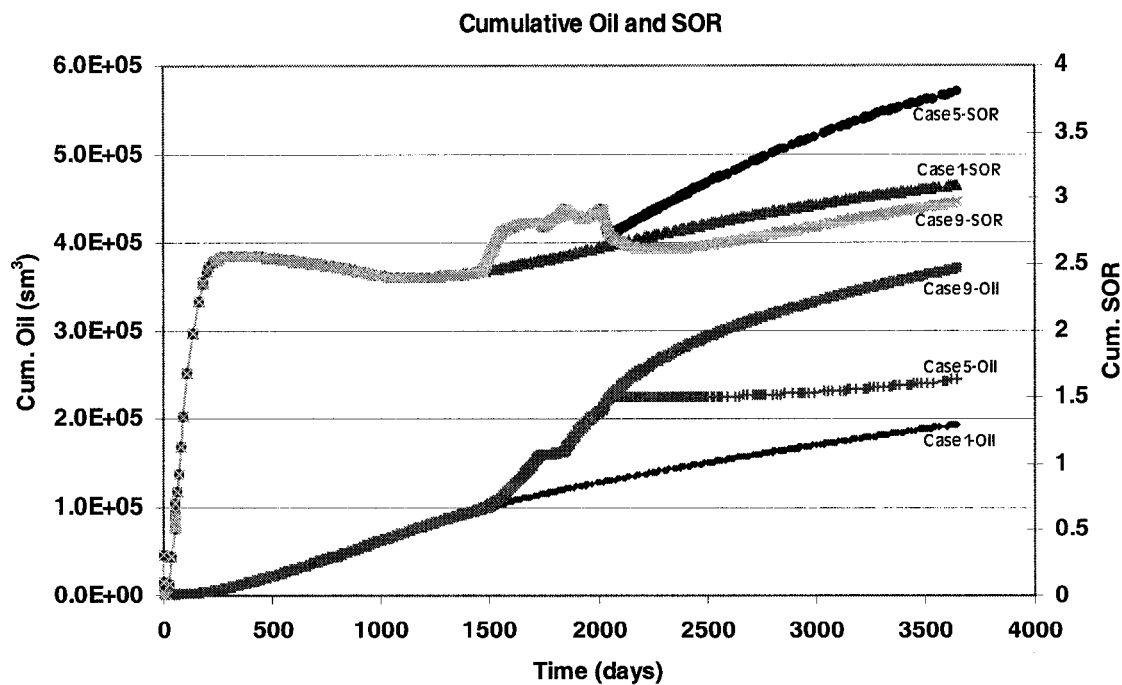


Figure C-40. Cumulative Oil and SOR Curves for Cases 5 and 9

## Appendix D: Geomechanical Properties of Oil Sands

In saturated porous media, the total stress can be divided into two parts. One component, called pore pressure, is carried by the saturating fluid in the continuous void spaces, and the other component of the total stress, called effective stress, is carried by the solid skeleton at the points of contact of the soil particles. Equation (D-1) defines effective stress:

$$\sigma' = \sigma - p \quad (D-1)$$

where  $\sigma'$  = effective stress,  $\sigma$  = total stress and  $p$  = pore pressure. The behavior of all porous media is controlled by effective stresses and is generally described in terms of the three orthogonal principal effective stresses,  $\sigma'_1 \geq \sigma'_2 \geq \sigma'_3$  (Figure D-1). The subscripts “1”, “2” and “3” refer to the major, intermediate and minor principal effective stresses, respectively. The behavior of a porous material is determined not only by the magnitudes of these three principal stresses but also by its stress history.

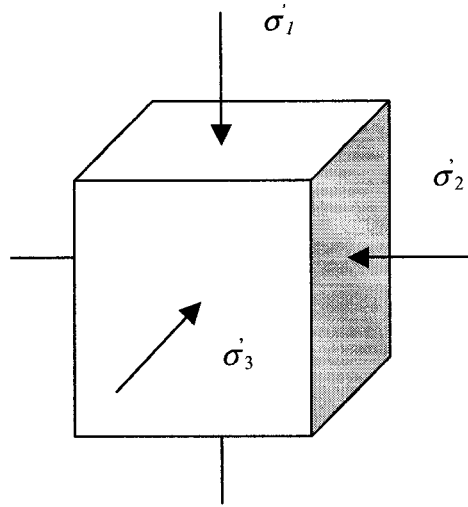


**Figure D-1. Principal Stresses**

Research<sup>(30)</sup> has shown that oil sands is a type of elastoplastic porous medium.

### *Yield and Potential Function*

With the ordering convention of Eq. (D-1), the failure criterion is presented by the Mohr-Coulomb failure criterion. The failure envelope is defined by the Mohr-Coulomb yield function:

$$f^s = \sigma_1' - \sigma_3' N_\phi + 2c' \sqrt{N_\phi} \quad (D-2)$$

and

$$N_\phi = \frac{1 + \sin \phi'}{1 - \sin \phi'} \quad (D-3)$$

where  $\phi'$  is the friction angle, and  $c'$ , the cohesion. If  $f^s > 0$ , the material is in a stable condition. If  $f^s = 0$ , the material is at the critical condition. Shear yield is detected if  $f^s < 0$ . The tensile strength,  $\sigma_t$ , is zero in unconsolidated models.

### *Initial stress*

From the stress measurements that have been made, it can be assumed that the assumption that the vertical stress is directly proportional to the overburden depth is justified.

$$\sigma_v = \gamma \times z \quad (D-4)$$

In Equation (D-4),  $\sigma_v$  is the vertical stress,  $\gamma$  is the unit weight of the overlying rock, and  $z$  is the depth below surface. The horizontal stresses acting on an element of rock at a depth  $z$  below the surface are much more difficult to estimate than the vertical stresses. In fact, measurements show that  $K_0$  ( $\sigma_h/\sigma_v$ ) is greater than 1 at depths shallower than 500 m, and that it approaches 1 at depths greater than 1 km (Figure D-2). It is assumed that the oil sands were deposited in a shallow environment<sup>(30)</sup>; therefore, the average horizontal stresses are significantly greater than the vertical stresses.

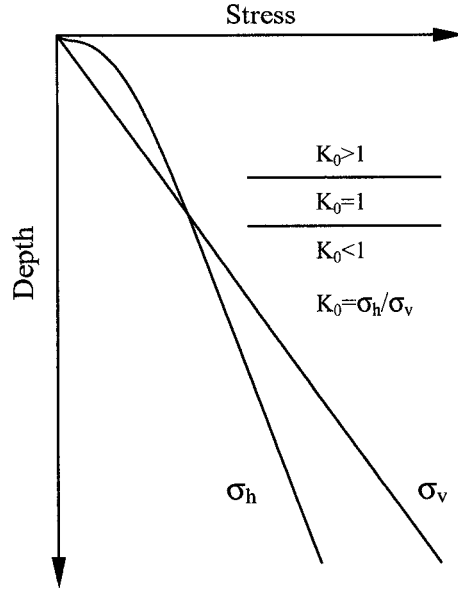


**Figure D-2. Stress Variation with Depth**

#### *Young's Modulus*

Substantial variations of Young's Modulus,  $E$ , a stiffness parameter, have been reported. In this study, a relationship that is obtained from a McMurray Oil Sand Formation sample<sup>(31)</sup> is used to calculate  $E$ .

$$E = 343\sigma_3'^{0.875} \quad (\text{MPa}) \quad (\text{D-5})$$

In the geomechanical model used, the effective mean stress  $(\frac{\sigma_1' + \sigma_2' + \sigma_3'}{3})$  is applied instead of the minimum effective stress  $\sigma_3'$ .

$$G = \frac{E}{2(1+\nu)} \quad (\text{D-6})$$

where  $G$  is the shear modulus, and  $\nu$  is Poisson's Ratio.

#### *Shear Dilatancy*

Shear Dilatancy is the change in volume that occurs with shear distortion of a material. Dilatancy is characterized by a dilation angle,  $\psi$ , which is related to the ratio of plastic volume change to plastic shear strain (Figure D-3).



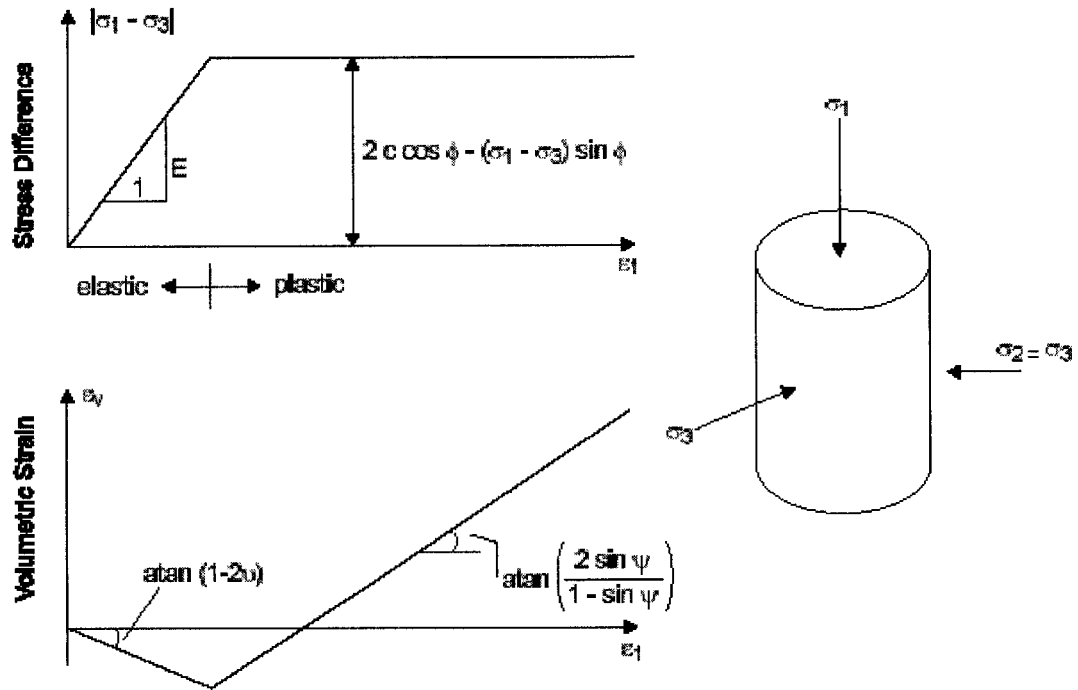


**Figure D-3. Idealized Relation for Dilation Angle**  
 ( from triaxial test result, Vermeer and de Borst <sup>(48)</sup>)

### *Thermal Expansion Coefficient of Bulk Rock*

Drained thermal expansion tests were conducted in which only the combined thermal expansion of the matrix was measured. The results from a thermal expansion test are presented as a volume change. In FLAC, the linear thermal expansion coefficient is required. So one third of the experimental data is applied in simulations.

### *Pore Volume Change*

The following equation<sup>(28,29)</sup> is used to illustrate the relationship between the porosity  $\phi$  (reservoir engineering concept) and volumetric strain  $\varepsilon_v$ .

$$\phi = \frac{\phi_0 + \varepsilon_v - (1 - \phi_0)\alpha\Delta T}{1 + \varepsilon_v} \quad (D-7)$$

where  $\Delta T$  is the change of temperature (K) and  $\alpha$  the coefficient of solid thermal expansion ( $K^{-1}$ ).

### *Absolute Permeability*

The most influential link between geomechanics concepts and the SAGD process occurs when dilation of the sand matrix causes the absolute permeability to increase. The following relationship developed by Tortike and Farouq Ali<sup>(28,29)</sup> describes a link between volumetric strain,  $\varepsilon_v$ , and absolute permeability,  $k$ :

$$\frac{k}{k_0} = \frac{\left[ 1 + \frac{\varepsilon_v}{\phi_0} - \frac{\alpha\Delta T(1 - \phi_0)}{\phi_0} \right]^3}{1 + \varepsilon_v} \quad (D-8)$$

where  $\Delta T$  and  $\alpha$  are the same as the above.

## APPENDIX E: GEOMECHANICAL SIMULATION RESULTS FOR CASES 1, 6 AND 8

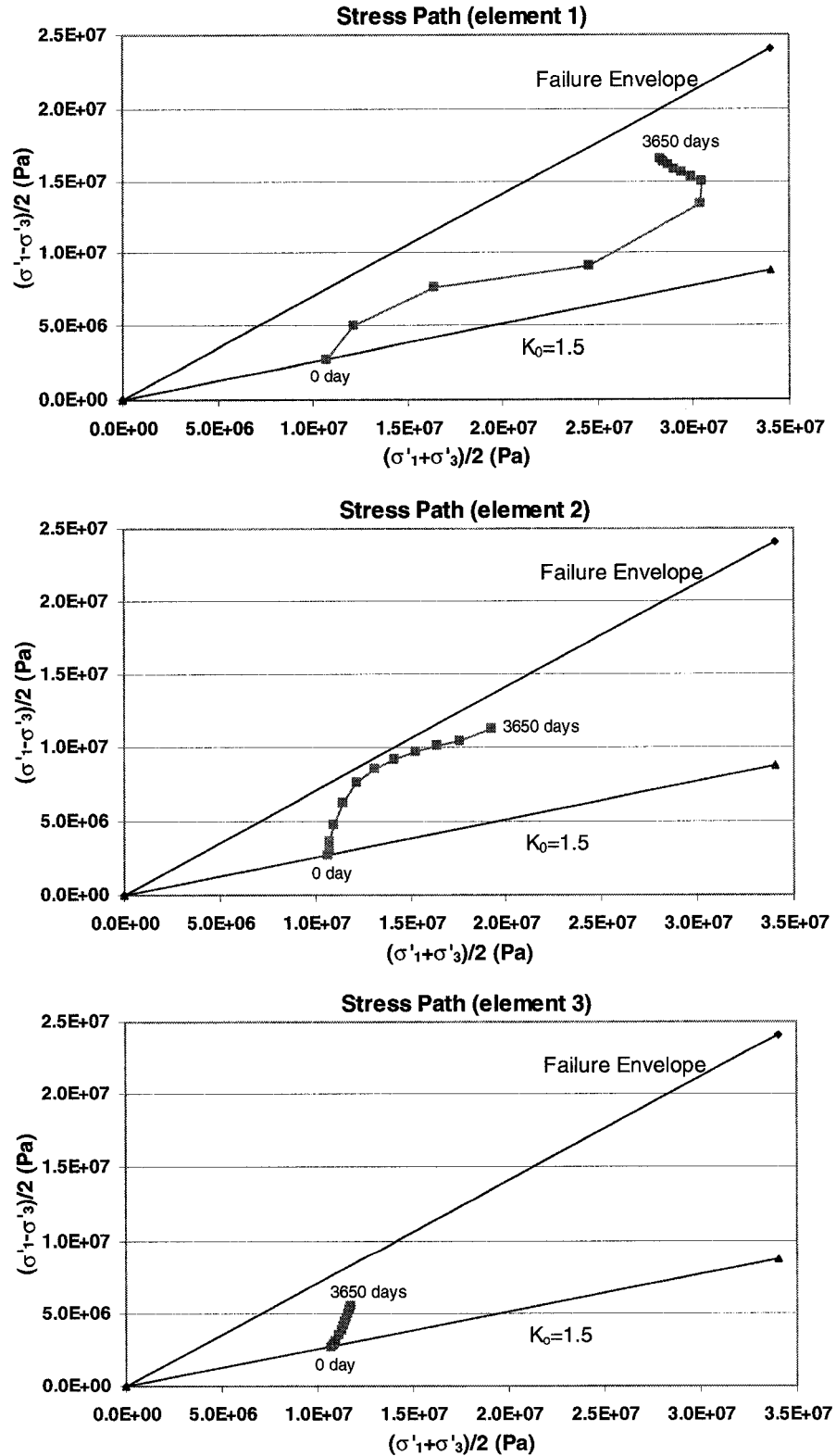
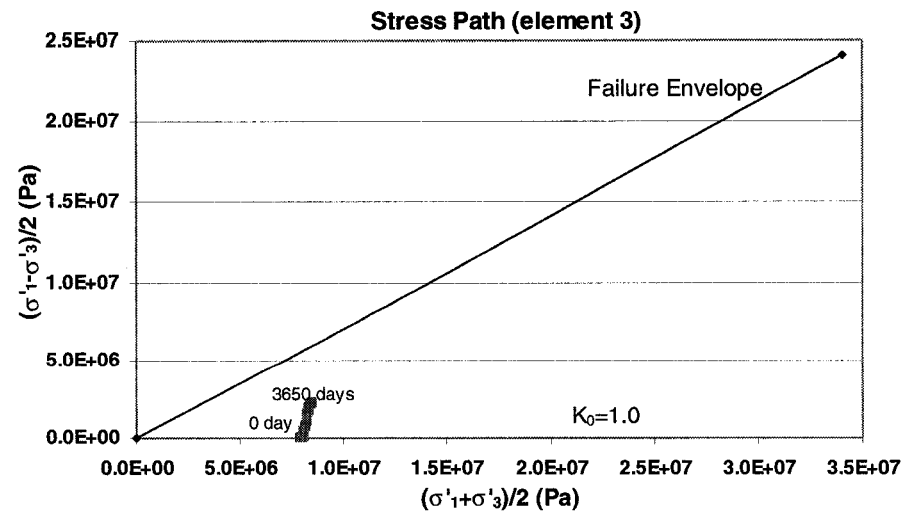
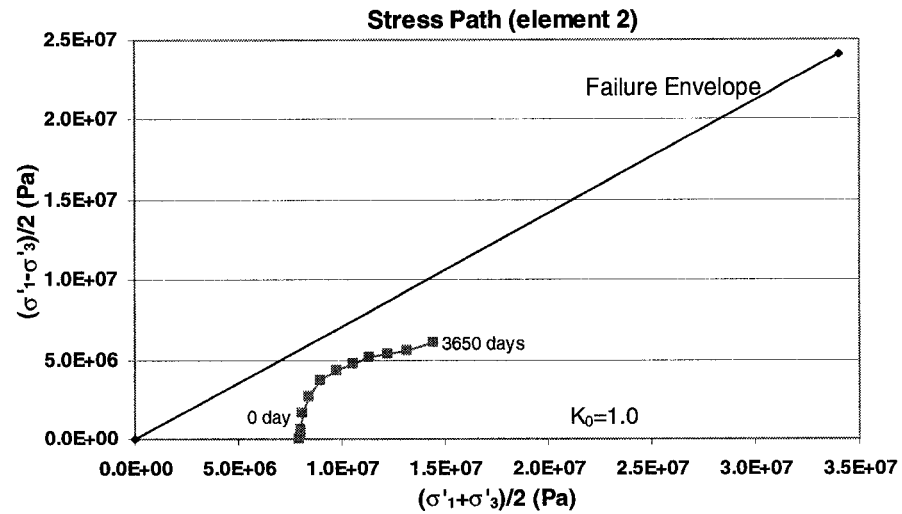
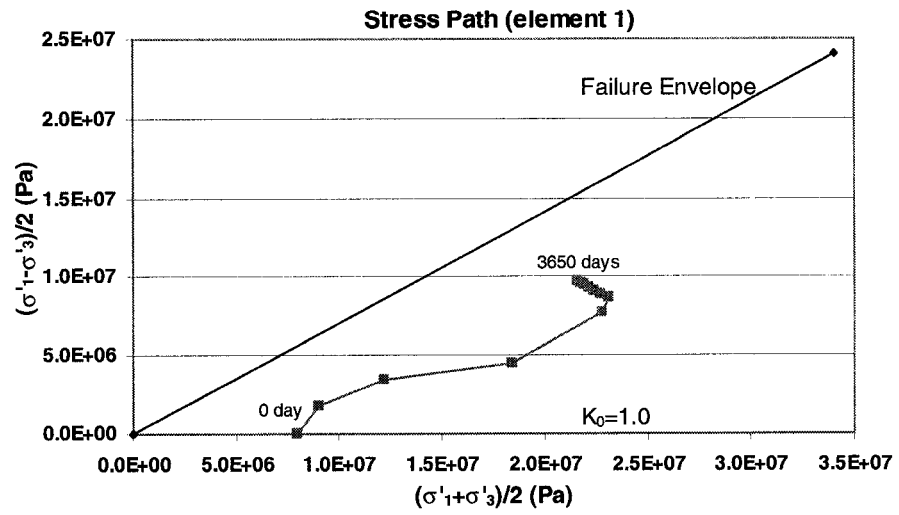
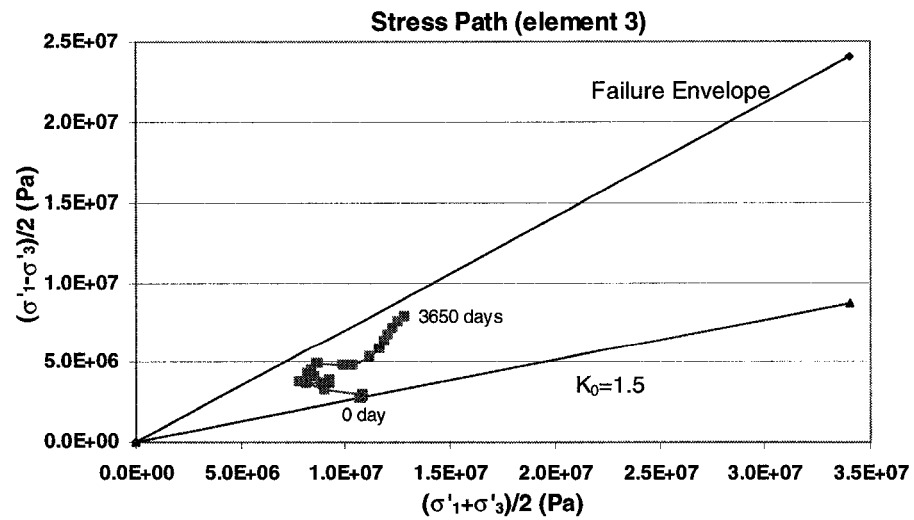
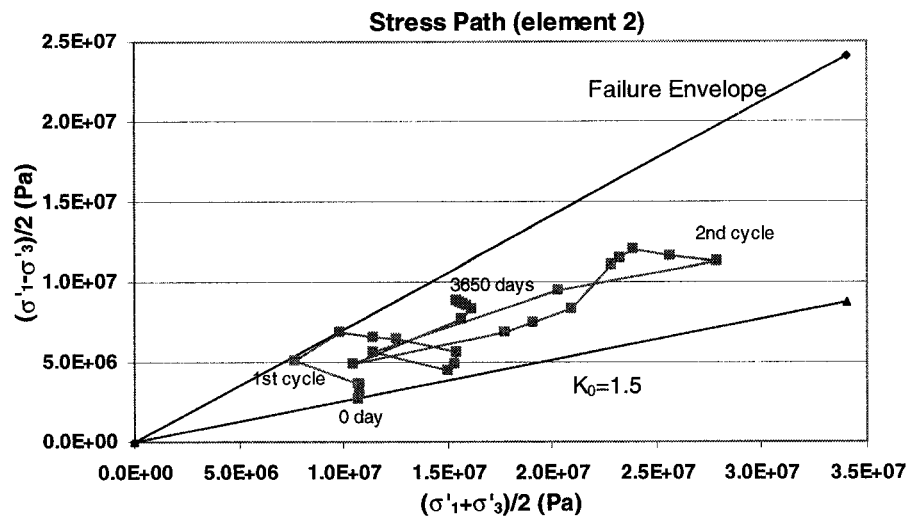
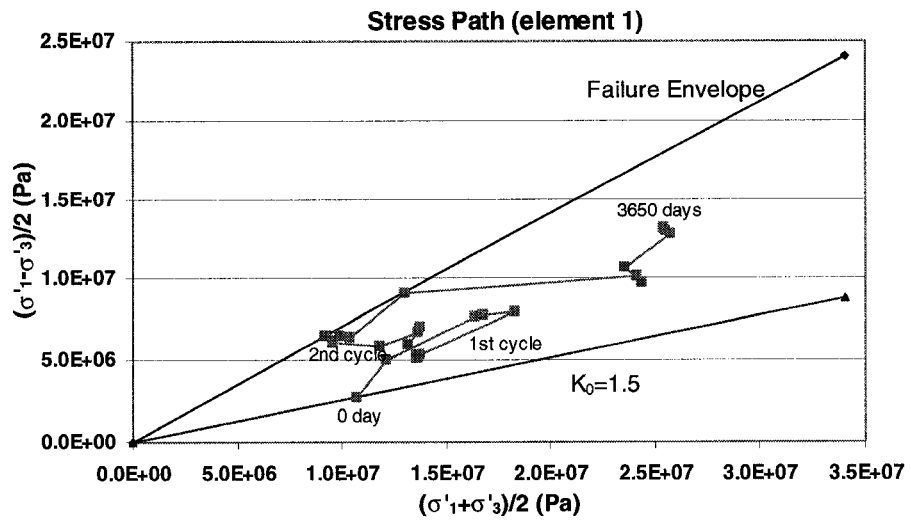


Figure E-1. Stress Paths for Case 1 ( $K_0=1.5$ )



**Figure E-2. Stress Paths for Case 1 ( $K_0=1.0$ )**



**Figure E-3. Stress Paths for Case 6 ( $K_0=1.5$ )**

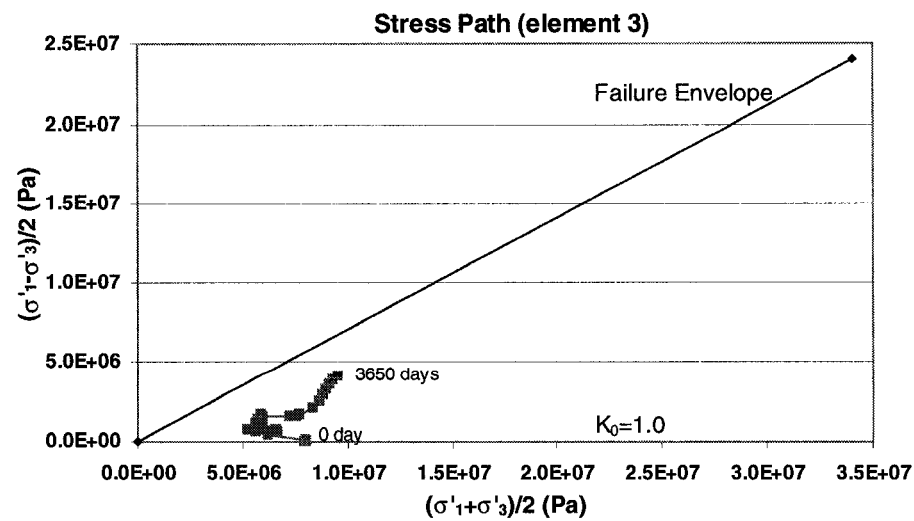
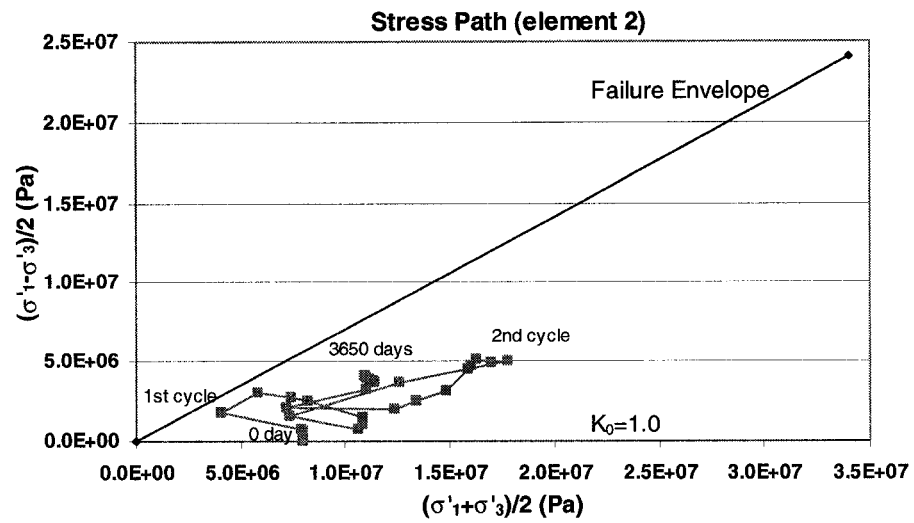
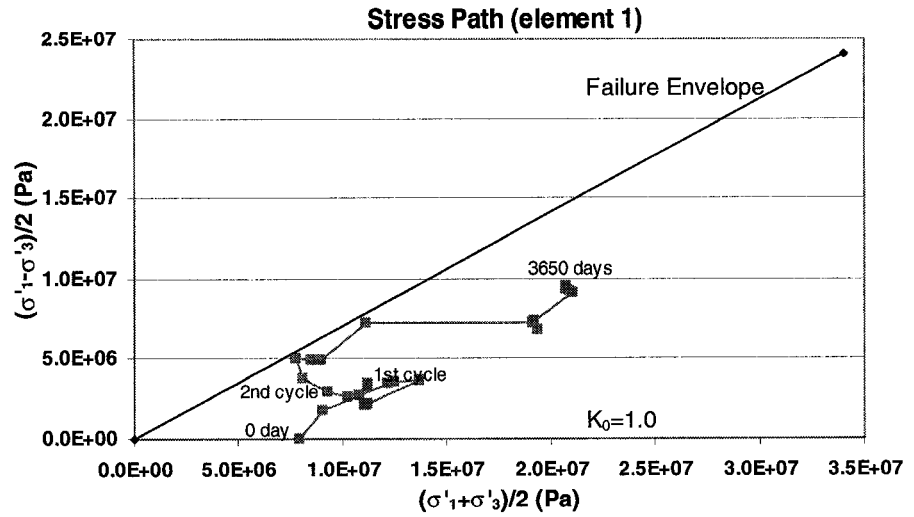


**Figure E-4. Stress Paths for Case 6 ( $K_0=1.0$ )**

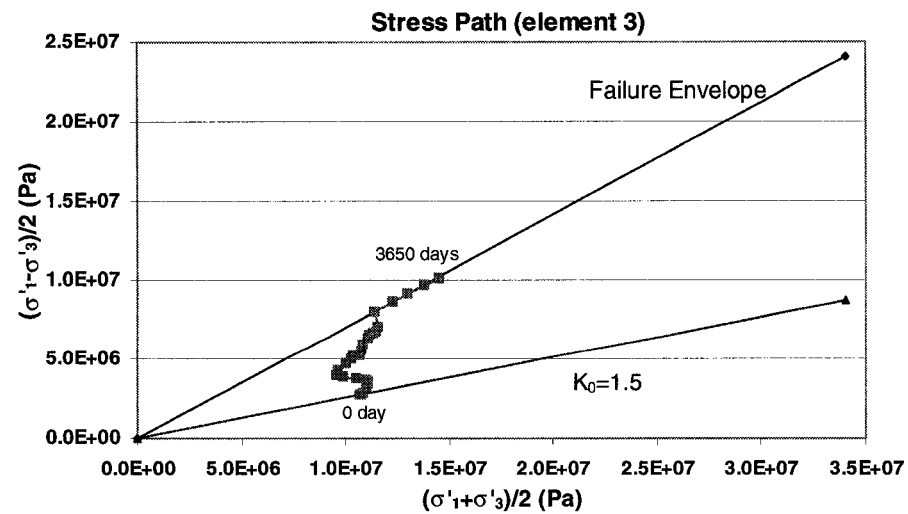
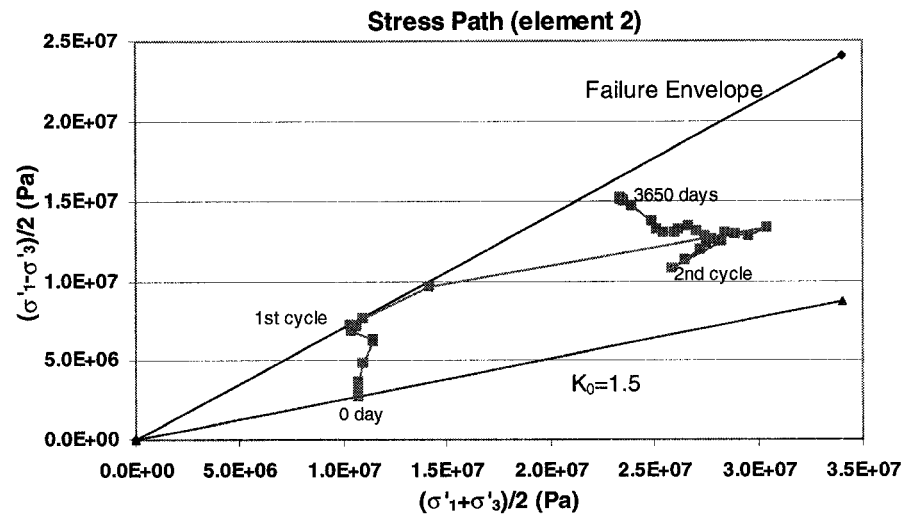
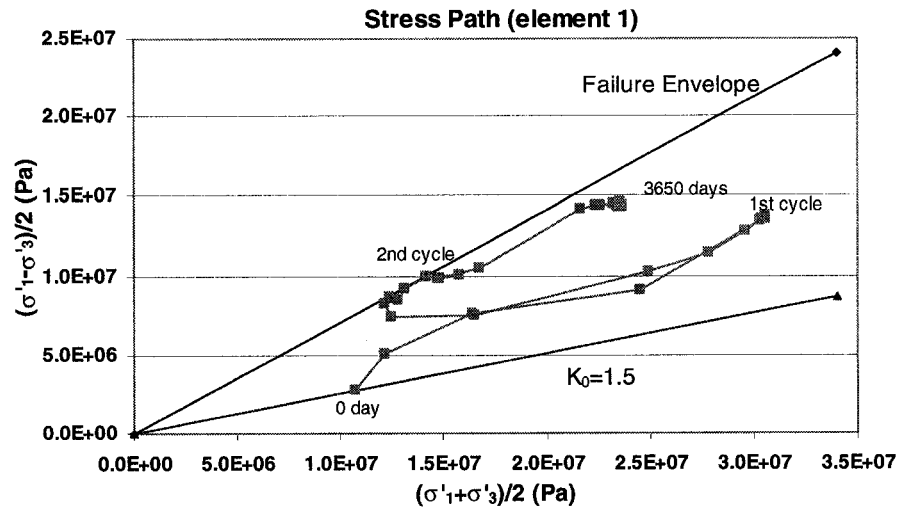


**Figure E-5. Stress Paths for Case 8 ( $K_0=1.5$ )**

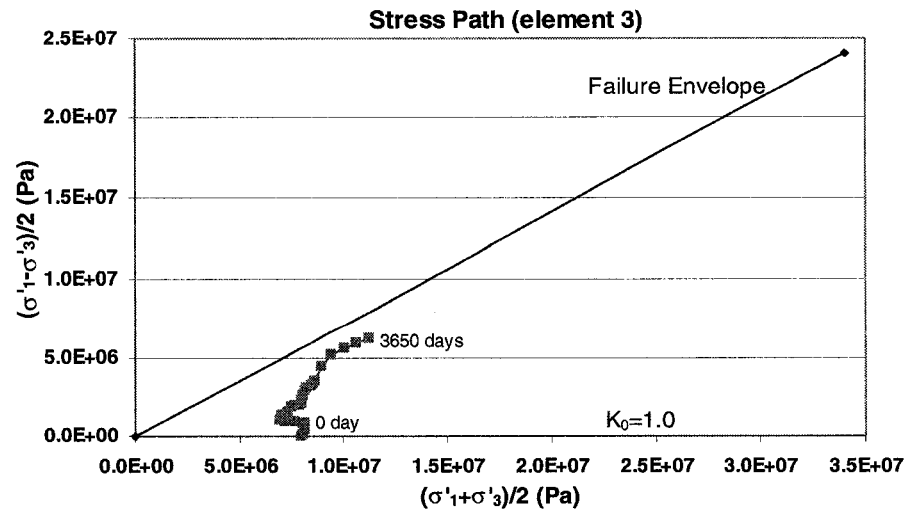
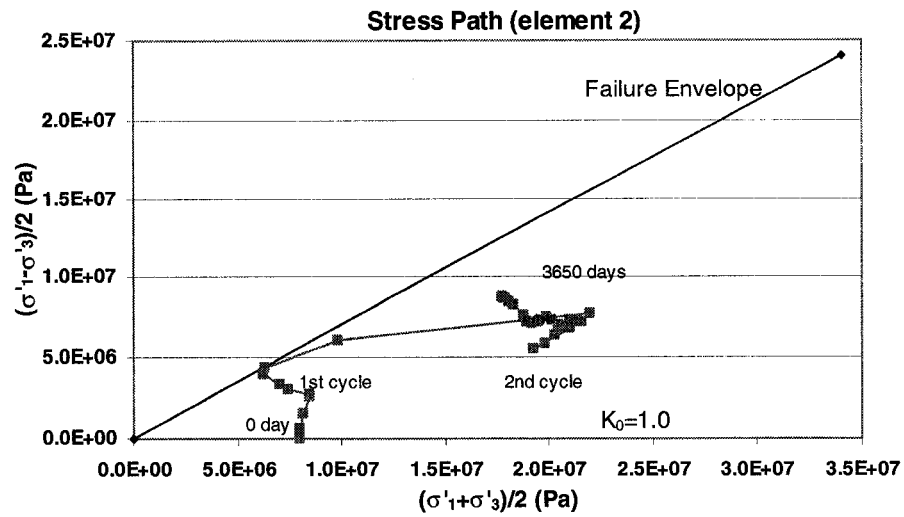
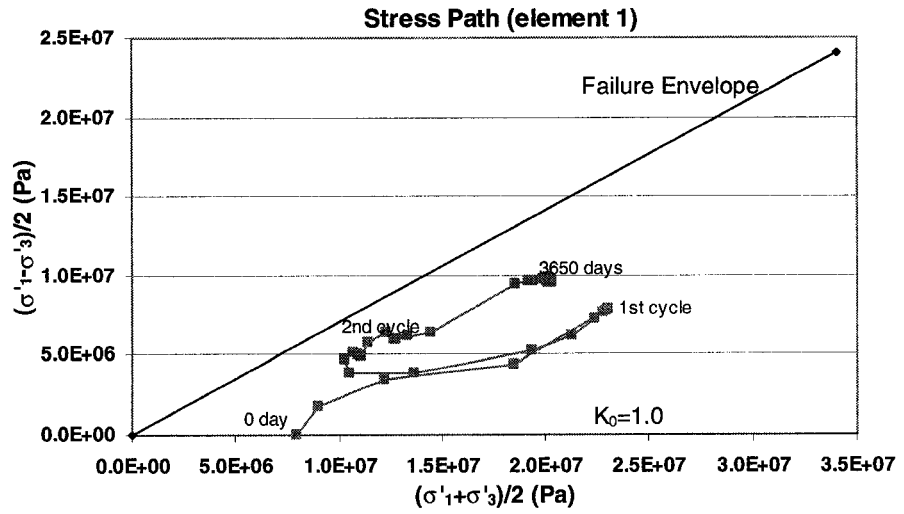


**Figure E-6. Stress Paths for Case 8 ( $K_0=1.0$ )**



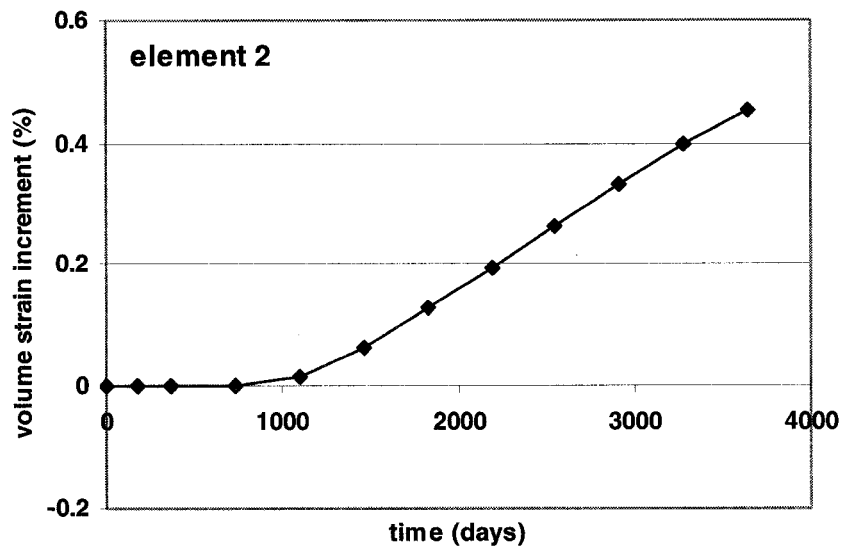
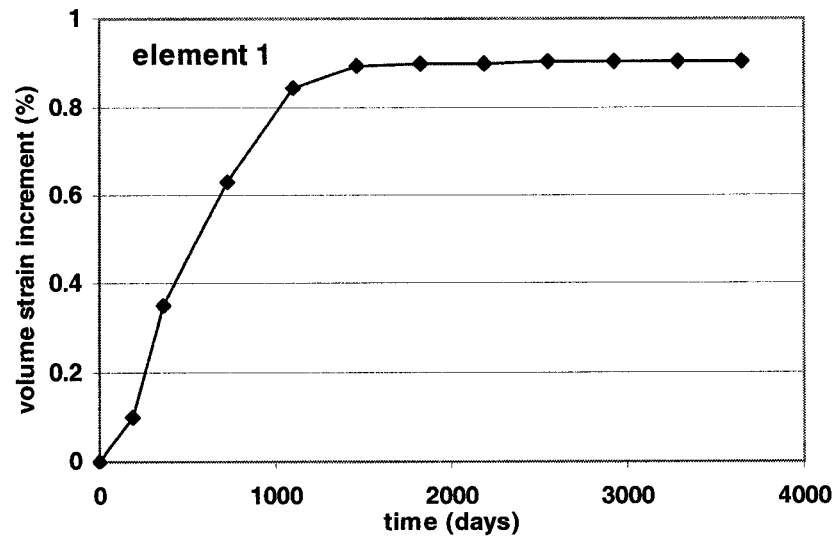


**Figure E-7. Volume Strain Increment for Case 1 ( $K_0=1.5$ )**

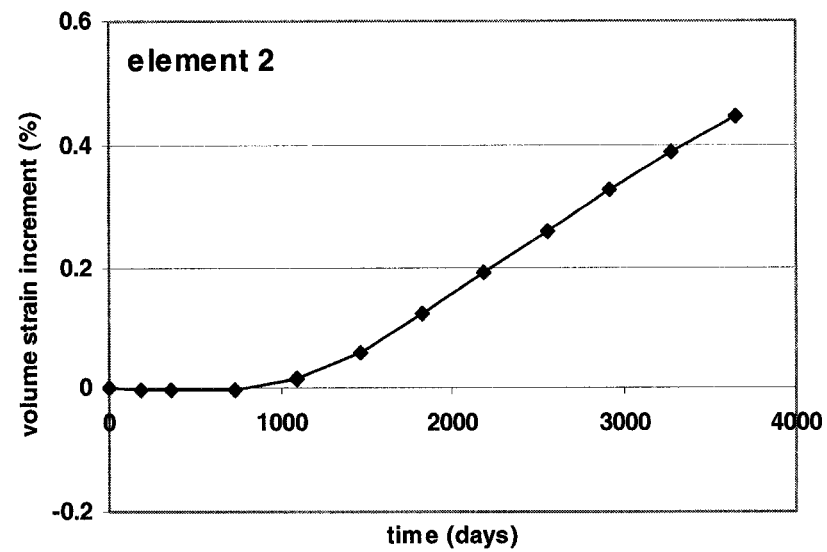
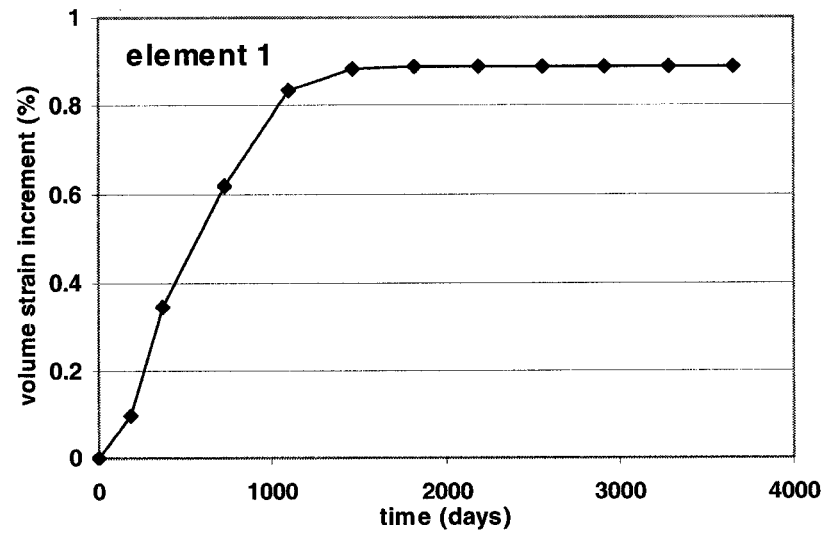
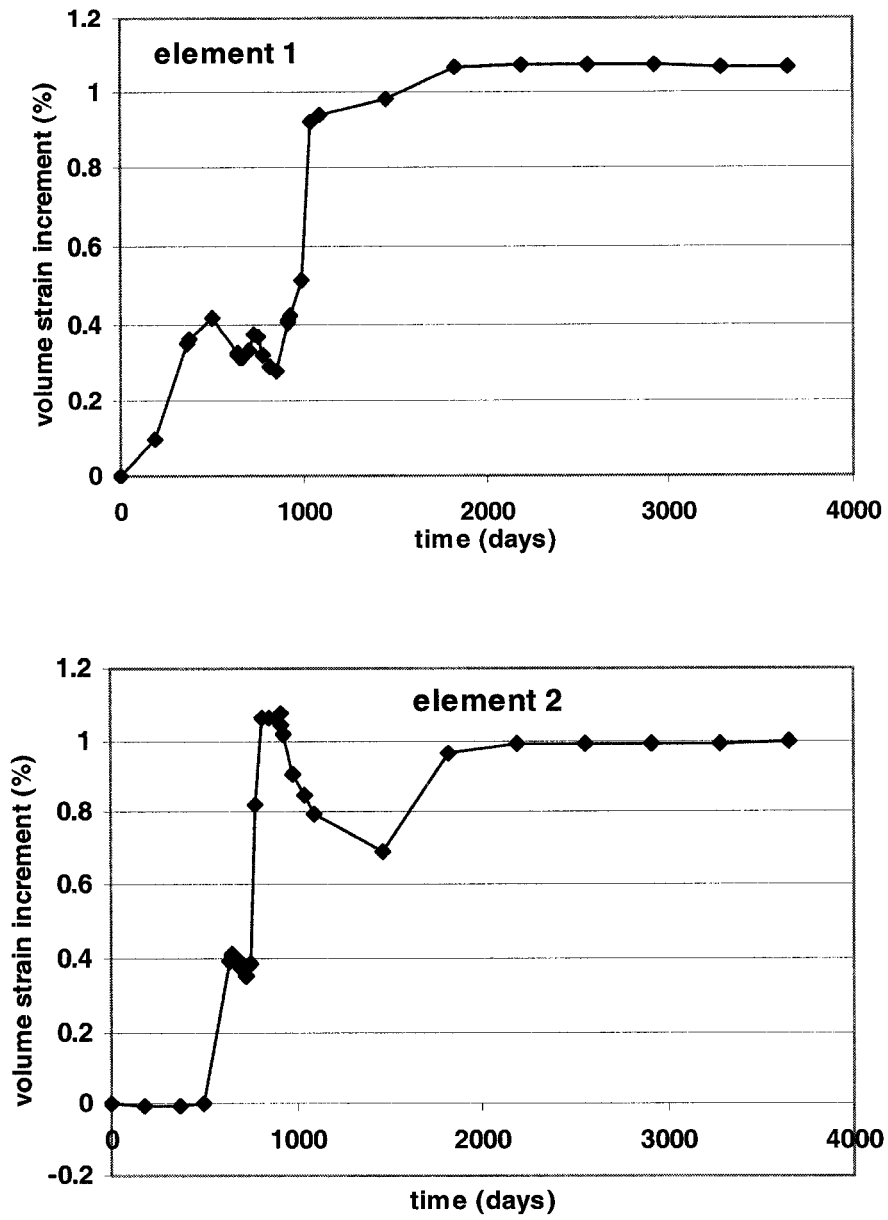
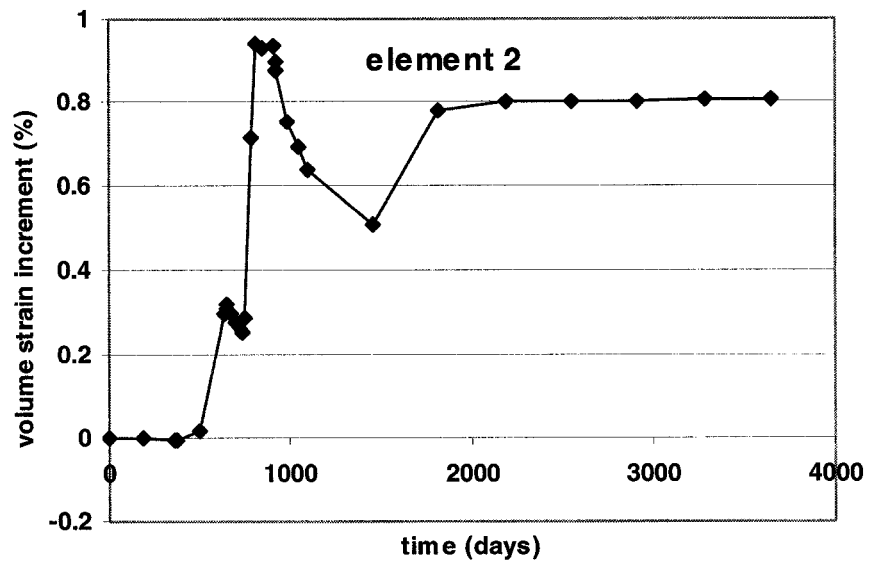
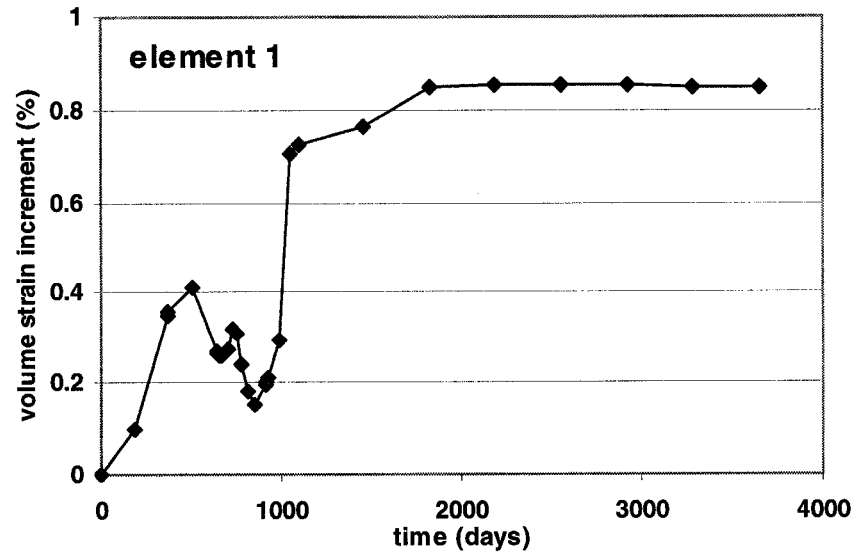


Figure E-8. Volume Strain Increment for Case 1 ( $K_0=1.0$ )



**Figure E-9. Volume Strain Increment for Case 6 ( $K_0=1.5$ )**



**Figure E-10. Volume Strain Increment for Case 6 ( $K_0=1.0$ )**

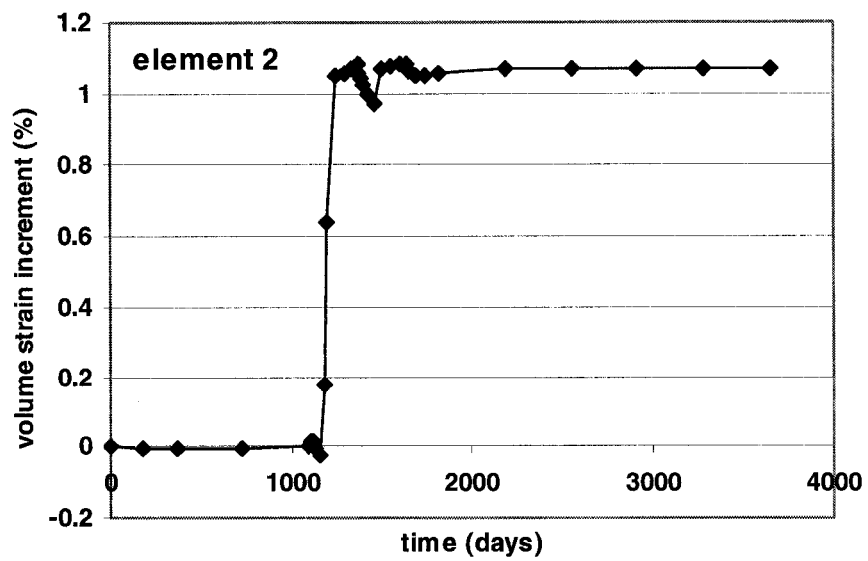
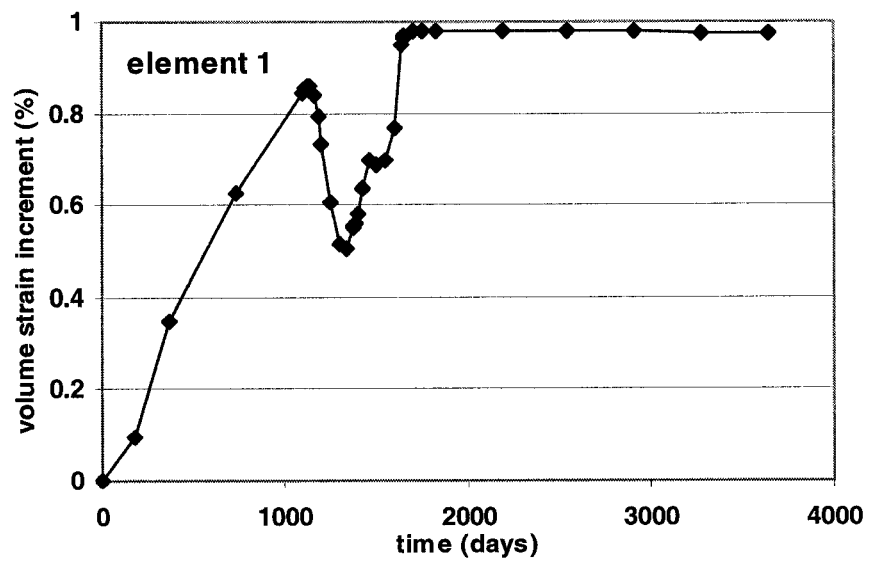


Figure E-11. Volume Strain Increment for Case 8 ( $K_0=1.5$ )

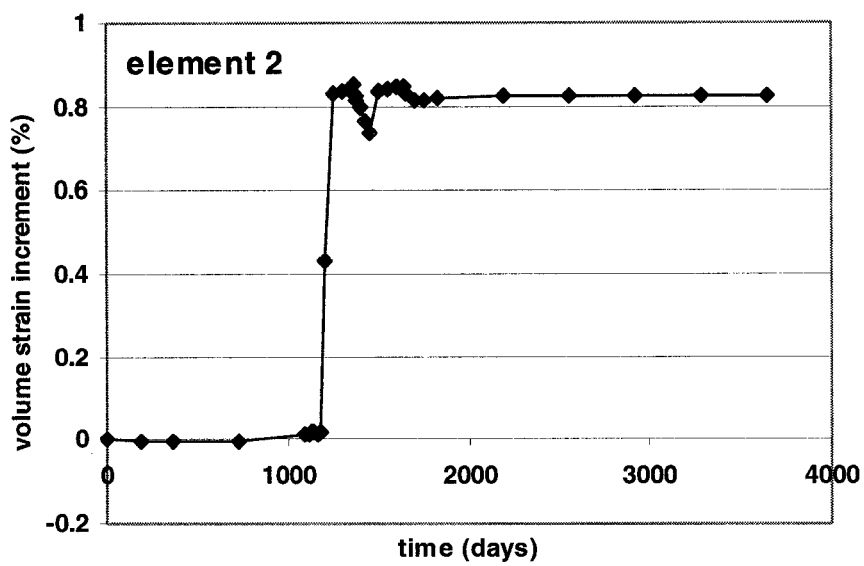
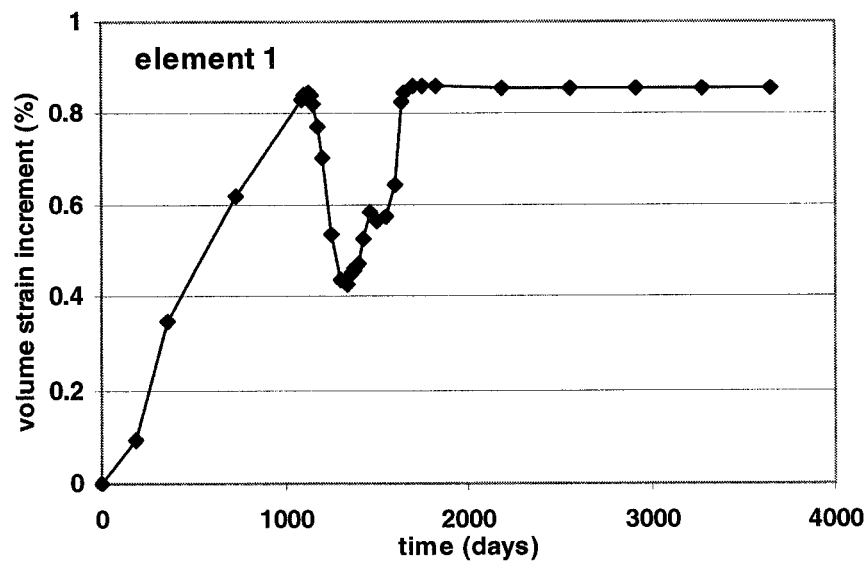
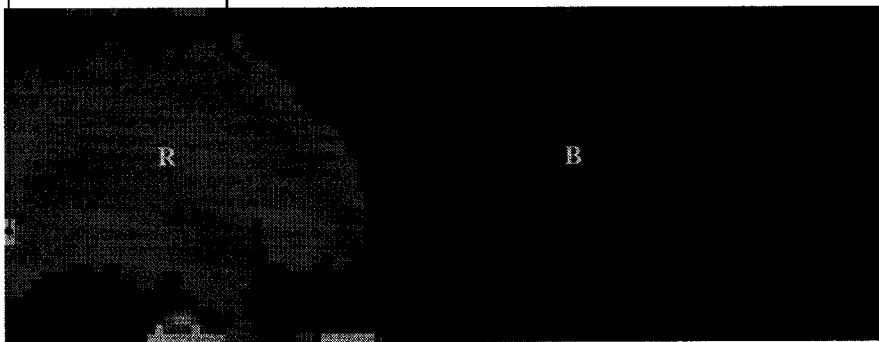


Figure E-12. Volume Strain Increment for Case 8 ( $K_0=1.0$ )



**Figure E-13. Failure Zone @ 10 Years for Case 6 ( $K_0=1.5$ )**

Red – post-failure, Green – currently in failure, Blue – elastic state



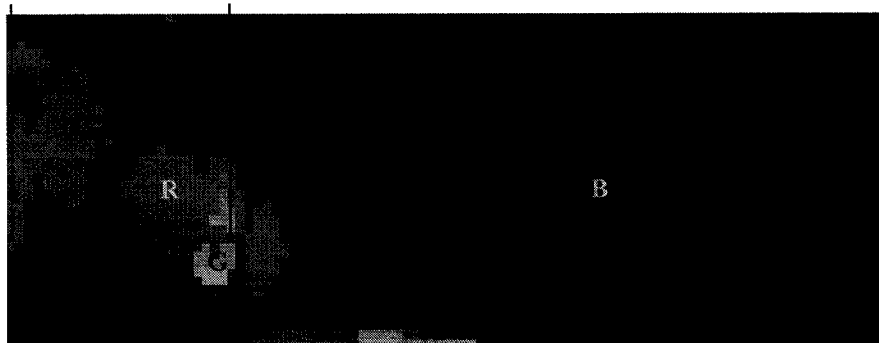
**Figure E-14. Failure Zone @ 10 Years for Case 6 ( $K_0=1.0$ )**

Red – post-failure, Green – currently in failure, Blue – elastic state



**Figure E-15. Failure Zone @ 10 Years for Case 8 ( $K_0=1.5$ )**

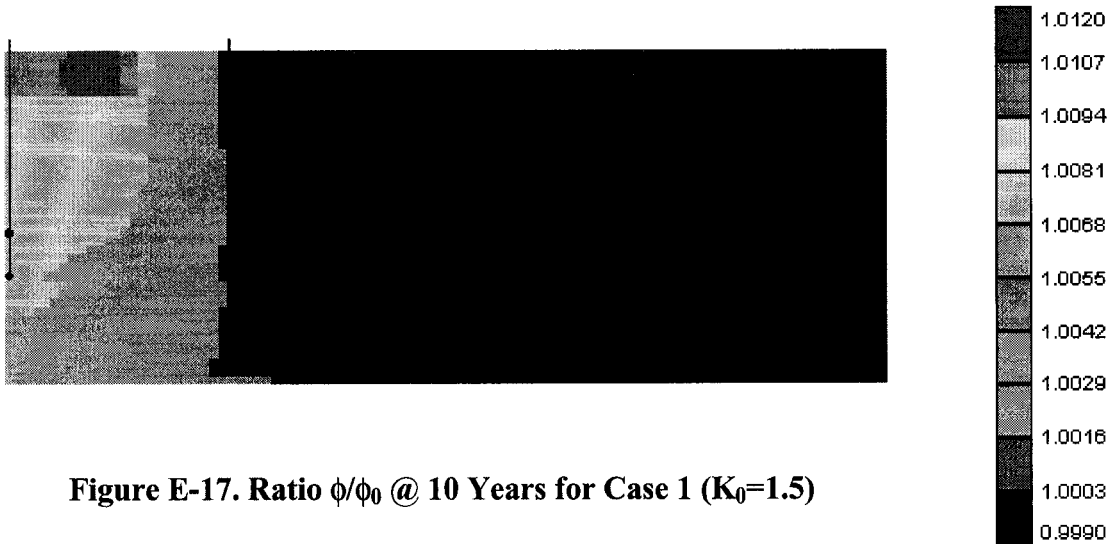
Red – post-failure, Green – currently in failure, Blue – elastic state



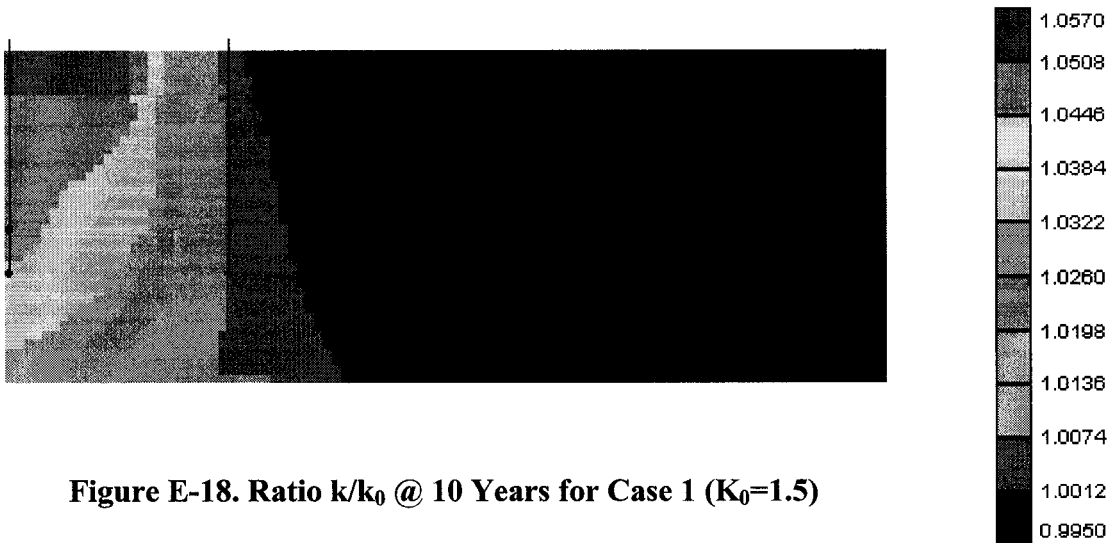
**Figure E-16. Failure Zone @ 10 Years for Case 8 ( $K_0=1.0$ )**

Red – post-failure, Green – currently in failure, Blue – elastic state

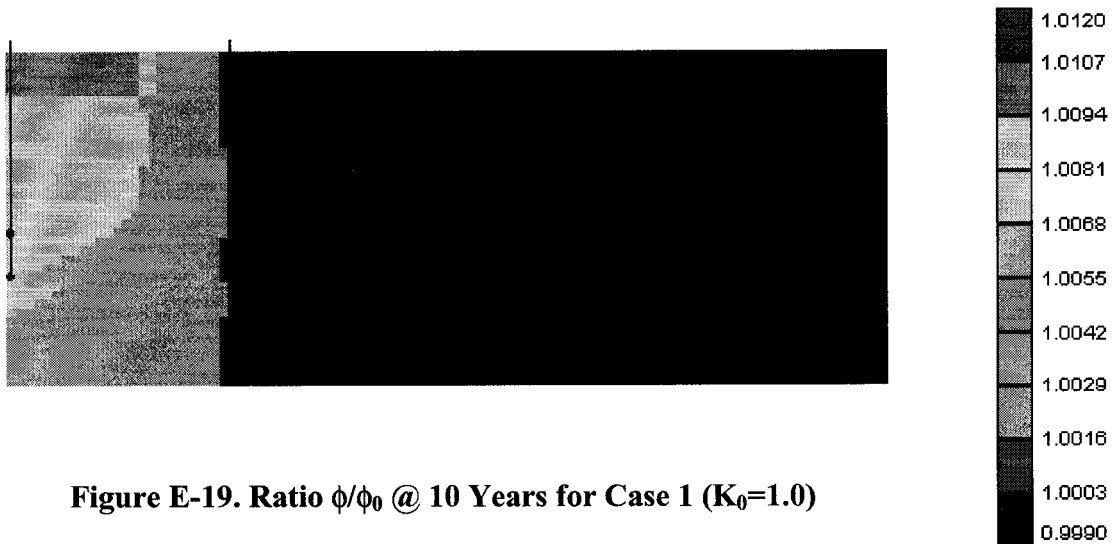




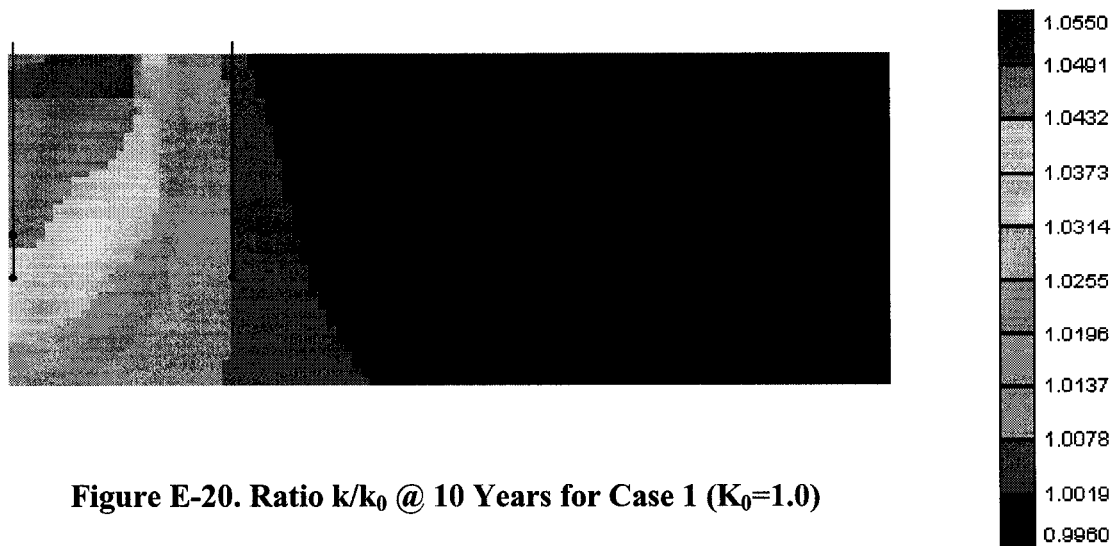
**Figure E-17. Ratio  $\phi/\phi_0$  @ 10 Years for Case 1 ( $K_0=1.5$ )**



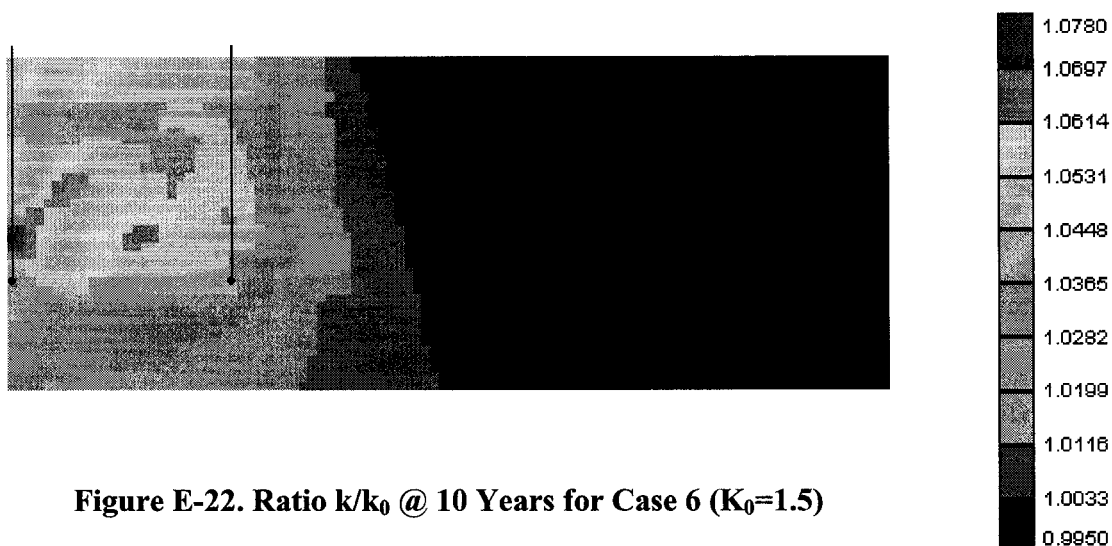
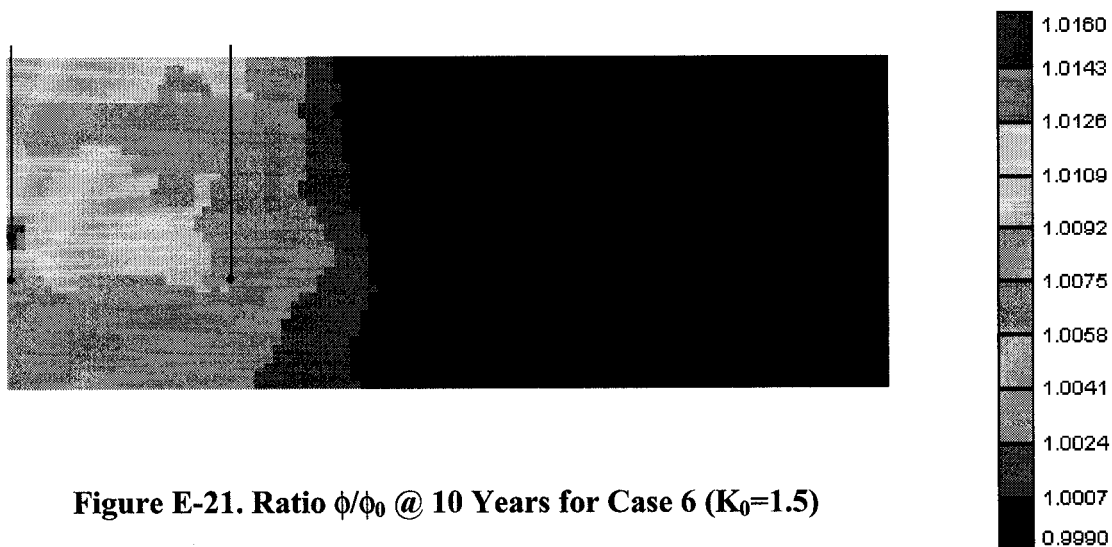
**Figure E-18. Ratio  $k/k_0$  @ 10 Years for Case 1 ( $K_0=1.5$ )**

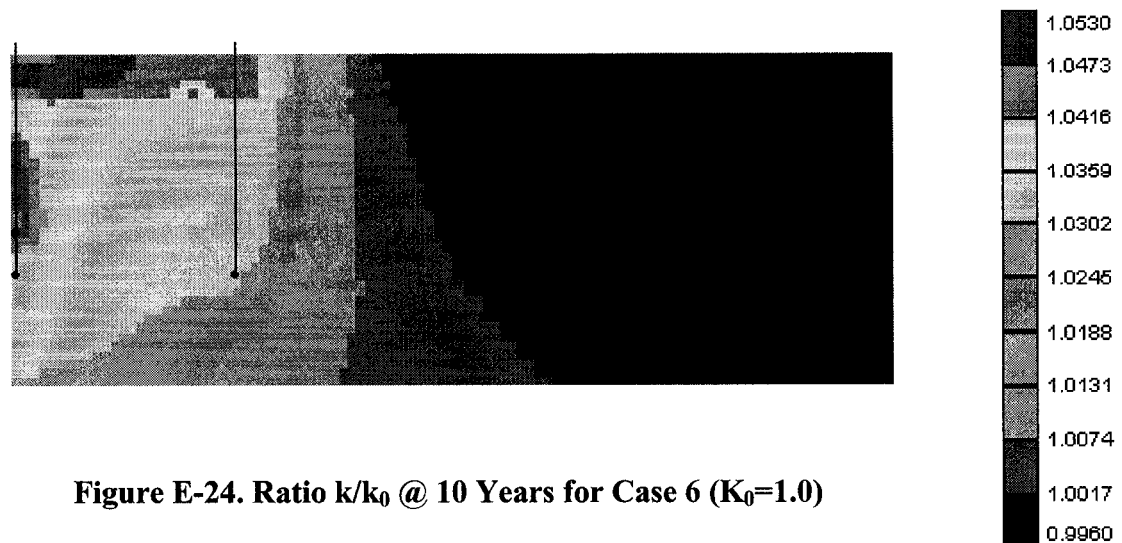
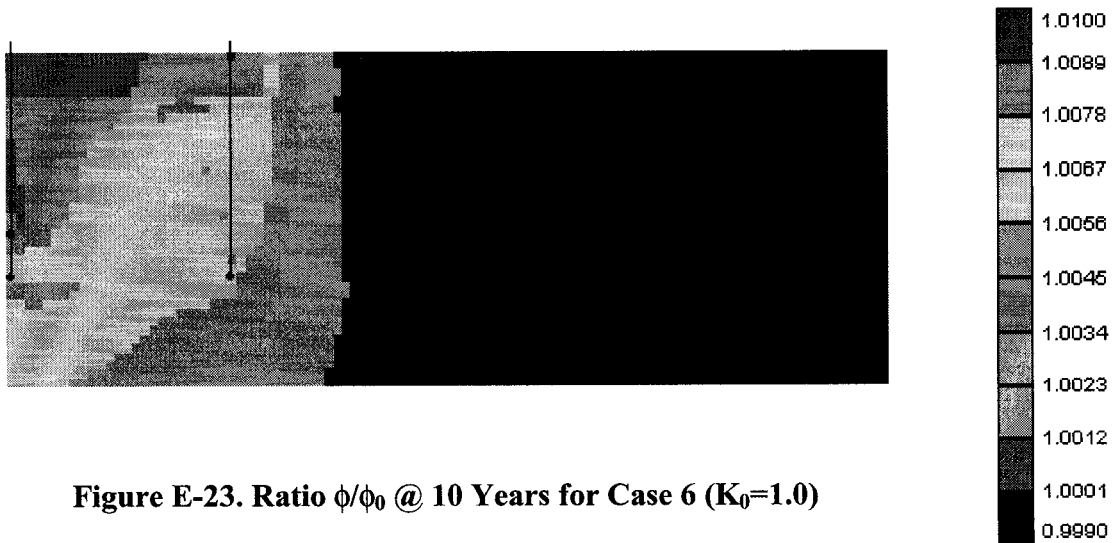


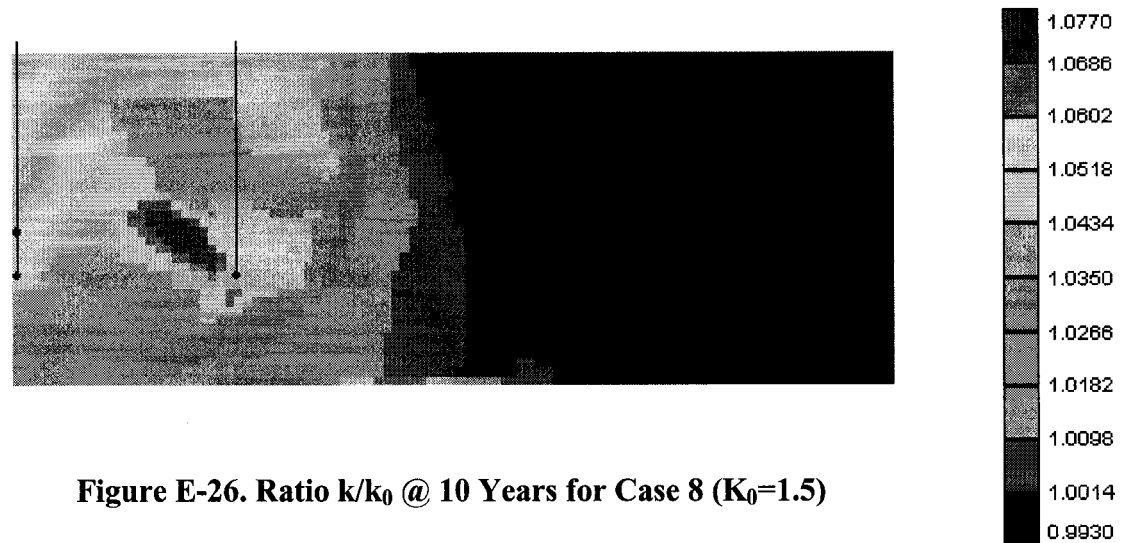
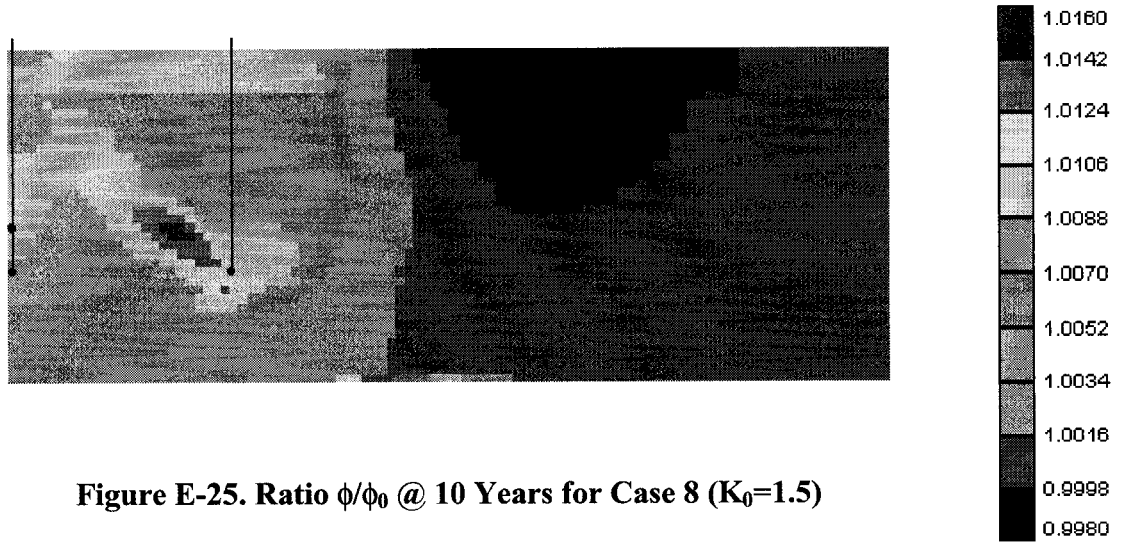
**Figure E-19. Ratio  $\phi/\phi_0$  @ 10 Years for Case 1 ( $K_0=1.0$ )**

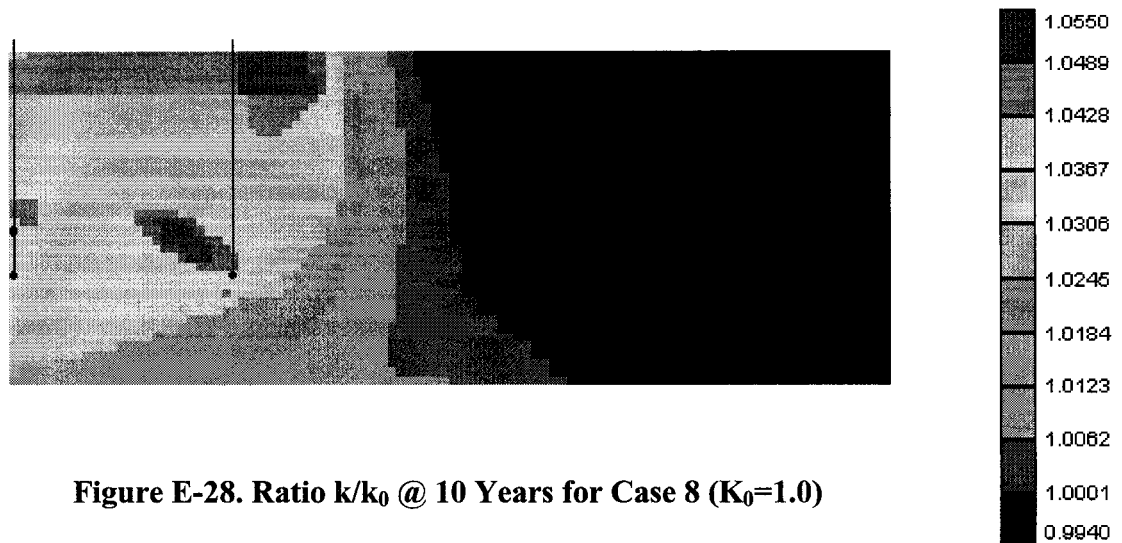
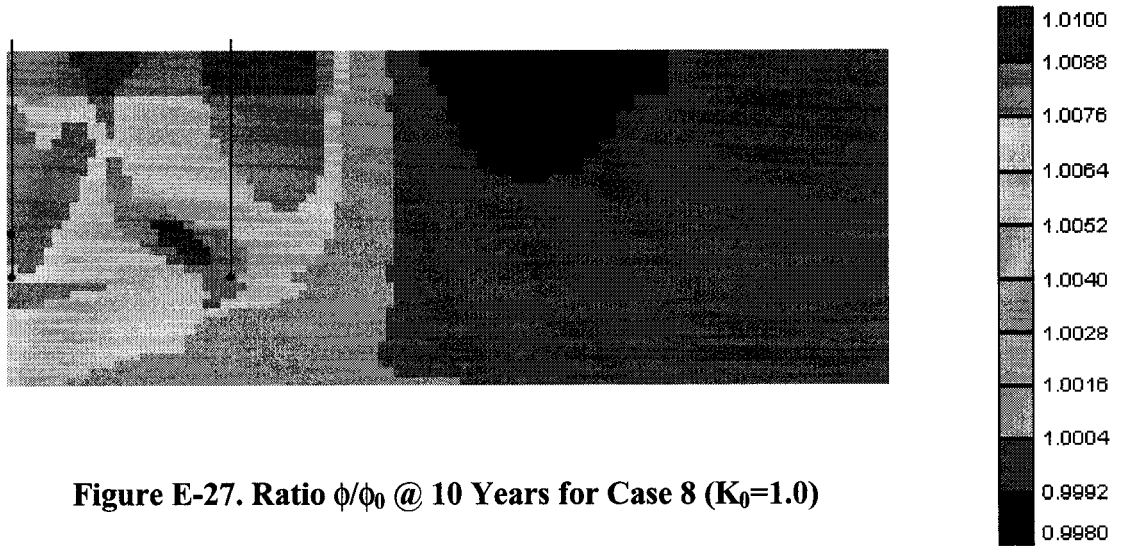


**Figure E-20. Ratio  $k/k_0$  @ 10 Years for Case 1 ( $K_0=1.0$ )**









## Appendix F: Reservoir Simulation Set (STARS)

```
** File Name: f-sagd-CSS03-extrasteam.dat
**
** Reservoir Thickness = 38 m
** Depth to Top of Reservoir = 402 m
** Overburden Thickness = 28 m
** Initial Reservoir Temperature = 18 C
** Initial Reservoir Pressure = 3100 kPa
**
** SAGD Production: 10 years (by Dual Horizontal wells)
** Production Pressure = 3100 kPa
** Steam Injection Pressure = 3110 kPa
** Steam Injection Rate = 400 m3/day
** Length of Horizontal Well = 900 m (8.7'' diameter)
** Well Horizontal Spacing = 100 m
** Injector Location = 21.5 m from Bottom of Reservoir
** Producer Location = 26.5 from Bottom of Reservoir
**
** Huff-Puff option: start offset well in year 3, two cycles
**                      9 mths inj + 3 mths prod, 6 mths inj + 6 mths prod
** Production Pressure = 3100 kPa
** Steam Injection Pressure = 8000 kPa
** Steam Injection Rate = 400 m3/day
** Length of Horizontal Well = 900 m (8.7'' diameter)
** Injector Location = 26.5 m from Bottom of Reservoir
** Producer Location = 26.5 m from Bottom of Reservoir
**
** SAGD Injection Rate = 800 m3/day after year 5
**
** Run on CMG's STARS

** ===== INPUT/OUTPUT CONTROL =====

*filename *output
        *index-out
        *main-results-out
        *main-results-in

**checkonly      ** check well data without running simulation

*title1 'bituman'
*title2 '2-D Fast-SAGD with Horizontal Wells'
*title3 'Data file: F-sagd-548x3'
*caseid '10-year'

*inunit *SI *except 6 1 ** darcy instead of md
*outunit *SI *except 6 1 ** darcy instead of md

**outprn *grid *pres *sw *so *sg *temp *x *y *vporos *obhloss *viso
*masdeno *masdenw
*outprn *grid *none
*outprn *iter *brief

*outsrf *grid *pres *sw *so *sg *temp *x *y *vporos
*outsrf *well *downhole *layer *all

*wrst      **write grid data to restart file at *time
**rewind 1  **only last restart is available
```

```

*prntorien 2 0    **I rows, K columns, J plane
**restart 184

** ===== GRID AND RESERVOIR DEFINITION =====

*grid *cart 151 1 38                ** Total gridblock number = 5738
*kdir *up                ** K = 1 at bottom of reservoir
*ninepoint *ik           ** this keyword isn't allowed in
Geomechanics Model

*di *ivar 10*1.0 36*1.0 9*1.0 36*1.0 10*1.0 50*2.0
** Gridblock size = 1.0 m*1.0 m around wellbores, 1.0 m*1.0 m in
between, 2.0 m far away
** for a total SAGD area 400 m * 900 m
*dj *jvar 900.0
*dk *kvar 38*1.0

** Half well along axis of symmetry (Gridblock size = 0.5 m 0.5 m)
*vamod 2 0.5 1.0 0.5 0.5 1.0 0.5 0.5    **9p 1.0 1.0 just for ninepoint
*vatype *con 1
      *mod 1 1 1:38 = 2
      ** 151 1 1:38 = 2

*dtop *con 402.0
*por *con 0.30                ** layer C3 porosity = 30.1%
      *mod 1:151 1 13:33 = 0.35 ** layer C2 porosity = 31.2%
      1:151 1 1:12 = 0.32 ** layer C1 porosity = 32.6%
*permi *con 1.5                ** layer C3 horizontal permeability =
0.16d
      *mod 1:151 1 13:33 = 2.5    ** layer C2 horizontal permeability =
1.97 d
      1:151 1 1:12 = 1.0    ** layer C1 horizontal permeability =
1.90 d
*permj *equalsi
*permk *con 0.3                ** layer C3 vertical permeability =
0.55 d
      *mod 1:151 1 13:33 = 1.25 ** layer C2 vertical permeability =
1.97 d
      1:151 1 1:12 = 0.2    ** layer C1 vertical permeability =
1.90 d
*end-grid
*prpor 3100.0

** USE STARS default values for sandstone thermal properties
*rocktype 1                ** Sandstone formation
*cpor 9.6e-6                ** formation compressibility = 9.6e-6/kPa (AOSTAR
Burnt Lake Study)
*rockcp 2.35e6                ** volumetric heat capacity of formation =2.35e6 J/m3-
C (UTF 2.39e6)

*thconr 6.6000e5            ** thermal conductivity of matrix (J/m-days-C)
*thconw 5.3496e4            ** thermal conductivity of water (J/m-days-C)
*thcono 1.1500e4            ** thermal conductivity of oil (J/m-days-c)
*thcong 1.3997e2            ** thermal conductivity of gas (J/m-days-c)

*thconmix *simple            ** Simple Volume Weighting (Default Value)
** Assumed Reservoir Temperature Above/Below Pay is 18 C
*hlossprop *overbur 2.35e6 1.469e5 *hlosst 18.0 *hlosstdiff 0.1
*hlossprop *underbur 2.35e6 1.469e5 *hlosst 18.0 *hlosstdiff 0.1
** ===== FULD DEFINITIONS =====

```



\*MODEL 3 3 3      \*\* Components are water, oil and dissolved gas

                 \*\* Standard water properties

*compname	'WATER'	'OIL'	'METHANE'	
*cmm	0	0.5	0.01604	
*pcrit	0	1360.0	4600.00	
*tcrit	0	624.65	-82.55	
*molden	0	1848.0	18750.9	**Live oil=
*cp	0	5.5e-7	5.5e-7	
*ct1	0	8.00e-4	8.00e-4	
*ct2	0	0	0	
*kv1	0	0	31914.0	
*kv2	0	0	0	
*kv3	0	0	0	
*kv4	0	0	-33.067	
*kv5	0	0	-27.71	
*cpl1	0	1060	67.2	**J/gmol-C
*cpg1	0	841	35.2	
*hvapr	0	1346	1770	

\*visctable

**Temp (C)	Water	Oil	CH4	**Live oil
12.0	0	60590	450	
20.0	0	21540	211.3	
30.0	0	7000	46.08	
40.0	0	2261	30.00	
50.0	0	1153	13.76	
60.0	0	558	8.16	
70.0	0	296.4	4.80	
80.0	0	170.3	4.00	
100.0	0	68.14	3.40	
120.0	0	33.25	2.90	
140.0	0	18.83	2.50	
160.0	0	11.94	2.15	
180.0	0	8.256	1.85	
200.0	0	6.106	1.45	
220.0	0	4.761	1.16	
240.0	0	3.815	0.95	
260.0	0	3.257	0.79	
280.0	0	2.815	0.68	
300.0	0	2.488	0.548	

\*\*Reference and Surface Conditions

\*prsr 101.325 \*temr 20.0 \*psurf 101.325 \*tsurf 20.0

\*surflash w o g

\*\* ===== ROCK-FLUID PROPERTIES =====

\*rockfluid

\*\* Neglect capillary pressure effect (no available data)

\*krtype \*con 1                      \*\*layer c3

      \*mod 1:151 1 13:33 = 2      \*\*layer c2

          1:151 1 1:12 = 3      \*\*layer c1

\*rpt 1      \*\* layer c3

*swt	** Water-oil Relative Permeabilities			
** Sw	Krw	Krow	Pcow	
**	-----	-----	-----	-----
0.0000000	0.0000000	1.0000000	8.9218645	
0.0900000	0.0000000	0.8486012	8.9218645	
0.1800000	0.0000000	0.6877059	8.9218645	
0.2700000	0.0000000	0.5247213	8.9218645	
0.3600000	0.0000000	0.3675857	8.9218645	
0.4500000	0.0000000	0.2250000	8.9218645	
0.4625000	0.0002276	0.2051564	8.2203941	
0.4750000	0.0007924	0.1861311	7.6009393	
0.4875000	0.0016441	0.1679333	7.0538144	
0.5000000	0.0027595	0.1505721	6.5704565	
0.5125000	0.0041235	0.1340580	6.1433034	
0.5359375	0.0073149	0.1054162	5.4712076	
0.5593750	0.0112910	0.0798736	4.9366956	
0.5828125	0.0160143	0.0575277	4.5102701	
0.6062500	0.0214563	0.0384981	4.1683998	
0.6296875	0.0275937	0.0229377	3.8922198	
0.6531250	0.0344074	0.0110557	3.6664891	
0.6765625	0.0418809	0.0031749	3.4787507	
0.7000000	0.0500000	0.0000000	3.3186455	
0.7375000	0.0951516	0.0000000	3.0983009	
0.7750000	0.1571142	0.0000000	2.8950715	
0.8125001	0.2380628	0.0000000	2.6800408	
0.8500001	0.3401130	0.0000000	2.4226151	
0.8875001	0.4653299	0.0000000	2.0861671	
0.9250001	0.6157349	0.0000000	1.6228262	
0.9625002	0.7933096	0.0000000	0.9666687	
1.0000000	1.0000000	0.0000000	0.0000000	

*slt	**Gas - liquid relative permeabilities			
** Sl	Krg	Krog	Pcgo	
**	-----	-----	-----	-----
0.0000000	1.0000000	0.0000000	11.8852911	
0.1000000	0.8810555	0.0000000	11.8852911	
0.2000000	0.7532181	0.0000000	11.8852911	
0.3000000	0.6207352	0.0000000	11.8852911	
0.4000000	0.4880767	0.0000000	11.8852911	
0.5000000	0.3600000	0.0000000	11.8852911	
0.5250000	0.3282502	0.0004556	10.2784863	
0.5450000	0.2978098	0.0018225	8.9923592	
0.5675000	0.2686931	0.0041006	7.9615321	
0.5900000	0.2409154	0.0072900	7.1335955	
0.6125000	0.2144928	0.0113906	6.4664559	
0.6338599	0.1906792	0.0161266	5.9509768	
0.6552197	0.1681191	0.0216839	5.5261912	
0.6765796	0.1468303	0.0280623	5.1726456	
0.6979395	0.1268320	0.0352620	4.8741474	
0.7192993	0.1081454	0.0432830	4.6170259	
0.7406592	0.0907940	0.0521252	4.3895054	
0.7620190	0.0748040	0.0617886	4.1811671	
0.7833789	0.0602052	0.0722732	3.9824681	
0.8047388	0.0470316	0.0835791	3.7843089	
0.8260986	0.0353230	0.0957063	3.5776145	
0.8474585	0.0251269	0.1086547	3.3529179	
0.8688183	0.0165023	0.1224243	3.0999289	
0.8901782	0.0095250	0.1370151	2.8070612	
0.9115381	0.0043011	0.1524272	2.4609025	
0.9328979	0.0010000	0.1686606	2.0455976	
0.9401156	0.0003728	0.1743316	1.8863907	

0.9442871	0.0001389	0.1776519	1.7894783
0.9466981	0.0000518	0.1795853	1.7317457
0.9480916	0.0000193	0.1807075	1.6977863
0.9488970	0.0000072	0.1813577	1.6779585
0.9493625	0.0000027	0.1817340	1.6664302
0.9500000	0.0000000	0.1822500	1.6505624
0.9666666	0.0000000	0.1960000	1.2002422
0.9833333	0.0000000	0.2102499	0.6727865
1.0000000	0.0000000	0.2250000	0.0000000

\*rpt 2 \*copy 1 \*\* layer C2

\*swt \*\* Water-oil Relative Permeabilities

** Sw	Krw	Krow	Pcow
0.0000000	0.0000000	1.0000000	6.6102490
0.0600000	0.0000000	0.9604667	6.6102490
0.1200000	0.0000000	0.8961671	6.6102490
0.1800000	0.0000000	0.8115541	6.6102490
0.2400000	0.0000000	0.7112345	6.6102490
0.3000000	0.0000000	0.6000000	6.6102490
0.3200000	0.0002276	0.5470836	5.8107371
0.3400000	0.0007924	0.4963496	5.1559744
0.3600000	0.0016441	0.4478219	4.6196809
0.3800000	0.0027595	0.4015256	4.1803331
0.4000000	0.0041235	0.3574881	3.8202991
0.4375000	0.0073149	0.2811098	3.3106978
0.4750000	0.0112909	0.2129961	2.9585462
0.5125000	0.0160143	0.1534072	2.7137392
0.5500000	0.0214563	0.1026615	2.5414460
0.5875000	0.0275937	0.0611671	2.4171529
0.6250000	0.0344074	0.0294817	2.3231745
0.6625001	0.0418810	0.0084664	2.2461400
0.7000000	0.0500000	0.0000000	2.1750901
0.7375000	0.1050487	0.0000000	2.0999134
0.7750000	0.1754919	0.0000000	2.0099154
0.8125001	0.2627652	0.0000000	1.8922905
0.8500001	0.3682758	0.0000000	1.7303030
0.8875001	0.4934058	0.0000000	1.5009053
0.9250001	0.6395141	0.0000000	1.1714581
0.9625002	0.8079394	0.0000000	0.6950878
1.0000000	1.0000000	0.0000000	0.0000000

\*slt \*\* Gas-liquid Relative Permeabilities

** Sl	Krg	Krog	Pcgo
0.0000000	1.0000000	0.0000000	8.8119259
0.0700000	0.9361368	0.0000000	8.8119259
0.1400000	0.8622400	0.0000000	8.8119259
0.2100000	0.7802442	0.0000000	8.8119259
0.2800000	0.6921435	0.0000000	8.8119259
0.3500000	0.6000000	0.0000000	8.8119259
0.3800000	0.5470837	0.0012781	7.2870235
0.4100000	0.4963497	0.0051124	6.1564059
0.4400000	0.4478219	0.0115030	5.3175530
0.4700000	0.4015256	0.0204497	4.6943998
0.5000000	0.3574880	0.0319527	4.2304420
0.5288554	0.3172891	0.0454285	3.8950956
0.5577109	0.2792353	0.0612693	3.6399288
0.5865663	0.2433573	0.0794750	3.4435489
0.6154218	0.2096886	0.1000455	3.2894900
0.6442772	0.1782663	0.1229809	3.1648359

0.6731327	0.1491311	0.1482812	3.0591342
0.7019881	0.1223291	0.1759464	2.9635236
0.7308435	0.0979122	0.2059765	2.8699872
0.7596990	0.0759404	0.2383715	2.7706833
0.7885544	0.0564841	0.2731314	2.6572852
0.8174099	0.0396277	0.3102561	2.5202856
0.8462653	0.0254766	0.3497457	2.3481982
0.8751208	0.0141687	0.3916002	2.1265948
0.9039762	0.0058999	0.4358196	1.8368946
0.9328316	0.0010000	0.4824039	1.4548093
0.9400771	0.0003728	0.4944725	1.3407885
0.9442649	0.0001389	0.5015159	1.2710992
0.9466853	0.0000518	0.5056095	1.2294959
0.9480842	0.0000193	0.5079830	1.2049950
0.9488927	0.0000072	0.5093574	1.1906799
0.9493600	0.0000027	0.5101526	1.1823543
0.9500000	0.0000000	0.5112426	1.1708897
0.9666666	0.0000000	0.5400394	0.8453855
0.9833333	0.0000000	0.5696252	0.4615968
1.0000000	0.0000000	0.6000000	0.0000000

\*rpt 3 \*copy 1 \*\* layer C1

\*swt \*\* water-oil relative permeabilities

** Sw	Krw	Krow	Pcow
0.0000000	0.0000000	1.0000000	8.0950136
0.1200000	0.0000000	0.9016334	8.0950136
0.2400000	0.0000000	0.7184374	8.0950136
0.3600000	0.0000000	0.4891419	8.0950136
0.4800000	0.0000000	0.2563998	8.0950136
0.6000000	0.0000000	0.0700000	8.0950136
0.6050000	0.0002276	0.0638264	7.8276482
0.6100000	0.0007924	0.0579075	7.5730677
0.6150000	0.0016441	0.0522459	7.3306351
0.6200000	0.0027595	0.0468447	7.0997438
0.6250000	0.0041235	0.0417070	6.8798175
0.6343750	0.0073149	0.0327962	6.4951138
0.6437500	0.0112909	0.0248496	6.1436582
0.6531249	0.0160143	0.0178976	5.8223605
0.6624999	0.0214562	0.0119772	5.5283937
0.6718749	0.0275936	0.0071362	5.2591729
0.6812499	0.0344073	0.0034396	5.0123296
0.6906248	0.0418808	0.0009878	4.7856936
0.7000000	0.0500000	0.0000000	4.5772672
0.7375000	0.0958982	0.0000000	3.8911202
0.7750000	0.1591381	0.0000000	3.3723254
0.8125001	0.2414732	0.0000000	2.9470670
0.8500001	0.3446493	0.0000000	2.5548403
0.8875001	0.4703946	0.0000000	2.1398385
0.9250001	0.6204156	0.0000000	1.6430143
0.9625002	0.7963969	0.0000000	0.9936792
1.0000000	1.0000000	0.0000000	0.0000000

\*slt \*\* Gas - liquid Relative Permeabilities

** Sl	Krg	Krog	Kcgo
0.0000000	1.0000000	0.0000000	10.7503405
0.1300000	0.9804409	0.0000000	10.7503405
0.2600000	0.8748173	0.0000000	10.7503405
0.3900000	0.7080842	0.0000000	10.7503405
0.5200000	0.5068279	0.0000000	10.7503405

0.6500000	0.3000000	0.0000000	10.7503405
0.6650000	0.2735419	0.0001286	9.7242098
0.6800000	0.2481749	0.0005143	8.8356829
0.6950001	0.2239109	0.0011571	8.0647287
0.7100000	0.2007628	0.0020571	7.3939753
0.7250000	0.1787441	0.0032143	6.8082962
0.7391589	0.1590093	0.0045425	6.3216057
0.7533178	0.1403073	0.0060998	5.8891683
0.7674767	0.1226524	0.0078862	5.5023003
0.7816356	0.1060605	0.0099017	5.1532326
0.7957945	0.0905488	0.0121463	4.8349562
0.8099535	0.0761366	0.0146201	4.5410795
0.8241124	0.0628453	0.0173229	4.2657018
0.8382713	0.0506991	0.0202549	4.0032921
0.8524302	0.0397257	0.0234160	3.7485824
0.8665891	0.0299574	0.0268062	3.4964564
0.8807480	0.0214329	0.0304255	3.2418520
0.8949069	0.0141997	0.0342739	2.9796565
0.9090658	0.0083188	0.0383515	2.7046046
0.9232247	0.0038746	0.0426581	2.4111731
0.9373836	0.0010000	0.0471939	2.0934696
0.9427080	0.0003728	0.0489588	1.9664288
0.9457855	0.0001389	0.0499937	1.8908864
0.9475641	0.0000518	0.0505968	1.8464833
0.9485921	0.0000193	0.0509470	1.8205651
0.9491863	0.0000072	0.0511500	1.8054974
0.9495297	0.0000027	0.0512675	1.7967606
0.9500000	0.0000000	0.0514286	1.7847605
0.9666666	0.0000000	0.0573016	1.3312364
0.9833333	0.0000000	0.0634921	0.8139912
1.0000000	0.0000000	0.0700000	0.0000000

\*\* Consider Foamy Oil Effect

\*\* krtemtab \*sgr

\*\* Temp(c) Sgr

\*\*-----

\*\* 12.0 0.10

\*\* 250.0 0.00 \*\* No foamy oil effect

\*\* ===== INTIAL CONDITIONS =====

\*initial

\*pres \*con 3100.00

\*sw \*con 0.45

\*mod 1:151 1 13:33 = 0.3

1:151 1 1:12 = 0.6

\*so \*con 0.55

\*mod 1:151 1 13:33 = 0.7

1:151 1 1:12 = 0.4

\*sg \*con 0.0

\*temp \*con 18.0

\*molefrac \*oil \*con 0.0 0.89 0.11 \*\* Live Oil

\*\*molefrac \*oil \*con 0.0 1.00 0.00 \*\* Dead Oil

\*vertical \*on

\*refpres 3100

\*refdepth 427.5

\*refblock 1 1 13

```

** ===== Numerical Control =====

*numerical

** ===== RECURRENT DATA =====

*run

*time 0.0 *dtwell 1.0e-4

*well 1 'InjectorB1' *frac 0.5    ** 900 m standard SAGD wells
*well 2 'ProducerB1' *frac 0.5    ** 900 m standard SAGD wells
*well 3 'Injector_S' *frac 1.0    ** 900 m single well (huff & puff)
*well 4 'Producer_S' *frac 1.0    ** 900 m single well (huff & puff)

*injector *mobweight 1
*operate *bhp 3110.0
*operate *max *water 400.0    **max. steam injection rate = 400 m3/d
CWE (full well)
*tinwj 235.0 *qual 0.95    **3110 - 235
*incomp *water 1 0 0
*geometry *j 0.11 0.249 1.0 0    ** well diameter = 8.7"
*perf *geo 1    ** i j k
                        1 1 18    ** injector 21.5 m from bottom of
reservoir
*uhtr *ijk 1:1 1:1 18 1.95e9
*tmpset *ijk 1:1 1:1 18 265.0

*producer 2
*operate *bhp 3100.0
*operate *steamtrap 5.0
*geometry *j 0.11 0.249 1.0 0    ** well diameter = 8.7"
*perf *geo 2    ** i j k
                        1 1 13    ** producer 26.5 m from bottom of
reservoir
*uhtr *ijk 1:1 1:1 13 1.95e9
*tmpset *ijk 1:1 1:1 13 265.0

*injector *mobweight 3
*operate *bhp 8000.0
*operate *max *water 800.0    ** max. steam injection rate = 800
m3/d CWE (full well)
*tinwj 295 *qual 0.98
*incomp *water 1 0 0
*geometry *j 0.11 0.249 1.0 0    ** well diameter = 8.7"
*perf *geo 3    ** i j k
                        51 1 13    ** injector 26.5 m from bottom of
reservoir

*producer 4
*operate *bhp 3100.0
*operate *steamtrap 5.0
*geometry *j 0.11 0.249 1.0 0    ** well diameter = 8.7"
*perf *geo 4    ** i j k
                        51 1 13    ** producer 26.5 m from bottom of
reservoir

*shutin 3 4
** producer 2 kept open for release of fluid while heating the SAGD pair

*time 52.0 *dtwell 1.0e-3    ** Standard SAGD Started

```

*uhtr *con 0.0	** turn heater off after startup
period of 52 days	
*time 91.25	
*time 182.5	
*time 273.75	
*time 365	** after 1 year
*time 730	** after 2 years
*time 1095	** after 3 years
*open 3	
*time 1370	** after 3 years 9 mths
*shutin 3	
*time 1384	** after 3 years 9 mths 2 weeks
*open 4	
*time 1460.0	** after 4 years
*shutin 4	
*open 3	
*time 1641	** after 4 years 6 mths
*shutin 3	
*injector *mobweight 1	
*operate *bhp 3110.0	
*operate *max *water 800.0	**max. steam injection rate = 800 m3/d
CWE (full well)	
*time 1655	** after 4 years 6 mths 2 weeks
*open 4	
*time 1825	** after 5 years
*time 2190	** after 6 years
*time 2555	** after 7 years
*time 2920	** after 8 years
*time 3285	** after 9 years
*time 3650	** after 10 years
*stop	

## Appendix G: Geomechanical Simulation Set (FLAC)

```

;Fast-SAGD-CSS@3-extrasteam-Ko=1.5
tit
Geomechanics in Fast SAGD process
config thermal gw extra 5

grid 76 52
mo el th_iso

gen 0,0    0,38    1,38    1,0    rat 1 1          i=1,2    j=1,39
gen 1,0    1,38    101,38  101,0   rat 1 1          i=2,52   j=1,39
gen 101,0  101,38  201,38  201,0   rat 1 1          i=52,77  j=1,39

gen 0,38    0,331    1,331    1,38    rat 1 1.408667    i=1,2    j=39,52
gen 1,38    1,331    101,331  101,38  rat 1 1.408667    i=2,52   j=39,52
gen 101,38  101,331  201,331  201,38  rat 1 1.408667    i=52,77  j=39,52

gen 0,331    0,440    1,440    1,331    rat 1 1          i=1,2    j=52,53
gen 1,331    1,440    101,440  101,331  rat 1 1          i=2,52   j=52,53
gen 101,331  101,440  201,440  201,331  rat 1 1          i=52,77  j=52,53

;ret

fix x y          i=1,77 j=1
fix x            i=1 j=1,53
fix x            i=77 j=1,53

set flow off
;
;Material Properties for Oil Sands
;
pro den 3000          j=1,38
pro bulk 3.60e8        j=1,38
pro she 3.54e8         j=1,38
pro cond 1 sp 1 thexp 2e-5
water dens 1000 bulk 2e9 tens 5e5
pro por 0.32          j=1,12
pro por 0.35          j=13,33
pro por 0.30          j=34,38

;
;Material Properties for Water Saturated Overburden
;
pro den 3000          j=39,51
pro bulk 5.56e8        j=39,51
pro she 3.57e8         j=39,51
pro por 1e-8          j=39,51

;
;Material Properties for Dry Overburden
;
pro den 1700          j=52
pro bulk 3.75e8        j=52
pro she 1.73e8         j=52
pro por 1e-8          j=52

```



```

ini sat 1 j=1,39
ini sat 1 j=39,52
ini sat 0 j=52,53
fix sat

set grav 9.81

ini sxx -1.73386845e7 var 0 1677510 j=1,38
ini syy -1.1559123e7 var 0 1118340 j=1,38
ini szz -1.73386845e7 var 0 1677510 j=1,38

ini sxx -1.56611745e7 var 0 12934485 j=39,51
ini syy -1.0440783e7 var 0 8622990 j=39,51
ini szz -1.56611745e7 var 0 12934485 j=39,51

ini sxx -1363344.75 j=52
ini syy -908896.5 j=52
ini szz -1363344.75 j=52

ini pp 3213100 var 0 -342600 j=1,39
ini pp 2870500 var 0 -2870500 j=39,52

;
;Equilibrium with initial in situ stress
;
set mech on flow off
water bulk 0
set therm off
solve force=10000

;ret

ini xd=0
ini yd 0

save f-sagd-0.sav

;Day 182
model mohr i=1,76 j=1,38
prop coh 0 dens 3000 dil 20 friction 45 i=1,76 j=1,38

def calmodulus
  loop i (1, izonas)
    loop j (1, 38)
      ps=-(sxx(i,j)+syy(i,j)+szz(i,j))/3.0-pp(i,j)
      if ps < 0 then
        ps=10000
      end_if
      y_mod=343*(ps/10e6)^0.875
      bulk_mod(i,j)=y_mod/(3.0*(1.0-2.0*p_ratio))*10e6
      shear_mod(i,j)=y_mod/(2.0*(1.0+p_ratio))*10e6
    end_loop
  end_loop
end
set p_ratio=0.3
set therm off flow off
call f-sagd-548x3-css@3-flac-p182.dat

```

```

calmodulus
solve force 10000
set therm on flow off
call f-sagd-548x3-css@3-flac-t182.dat
solve force 10000
save f-sagd-182.sav

;Day 365

set therm off flow off
call f-sagd-548x3-css@3-flac-p365.dat
calmodulus
solve force 10000
set therm on flow off
call f-sagd-548x3-css@3-flac-t365.dat
solve force 10000
save f-sagd-365.sav

;Day 730

set therm off flow off
call f-sagd-548x3-css@3-flac-p730.dat
calmodulus
solve force 10000
set therm on flow off
call f-sagd-548x3-css@3-flac-t730.dat
solve force 10000
save f-sagd-730.sav

;Day 1095

set therm off flow off
call f-sagd-548x3-css@3-flac-p1095.dat
calmodulus
solve force 10000
set therm on flow off
call f-sagd-548x3-css@3-flac-t1095.dat
solve force 10000
save f-sagd-1095.sav

;Day 1110

set therm off flow off
call f-sagd-548x3-css@3-flac-p1110.dat
calmodulus
solve force 10000
set therm on flow off
call f-sagd-548x3-css@3-flac-t1110.dat
solve force 10000
save f-sagd-1110.sav

;Day 1125

set therm off flow off
call f-sagd-548x3-css@3-flac-p1125.dat
calmodulus
solve force 10000

```

```
set therm on flow off
call f-sagd-548x3-css@3-flac-t1125.dat
solve force 10000
save f-sagd-1125.sav
```

```
;Day 1140
```

```
set therm off flow off
call f-sagd-548x3-css@3-flac-p1140.dat
calmodulus
solve force 10000
set therm on flow off
call f-sagd-548x3-css@3-flac-t1140.dat
solve force 10000
save f-sagd-1140.sav
```

```
;Day 1160
```

```
set therm off flow off
call f-sagd-548x3-css@3-flac-p1160.dat
calmodulus
solve force 10000
set therm on flow off
call f-sagd-548x3-css@3-flac-t1160.dat
solve force 10000
save f-sagd-1160.sav
```

```
;Day 1180
```

```
set therm off flow off
call f-sagd-548x3-css@3-flac-p1180.dat
calmodulus
solve force 10000
set therm on flow off
call f-sagd-548x3-css@3-flac-t1180.dat
solve force 10000
save f-sagd-1180.sav
```

```
;Day 1200
```

```
set therm off flow off
call f-sagd-548x3-css@3-flac-p1200.dat
calmodulus
solve force 10000
set therm on flow off
call f-sagd-548x3-css@3-flac-t1200.dat
solve force 10000
save f-sagd-1200.sav
```

```
;Day 1250
```

```
set therm off flow off
call f-sagd-548x3-css@3-flac-p1250.dat
calmodulus
solve force 10000
set therm on flow off
call f-sagd-548x3-css@3-flac-t1250.dat
```

```

solve force 10000
save f-sagd-1250.sav

;Day 1300

set therm off flow off
call f-sagd-548x3-css@3-flac-p1300.dat
calmodulus
solve force 10000
set therm on flow off
call f-sagd-548x3-css@3-flac-t1300.dat
solve force 10000
save f-sagd-1300.sav

;Day 1340

set therm off flow off
call f-sagd-548x3-css@3-flac-p1340.dat
calmodulus
solve force 10000
set therm on flow off
call f-sagd-548x3-css@3-flac-t1340.dat
solve force 10000
save f-sagd-1340.sav

;Day 1370

set therm off flow off
call f-sagd-548x3-css@3-flac-p1370.dat
calmodulus
solve force 10000
set therm on flow off
call f-sagd-548x3-css@3-flac-t1370.dat
solve force 10000
save f-sagd-1370.sav

;Day 1377

set therm off flow off
call f-sagd-548x3-css@3-flac-p1377.dat
calmodulus
solve force 10000
set therm on flow off
call f-sagd-548x3-css@3-flac-t1377.dat
solve force 10000
save f-sagd-1377.sav

;Day 1384

set therm off flow off
call f-sagd-548x3-css@3-flac-p1384.dat
calmodulus
solve force 10000
set therm on flow off
call f-sagd-548x3-css@3-flac-t1384.dat
solve force 10000
save f-sagd-1384.sav

```

```

;Day 1400

set therm off flow off
call f-sagd-548x3-css@3-flac-p1400.dat
calmodulus
solve force 10000
set therm on flow off
call f-sagd-548x3-css@3-flac-t1400.dat
solve force 10000
save f-sagd-1400.sav

;Day 1430

set therm off flow off
call f-sagd-548x3-css@3-flac-p1430.dat
calmodulus
solve force 10000
set therm on flow off
call f-sagd-548x3-css@3-flac-t1430.dat
solve force 10000
save f-sagd-1430.sav

;Day 1460

set therm off flow off
call f-sagd-548x3-css@3-flac-p1460.dat
calmodulus
solve force 10000
set therm on flow off
call f-sagd-548x3-css@3-flac-t1460.dat
solve force 10000
save f-sagd-1460.sav

;Day 1500

set therm off flow off
call f-sagd-548x3-css@3-flac-p1500.dat
calmodulus
solve force 10000
set therm on flow off
call f-sagd-548x3-css@3-flac-t1500.dat
solve force 10000
save f-sagd-1500.sav

;Day 1550

set therm off flow off
call f-sagd-548x3-css@3-flac-p1550.dat
calmodulus
solve force 10000
set therm on flow off
call f-sagd-548x3-css@3-flac-t1550.dat
solve force 10000
save f-sagd-1550.sav

;Day 1600

```

```
set therm off flow off
call f-sagd-548x3-css@3-flac-p1600.dat
calmodulus
solve force 10000
set therm on flow off
call f-sagd-548x3-css@3-flac-t1600.dat
solve force 10000
save f-sagd-1600.sav
```

;Day 1641

```
set therm off flow off
call f-sagd-548x3-css@3-flac-p1641.dat
calmodulus
solve force 10000
set therm on flow off
call f-sagd-548x3-css@3-flac-t1641.dat
solve force 10000
save f-sagd-1641.sav
```

;Day 1648

```
set therm off flow off
call f-sagd-548x3-css@3-flac-p1648.dat
calmodulus
solve force 10000
set therm on flow off
call f-sagd-548x3-css@3-flac-t1648.dat
solve force 10000
save f-sagd-1648.sav
```

;Day 1655

```
set therm off flow off
call f-sagd-548x3-css@3-flac-p1655.dat
calmodulus
solve force 10000
set therm on flow off
call f-sagd-548x3-css@3-flac-t1655.dat
solve force 10000
save f-sagd-1655.sav
```

;Day 1700

```
set therm off flow off
call f-sagd-548x3-css@3-flac-p1700.dat
calmodulus
solve force 10000
set therm on flow off
call f-sagd-548x3-css@3-flac-t1700.dat
solve force 10000
save f-sagd-1700.sav
```

;Day 1750

```
set therm off flow off
```

```

call f-sagd-548x3-css@3-flac-p1750.dat
calmodulus
solve force 10000
set therm on flow off
call f-sagd-548x3-css@3-flac-t1750.dat
solve force 10000
save f-sagd-1750.sav

;Day 1825

set therm off flow off
call f-sagd-548x3-css@3-flac-p1825.dat
calmodulus
solve force 10000
set therm on flow off
call f-sagd-548x3-css@3-flac-t1825.dat
solve force 10000
save f-sagd-1825.sav

;Day 2190

set therm off flow off
call f-sagd-548x3-css@3-flac-p2190.dat
calmodulus
solve force 10000
set therm on flow off
call f-sagd-548x3-css@3-flac-t2190.dat
solve force 10000
save f-sagd-2190.sav

;Day 2555

set therm off flow off
call f-sagd-548x3-css@3-flac-p2555.dat
calmodulus
solve force 10000
set therm on flow off
call f-sagd-548x3-css@3-flac-t2555.dat
solve force 10000
save f-sagd-2555.sav

;Day 2920

set therm off flow off
call f-sagd-548x3-css@3-flac-p2920.dat
calmodulus
solve force 10000
set therm on flow off
call f-sagd-548x3-css@3-flac-t2920.dat
solve force 10000
save f-sagd-2920.sav

;Day 3285

set therm off flow off
call f-sagd-548x3-css@3-flac-p3285.dat
calmodulus

```

```
solve force 10000
set therm on flow off
call f-sagd-548x3-css@3-flac-t3285.dat
solve force 10000
save f-sagd-3285.sav
```

```
;Day 3650
```

```
set therm off flow off
call f-sagd-548x3-css@3-flac-p3650.dat
calmodulus
solve force 10000
set therm on flow off
call f-sagd-548x3-css@3-flac-t3650.dat
solve force 10000
save f-sagd-3650.sav
```



## Appendix H: Interfacial Program of Data Transformation

### H-1. Code for data transformation from STARS to FLAC

Dim Ps, Pf, Ts, Tf, Sum\_P, Sum\_T As Single

Dim I, J, N, K As Integer

Dim Title, Grid\_N As String

Open "E:\jian\vb\f-sagd-548x3-@3-vb\f-sagd-548x3-css@3-stars-p3650.txt" For Input As #1

Open "E:\jian\vb\f-sagd-548x3-@3-vb\f-sagd-548x3-css@3-flac-p3650.dat" For Output As #2

N = 0

Sum\_P = 0

For K = 1 To 6

Line Input #1, Title

Next K

For J = 1 To 38

Line Input #1, Grid\_N

For I = 1 To 2

Input #1, Ps

Pf = Ps \* 1000

Sum\_P = Pf + Sum\_P

If I = 2 Then

Pf = Int(Sum\_P / 2)

N = 0

Sum\_P = 0

End If

Print #2, "ini pp", Pf, "i", I, "j", J

Print #2, "fix pp", "i", I, "j", J

Next I

For I = 3 To 151

Input #1, Ps

N = N + 1

```

    Pf = Ps * 1000
    Sum_P = Pf + Sum_P
    If N = 2 Then
        Pf = Int(Sum_P / N)
        Print #2, "ini pp", Pf, "i", (I + 2) / 2, "j", J
        Print #2, "fix pp", "i", (I + 2) / 2, "j", J
        N = 0
        Sum_P = 0
    End If
    If I = 151 Then
        Pf = Int(Sum_P)
        Print #2, "ini pp", Pf, "i", (I + 3) / 2, "j", J
        Print #2, "fix pp", "i", (I + 3) / 2, "j", J
        N = 0
        Sum_P = 0
    End If
Next I
Next J
Close #1
Close #2

Open "E:\jian\vb\fsagd-548x3-@3-vb\fsagd-548x3-css@3-stars-t3650.txt" For Input As #3
Open "E:\jian\vb\fsagd-548x3-@3-vb\fsagd-548x3-css@3-flac-t3650.dat" For Output As #4
N = 0
Sum_T = 0

For K = 1 To 6
    Line Input #3, Title
Next K

For J = 1 To 38
    Line Input #3, Grid_N
    For I = 1 To 1
        Input #3, Ts

```

```

        Tf = Ts - 18
        Print #4, "fix te", Tf, "i", I, "j", J
    Next I

    For I = 2 To 151
        Input #3, Ts
        N = N + 1
        Tf = Ts - 18
        Sum_T = Tf + Sum_T
        If N = 2 Then
            Tf = Sum_T / N
            Print #4, "fix te", Tf, "i", (I + 1) / 2, "j", J
            N = 0
            Sum_T = 0
        End If
    Next I
Next J
Close #3
Close #4

End Sub

```

## **H-2. Code for Calculating the Stress-Induced Permeability Change**

```

Dim vsi, te, por_ratio, perm_ratio, layer_number As Single
Dim v(76, 52), t(76, 52) As Single
Dim I, J, N, k As Integer
Dim Title As String

Open "E:\jian\vb\sagd-15-vsi-3650.dat" For Input As #1
For k = 1 To 3
    Line Input #1, Title
Next k

```

```

For N = 0 To 7
    For k = 1 To 5
        Line Input #1, Title
    Next k

    For J = 52 To 1 Step -1
        For I = 1 + (N * 10) To 10 + (N * 10)
            If I = 77 Then GoTo 100
            If I = 1 + (N * 10) Then
                Input #1, layer_number, vsi
            Else
                Input #1, vsi
            End If
            v(I, J) = vsi * 0.001
        Next I
    Next J
Next N
Close #1

```

```

Open "E:\jian\vb\sagd-15-te-3650.dat" For Input As #2
For k = 1 To 3
    Line Input #2, Title
Next k

```

```

For N = 0 To 7
    For k = 1 To 5
        Line Input #2, Title
    Next k

    For J = 52 To 1 Step -1
        For I = 1 + (N * 10) To 10 + (N * 10)
            If I = 77 Then GoTo 200
            If I = 1 + (N * 10) Then
                Input #2, layer_number, te
            End If
        Next I
    Next J
Next N

```

```

Else
    Input #2, te
End If
t(I, J) = te * 100
Next I
200 Next J
Next N
Close #2

Open "E:\jian\vb\sagd-15-por-3650.dat" For Output As #3
Print #3, "*POR *ijk"
For J = 38 To 34 Step -1
    For I = 1 To 76
        por_ratio = (0.3 + v(I, J) - (1 - 0.3) * 0.00002 * t(I, J)) / (1 + v(I, J)) / 0.3
        por_ratio = Round(por_ratio, 3)
        If I = 76 Then
            Print #3, Format(2 * I - 1, "00"); ":", Format(2 * I - 1, "00"), "1:1",
            Format(J, "00"); ":", Format(J, "00"), Int(por_ratio * 1000) / 1000
        Else
            Print #3, Format(2 * I - 1, "00"); ":", Format(2 * I - 1, "00"), "1:1",
            Format(J, "00"); ":", Format(J, "00"), Int(por_ratio * 1000) / 1000
            Print #3, Format(2 * I, "00"); ":", Format(2 * I, "00"), "1:1", Format(J,
            "00"); ":", Format(J, "00"), Int(por_ratio * 1000) / 1000
        End If
    Next I
Next J

For J = 33 To 13 Step -1
    For I = 1 To 76
        por_ratio = (0.35 + v(I, J) - (1 - 0.35) * 0.00002 * t(I, J)) / (1 + v(I, J)) / 0.35
        por_ratio = Round(por_ratio, 3)
        If I = 76 Then
            Print #3, Format(2 * I - 1, "00"); ":", Format(2 * I - 1, "00"), "1:1",
            Format(J, "00"); ":", Format(J, "00"), Int(por_ratio * 1000) / 1000

```

```

Else
    Print #3, Format(2 * I - 1, "00"); ":"; Format(2 * I - 1, "00"), "1:1",
    Format(J, "00"); ":"; Format(J, "00"), Int(por_ratio * 1000) / 1000
    Print #3, Format(2 * I, "00"); ":"; Format(2 * I, "00"), "1:1", Format(J,
    "00"); ":"; Format(J, "00"), Int(por_ratio * 1000) / 1000
End If
Next I
Next J

For J = 12 To 1 Step -1
    For I = 1 To 76
        por_ratio = (0.32 + v(I, J) - (1 - 0.32) * 0.00002 * t(I, J)) / (1 + v(I, J)) / 0.32
        por_ratio = Round(por_ratio, 3)
        If I = 76 Then
            Print #3, Format(2 * I - 1, "00"); ":"; Format(2 * I - 1, "00"), "1:1",
            Format(J, "00"); ":"; Format(J, "00"), Int(por_ratio * 1000) / 1000
        Else
            Print #3, Format(2 * I - 1, "00"); ":"; Format(2 * I - 1, "00"), "1:1",
            Format(J, "00"); ":"; Format(J, "00"), Int(por_ratio * 1000) / 1000
            Print #3, Format(2 * I, "00"); ":"; Format(2 * I, "00"), "1:1", Format(J,
            "00"); ":"; Format(J, "00"), Int(por_ratio * 1000) / 1000
        End If
    Next I
Next J

Close #3
End Sub

```

### **H-3. Code for Calculating the Stress-Induced Permeability Change**

```

Dim vsi, te, perm_ratio, layer_number As Single
Dim v(76, 52), t(76, 52) As Single
Dim I, J, N, k As Integer
Dim Title As String

```

```

Open "E:\jian\vb\sagd-15-vsi-3650.dat" For Input As #1

For k = 1 To 3
    Line Input #1, Title
Next k

For N = 0 To 7
    For k = 1 To 5
        Line Input #1, Title
    Next k

    For J = 52 To 1 Step -1
        For I = 1 + (N * 10) To 10 + (N * 10)
            If I = 77 Then GoTo 100
            If I = 1 + (N * 10) Then
                Input #1, layer_number, vsi
            Else
                Input #1, vsi
            End If
            v(I, J) = vsi * 0.001
        Next I
    Next J
100 Next J
Next N
Close #1

```

```

Open "E:\jian\vb\sagd-15-te-3650.dat" For Input As #2

For k = 1 To 3
    Line Input #2, Title
Next k

For N = 0 To 7
    For k = 1 To 5
        Line Input #2, Title
    Next k

```

```

For J = 52 To 1 Step -1
    For I = 1 + (N * 10) To 10 + (N * 10)
        If I = 77 Then GoTo 200
        If I = 1 + (N * 10) Then
            Input #2, layer_number, te
        Else
            Input #2, te
        End If
        t(I, J) = te * 100
    Next I
200    Next J
Next N
Close #2

Open "E:\jian\vb\sagd-15-perm-3650.dat" For Output As #3
Print #3, "**Perm *ijk"
For J = 38 To 34 Step -1
    For I = 1 To 76
        perm_ratio = (1 + v(I, J) / 0.3 - 0.00002 * t(I, J) * (1 - 0.3) / 0.3) ^ 3 / (1 + v(I, J))
        perm_ratio = Round(perm_ratio, 3)
        If I = 76 Then
            Print #3, Format(2 * I - 1, "00"); ":"; Format(2 * I - 1, "00"), "1:1",
            Format(J, "00"); ":"; Format(J, "00"), Int(perm_ratio * 1000) / 1000
        Else
            Print #3, Format(2 * I - 1, "00"); ":"; Format(2 * I - 1, "00"), "1:1",
            Format(J, "00"); ":"; Format(J, "00"), Int(perm_ratio * 1000) / 1000
            Print #3, Format(2 * I, "00"); ":"; Format(2 * I, "00"), "1:1", Format(J,
            "00"); ":"; Format(J, "00"), Int(perm_ratio * 1000) / 1000
        End If
    Next I
Next J

For J = 33 To 13 Step -1

```



```

For I = 1 To 76
    perm_ratio = (1 + v(I, J) / 0.35 - 0.00002 * t(I, J) * (1 - 0.35) / 0.35) ^ 3 / (1 + v(I,
    J))
    perm_ratio = Round(perm_ratio, 3)
    If I = 76 Then
        Print #3, Format(2 * I - 1, "00"); ":"; Format(2 * I - 1, "00"), "1:1",
        Format(J, "00"); ":"; Format(J, "00"), Int(perm_ratio * 1000) / 1000
    Else
        Print #3, Format(2 * I - 1, "00"); ":"; Format(2 * I - 1, "00"), "1:1",
        Format(J, "00"); ":"; Format(J, "00"), Int(perm_ratio * 1000) / 1000
        Print #3, Format(2 * I, "00"); ":"; Format(2 * I, "00"), "1:1", Format(J,
        "00"); ":"; Format(J, "00"), Int(perm_ratio * 1000) / 1000
    End If
Next I
Next J

For J = 12 To 1 Step -1
    For I = 1 To 76
        perm_ratio = (1 + v(I, J) / 0.32 - 0.00002 * t(I, J) * (1 - 0.32) / 0.32) ^ 3 / (1 + v(I,
        J))
        perm_ratio = Round(perm_ratio, 3)
        If I = 76 Then
            Print #3, Format(2 * I - 1, "00"); ":"; Format(2 * I - 1, "00"), "1:1",
            Format(J, "00"); ":"; Format(J, "00"), Int(perm_ratio * 1000) / 1000
        Else
            Print #3, Format(2 * I - 1, "00"); ":"; Format(2 * I - 1, "00"), "1:1",
            Format(J, "00"); ":"; Format(J, "00"), Int(perm_ratio * 1000) / 1000
            Print #3, Format(2 * I, "00"); ":"; Format(2 * I, "00"), "1:1", Format(J,
            "00"); ":"; Format(J, "00"), Int(perm_ratio * 1000) / 1000
        End If
    Next I
Next J
Close #3
End Sub

```